ORIGINAL PAGE IS
OF POOR QUALITY

MTI-84TR35

Final Report

RESEARCH STUDY OF PRESSURE INSTRUMENTATION

Prepared for

George C. Marshall Space Flight Center

Prepared Under

NASA Contract NAS8-35015

July 1984

DRAFT

RESEARCH AND DEVELOPMENT DIVISION

MECHANICAL TECHNOLOGY INC.

MTI 84TR35

Final Report

RESEARCH STUDY OF PRESSURE INSTRUMENTATION

Prepared for:

George C. Marshall Space Flight Center
Marshall Space Flight Center
Alabama, 35812

Prepared under:

NASA Contract NAS8-35015

Prepared by:

Leo Hoogenboom
Greg Hull-Allen

July 1984

MECHANICAL TECHNOLOGY INCORPORATED
968 Albany-Shaker Road
Latham, New York 12110

SUMMARY

To obtain a more vibration-resistant pressure sensor for use on the Space Shuttle Main Engine, a proximity-probe-based, diaphragm-type pressure sensor breadboard was developed by Mechanical Technology Incorporated (MTI). A fiber optic proximity probe was selected as the sensor. In combination with existing electronics, a thermal stability evaluation of the entire probe system was made. Based upon the results, a breadboard design of the pressure sensor and electronics was made and fabricated. A brief series of functional experiments was made with the breadboard to calibrate, thermally compensate, and linearize its response. In these experiments, the performance obtained in the temperature range of -320°F (liquid N_2) to +200°F was comparable to that of the strain-gage-based sensor presently in use on the engine. In tests at NASA-Marshall Space Flight Center (MSFC), after some time at or near liquid nitrogen temperatures, the sensor output varied over the entire output range. These large spurious signals were attributed to condensation of air in the sensing gap.

In the next phase of development of this sensor, an evaluation of fabrication techniques toward greater thermal and mechanical stability of the fiber probe assembly must be made. In addition to this, a positive optics-to-metal seal must be developed to withstand the pressure that would result from a diaphragm failure.

TABLE OF CONTENTS

TABLE OF CONTENTS (CONT'D)

LIST OF FIGURES

1.0 INTRODUCTION

Pressure measurements on the Space Shuttle Main Engine are presently made with strain-gage-type transducers. The failure history of these transducers, however, has motivated the search for a more vibration-resistant transducer. The present study was aimed at the evaluation of transducer concepts in which the deflection of a diaphragm is measured with a proximity sensor. Two types of proximity sensors were originally considered: a capacitive and a fiber optic sensor.* The capacitive sensor has been used at Mechanical Technology Incorporated (MTI) in a variety of high-temperature pressure sensors and is a well-documented device. However, the electronics and cabling were considered to have a reliability penalty that would make it potentially less attractive than the fiber optic sensor. As a result, the fiber optic sensor was selected for a detailed evaluation resulting in the design and fabrication of an experimental pressure sensor model.

1.1 Transducer Design

The experimental transducer design was guided by the contract statement of work, a copy of which is presented in Appendix 6, together with a group of specifications assembled from other sources. The following seven items were determined to be the key requirements for the experimental design:

1. Pressure ranges from 300 psig FS to 9000 psig FS
2. Envelope dimensions no greater than those of existing pressure sensors**
3. Operating temperature limits: -452°F to +450°F
4. Thermal zero shift: <0.5% per 100°F
5. Thermal sensitivity shift: <0.5% per 100°F
6. Thermal gradient: 165°F across sensor (axially)
7. Response: 0 to 300 Hz and also 0 to 20,000 Hz

---

*MTI Proposal G2-457, "Research Study: Research of Pressure Instrumentation," March 12, 1982, in response to RFP 8-1-2-EC25722.

**The envelope dimensions given in Appendix 6 were taken from Rockwell International Corp., Rocketdyne Division, Specification RC7001 for a pressure transducer with low-level analog output.

The transducer design is a compromise among the following:

- Maximum practical diaphragm diameter
- Maximum allowable diaphragm stress
- Minimum acceptable diaphragm deflection.

The minimum deflection acceptable is a multiple (100 to 1000 times) of the sum of the:

- Thermally induced mechanical zero shift of the promimity sensor
- Thermally induced electro-optical and electronic zero shift of the proximity sensor
- Effect of thermally induced compliance change of diaphragm.

Since these three thermally induced effects are on the order of 1 to 10 μin. (minimum), the minimum diaphragm deflection acceptable under these constraints is 0.0005 to 0.0010 in.

The design of a diaphragm-type pressure transducer is a compromise between a number of factors such as: desired deflection, permissible stress level, diaphragm diameter and diaphragm thickness. Appendix 1 shows the formulas that are used in the design of the diaphragm and it applies them to the problem of reaching a satisfactory compromise between the factors mentioned above. The present design effort is complicated by the fact that not just one, but a total of seven similar transducers must be designed for a series of seven pressure ranges. Therefore an additional design input is that all the sensors will use a diaphragm of a given (maximum) diameter. To aid in reaching the final design compromise, two tables were set up that show various options. Table 1* lists as inputs four diaphragm sizes and two maximum stress levels and the resulting pressure range, diaphragm thickness and resonant frequency, each for three (input) values of deflection. The boxed-in area in the "q" column shows pressure ranges from 250 psi to 9000 psi, for deflections of 0.001 to 0.003 in. The diaphragm thickness associated with these pressure

*Tables and Figures are presented consecutively, beginning on page 8.

ranges are shown in the box in the next column. They range from 0.029 in. (pressure range q = 501 psi) to 0.173 in. ($q_{.}$ = 9000 psi). The conclusion is that the entire pressure range can be accommodated, with acceptable diaphragm thickness, but with deflections not more than 0.003 in., and with some diaphragms that are 1.6 in. in diameter. To get a different cross section of designs, Table 2 was made. The inputs in Table 2 are seven pressure ranges, from 300 psi to 9000 psi, two stress levels (70,000 and 35,000 psi) and four diaphragm diameters (0.5, 0.8, 1.12, and 1.6 in.). For each combination of these inputs, the resulting deflection, diaphragm thickness and resonant frequency are given. The most attractive solution is a design for all pressure ranges that has a fixed diameter and a thickness that varies with pressure range, and that has acceptable deflection. The diaphragm with a radius of 0.4 in. approaches the ideal when the maximum stress allowed is 70,000 psi. The minimum thickness is 0.023 in., which is practical, and the minimum deflection is 0.0007 in., a little less than desired, but still acceptable. In the final design, due to space constraints, it became necessary to reduce the diaphragm size to 0.7 in. diameter. The diaphragm design series for that diameter is listed in Table 3 as the final design. The transducer assembly drawing in Figure 1 shows the layout of a sensor with a 0.7 in. diameter diaphragm for the maximum pressure range of 9000 psi. Figure 1 was taken from MTI Drawing No. SK-B-8454 located in the pocket at the end of this report.

As shown in Table 3, the diaphragm thickness for the lowest pressure range (300 psi) is 0.020 in. and for the highest range it is 0.112 in. The deflections available from these diaphragms range between 0.0006 in. and 0.0034 in. Due to this range in deflections, the specifications for thermal stability for the 300-psi sensor will be better than those for the 9000-psi sensor by a factor of about 6 (maximum). This is because the fiber probe thermal drift is a fixed amount. For the demonstrator model, a pressure range (q) equal to 1000 psi was selected, for which the diaphragm thickness was 0.036 in., and the deflection was 0.0019 in. at full scale.

1.2 Evaluation of Commercial MTI Fiber Optic Proximity Probe

To guide the design of the electronics and the transducer, a preliminary experimental evaluation of MTI's fiber optic proximity probe, the Fotonic™

sensor, was made.* The principle of operation of this probe is shown in Figure 2 and a probe section is shown in Figure 3. The following information was needed from the experiment:

- Temperature effects on probe output
- Nonlinearity in response
- Temperature effects on stability of zero and gain of the fiber optic probe electronics.

The results of tests for the effect of temperature on probe output and nonlinearity of response are shown in Figures 4 and 5, respectively. The effect of temperature on the electronics is shown in Figures 6 to 9.

Figure 4 shows that as the temperature increases, the gap increases. The differential thermal expansion between the glass fiber bundle and the stainless steel sheath causes the fibers to withdraw into the sheath. At some point, the glass remains attached and moves with the sheath. In Appendix 7, it is calculated that the glass moves independent of the sheath to a depth of 0.36 to 0.45 in., depending upon the coefficient of expansion of the glass. This experiment, as well as others described in Appendix 7, led to the conclusion that the proximity sensor in the pressure transducer must be provided with a means of temperature compensation.

The basic fiber optic probe response shown in Figure 5 indicates that the sensor has a quasi-linear response around a gap of about 0.0035 in. The displacement range needed for the transducer (see Table 3) varies between 0.0006 in. for a 9000-psi sensor and 0.0034 in. for a 300-psi sensor.

The linearity requirements for the proximity probes are analyzed in Appendix 2. The conclusion is that a slope variation of 0.6 to 1.2% is permissible. In Figure 4 it can be seen that the gap range available within the 0.6 to 1.2% slope band is about 0.0004 in. at the peak of the slope curve. This is an insufficient gap range for any of the diaphragm designs in Table 3. Therefore, electronic linearization must be provided.

---

*See also Appendix 9 for more detail in some areas of the design.

The effect of temperature on the zero drift/stability of the electronic building blocks or components is documented in Figures 6 to 9. As shown on Figure 6, the total drift for the complete electronics circuit, including the effects of the incandescent lamp, was 135 μin./90°F. Three sources contributing to this drift were evaluated separately. A fourth source identified was the incandescent lamp. Its contribution to drift is calculated from the total drift minus that contributed by the three sources for which data is given in Figures 7 through 9.

Drift contributed by the unilluminated photo diode is shown in Figure 7, but it is only a few percent of the total in Figure 6, and it opposes the trend in Figure 6.

The effect of the elements in the lamp control circuit on drift is shown in Figure 8. The total effect of the lamp control unit is 0.3%/90°F. Using the response data given in Figure 5, this percentage is converted to an equivalent gap as follows.

When the sensing gap is set at the maximum slope point of the response curve, the sensitivity is roughly equal to 150×10^{-6} of the peak output per microinch. The output level at that gap is about 40% of the peak output. If the lamp intensity varies by 0.3%, the output will vary by 0.3% of 40% of the peak:

$$\frac{0.003 \times 0.40 \times \text{peak}}{1.50 \times 10^{-6} \times \text{peak}/\mu\text{in.}} = 8\ \mu\text{in.}/90°\text{F.}$$

The temperature effect on the electronics without the drift contributed by the photodiode is shown in Figure 9. That contribution is a few percent of the total in Figure 6, but the trend is also opposed to that in Figure 6.

In summary, it was found that:

1. Thermal effects of the probe materials are:

   $\frac{+320\ \mu\text{in.}}{180°\text{F}}$ (Figure 4).

2. Thermal effects of the electronics (including incandescent lamp effects) are:

   $\frac{+135\ \mu in.}{90°F}$ (Figure 6).

3. Thermal effects of the electronics alone (excluding incandescent lamp effects) are:

   - Electronics only: $\frac{-3\ \mu in.}{90°F}$ (Figure 7).
   - Lamp control circuit: $\frac{-8\ \mu in.}{90°F}$ (Figure 8).
   - Electronics without photodiode: $\frac{-3\ \mu in.}{90°F}$ (Figure 9).

Notice that the thermal effects of the electronics are small and of opposed sign to the large, positive contribution attributed to the thermal instability of the incandescent lamp. The thermal effect of the probe must be compensated by measuring the probe temperature. To eliminate the use of any electrical connections in the transducer, it was decided that a second fiber optic probe would be used with enhanced temperature sensitivity to measure probe temperature. In a gage length of about 0.6 in., the thermal differential expansion between glass and 304 stainless steel suffices to obtain a gap change of +0.0003 in./100°F (see Figure A7-2 for thermal expansion data). In Appendix 4, a calculation is made of the response of the probe to a rapid temperature change as may happen when it is exposed to a change from gaseous to liquid fuel or oxidizer. A 10 to 20 second delay in thermal response of the temperature sensor was calculated.

The thermal effects in the electronics shown in Figure 6 are an order of magnitude greater than those shown in Figures 7 to 9 and they are of opposed sign. There is obviously another element that contributes a major amount of thermal drift. The only likely source of this drift is the incandescent lamp. The effect of the lamp is a combination of the non-uniform intensity distribution of the light exiting the lamp and the non-uniformity of the distribution of illuminating fibers in the face of the probe. These two factors combined result in drift when the lamp filament shifts its position. The potential

magnitude of the lamp-related drift is quantized in Appendix 8. The results shown in Appendix 8 agree with the drift shown in Figure 6, thus confirming the hypothesis that blames the lamp for most of the drift.

The thermal drift effects ascribed to mechanical effects of the incandescent lamp are undesirable. In addition to these quasi-static effects, the filament can vibrate in many modes, which could cause dynamic noise comparable in amplitude to the thermally induced drift. The effect of vibration on the incandescent lamp was already considered a major liability before the thermal effects were identified. Therefore, solid-state light sources were investigated as a substitute. For the present application, in which the permissible fiber bundle size and the target reflectivity favor high light signal levels, the solid-state light-emitting diode (LED) is equivalent to an incandescent lamp. The spectral content of the light in an incandescent lamp and an IR LED source and the spectral response of the photodiode are compared in Figure 10. It can be seen that the LED output is centered on the response of the photodiode, which is a favorable match; whereas the incandescent lamp peaks well outside the photodiode response curve.

The effort described in this section was aimed at supporting and guiding the design of the breadboard. The critical evaluation of the commercial MTI fiber optic proximity sensor that was performed to provide the basic design inputs was not repeated on the finished breadboard. The work under the present contract was limited to the design and fabrication of a system most responsive to need. Actual performance evaluation will be made at MSFC. The results of three series of pressure calibrations of the system at NASA-MSFC are summarized and discussed in Appendix 10.

TABLE 1

PRESSURE TRANSDUCER DESIGN CHART

(See Graphs in Figures A1-1, A1-2, A1-3)

Modulus of Elasticity ($E = 29 \times 10^6$ psi)										
		Pressure (q) (psi)			Diaphragm Thickness (t) (in.)			Resonant Frequency (f) (kHz)		
Deflection (w) (in.)		0.001	0.003	0.010	0.001	0.003	0.010	0.001	0.003	0.010
Diaphragm Radius (a) (in.)	Max. Stress (σ^*) (psi)									
0.25	35,000	220	22.4	2.20	0.0172	0.0057	0.00172			
0.25	70,000	1,760	195	17.6	0.0344	0.0114	0.00344			
0.40	35,000	563	62.6	5.63	0.0440	0.0146	0.0044			
0.40	70,000	4,504	501	45	0.0880	0.0292	0.0088			
0.562	35,000	1,125	125	11.3	0.0880	0.0294	0.0088			
0.562	70,000	9,001	1000	90	0.1730	0.0579	0.0173			
0.80	35,000	2,253	250	22.5	0.1760	0.0587	0.0176			
0.80	70,000	18,024	2000	180	0.3520	0.1174	0.0352			
	35,000							26.3	8.76	2.63
	70,000							52.6	17.5	5.26

For σ = 35,000 psi:

$t = 0.275 \times 10^{-3} \frac{a^2}{w}$

$q = 3.52 \times 10^{-3} \left(\frac{a}{w}\right)^2$

$f = 26.3 \frac{1}{w}$ Hz

For σ = 70,000 psi

$t = 0.550 \times 10^{-3} \frac{a^2}{w}$

$q = 28.16 \times 10^{-3} \left(\frac{a}{w}\right)^2$

$f = 52.6 \frac{1}{w}$ Hz

NOTE: Stress level in strain gage transducer, made of A286, is 50,000 psi according to Don Rupar of Cons. Controls Corp. of America.

*Radial bending stress (σ_r) at outer edge. The tangential bending stress (σ_t) is 2 times the radial stress. The equivalent stress (σ_e) according to the maximum distortion energy criterion is $\sigma_e^2 = \sigma_r^2 + \sigma_t^2 - \sigma_r\sigma_t$, which is 89% of the radial bending stress (σ_r).

TABLE 2

DESIGN DATA MATRIX FOR SEVEN DIAPHRAGMS FOR PRESSURE RANGES OF 300-9000 PSI

n	q_n^* (psi)	q (psi)	a (in.)		σ = 70,000 psi					σ = 35,000 psi		
					0.25	0.40	0.56	0.80	0.25	0.40	0.56	0.80
0	300	300	w	inch	0.0024	0.0039	0.0055	0.0077		0.0014	0.0019	0.0027
			t	inch	0.014	0.023	0.032	0.046		0.031	0.047	0.065
			f	kHz	21.6	13.4	9.5	6 8		18.7	13.8	9.7
1	529	500	w	inch	0.0019	0.0030	0.0042	0.0060		0.0011	0.0015	0.0021
			t	inch	0.018	0 030	0 042	0 068		0.040	0.059	0.084
			f	kHz	27.5	17.5	12.4	8 7		23.8	17.5	12.5
2	932	1000	w	inch	0.0013	0.0021	0.0030	0 0042			0.0011	0.0015
			t	inch	0.026	0.042	0.059	0.083			0.080	0.117
			f	kHz	40.0	25.0	17.5	12.4			23.8	17.5
3	1643	1500	w	inch	0.0011	0.0017	0.0024	0.0034				0.0012
			t	inch	0.031	0.052	0.73	0.103				0.146
			f	kHz	47.5	30.8	21.6	15.4				21.8
4	2897	3000	w	inch	0.00077	0.0012	0.0017	0.0024				
			t	inch	0.044	0.073	0.103	0.146				
			f	kHz	69.	43.6	30.8	21.6				
5	5106	5000	w	inch	0.00059	0.00094	0.00135	0.0019				
			t	inch	0.058	0.94	0 130	0.184				
			f	kHz	89.	55.	38.6	27.5				
6	9000	9000	w	inch	0.00044	0.00071	0.0010	0.0014				
			t	inch	0.077	0.124	0.175	0 250				
			f	kHz	118.	74.	52.5	37.3				

q = pressure range; σ = maximum stress; 2a = diameter; t = thickness; w = diaphragm deflection (FS)

*$q_n = q_0(1.763)^n$

NOTE: For a given range q, at 50,000 psi, the available deflection (w) is:

$(5/7)^{3/2}$ times (= 60% of) that for 70,000 psi.

TABLE 3
FINAL DESIGN DATA FOR SEVEN DIAPHRAGMS FOR PRESSURE RANGES OF 300-9000 PSI

Diaphragm Diameter 2a = 0.7 in.

Maximum Stress σ = 70,000 psi

Pressure Range (q) (psi)	Diaphragm Deflection (w) (in.)	Diaphragm Thickness (t) (in.)	Resonant Frequency (f) (kHz)
300	0.0034	0.020	15.5
500	0.0026	0.026	20.2
1000	0.0019	0.036	27.7
1500	0.0015	0.045	35.1
3000	0.0011	0.061	47.8
5000	0.0008	0.084	65.8
9000	0.0006	0.112	87.7

$$w = \frac{0.0588}{\sqrt{q}} \text{ in.}, \quad t = \frac{0.0673 \times 10^{-3}}{w} \text{ in.}, \quad f = \frac{52.6}{w} \text{ Hz}$$

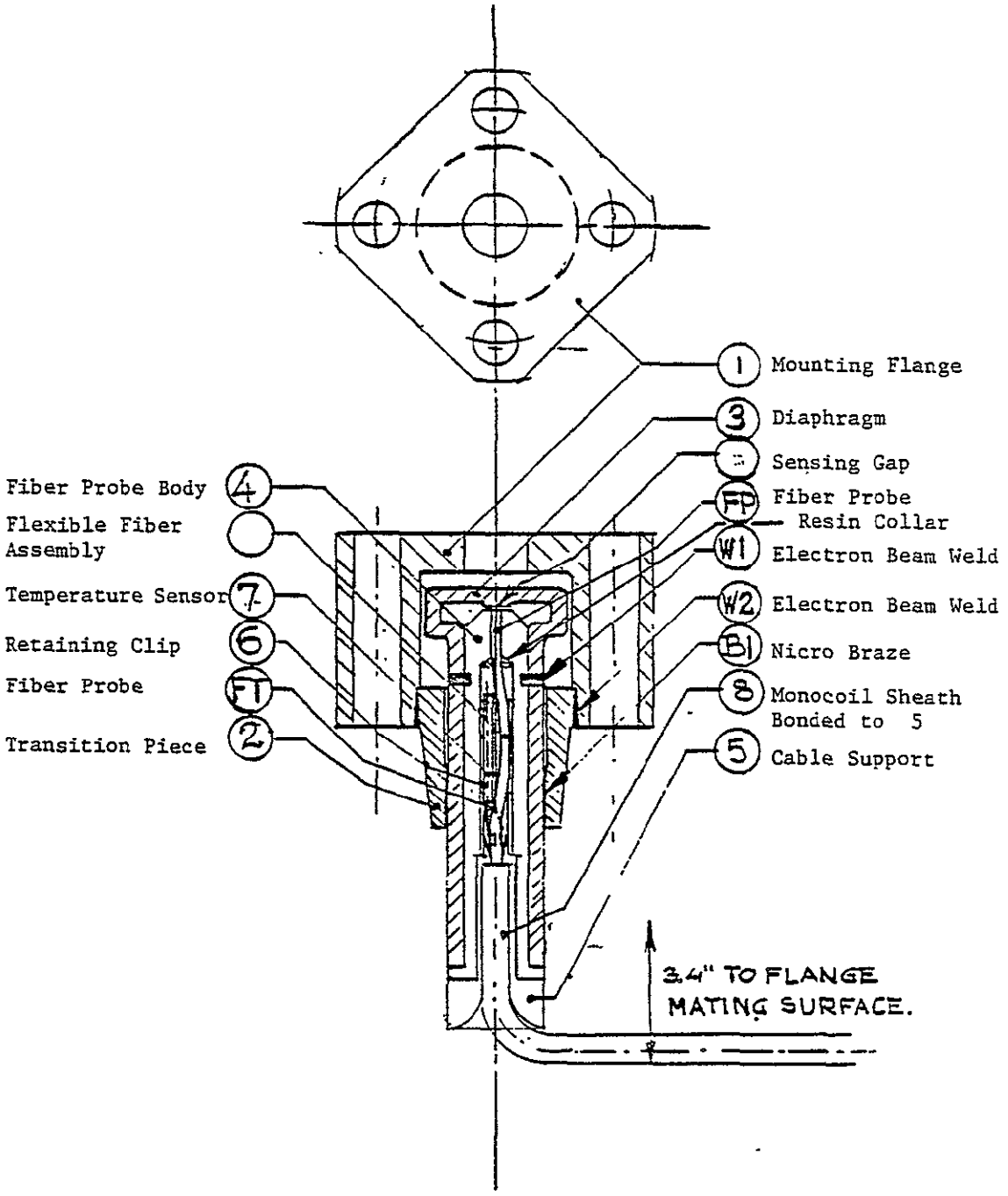

Fig. 1 Fiber Optic Pressure Transducer Assembly

SK-B-8454

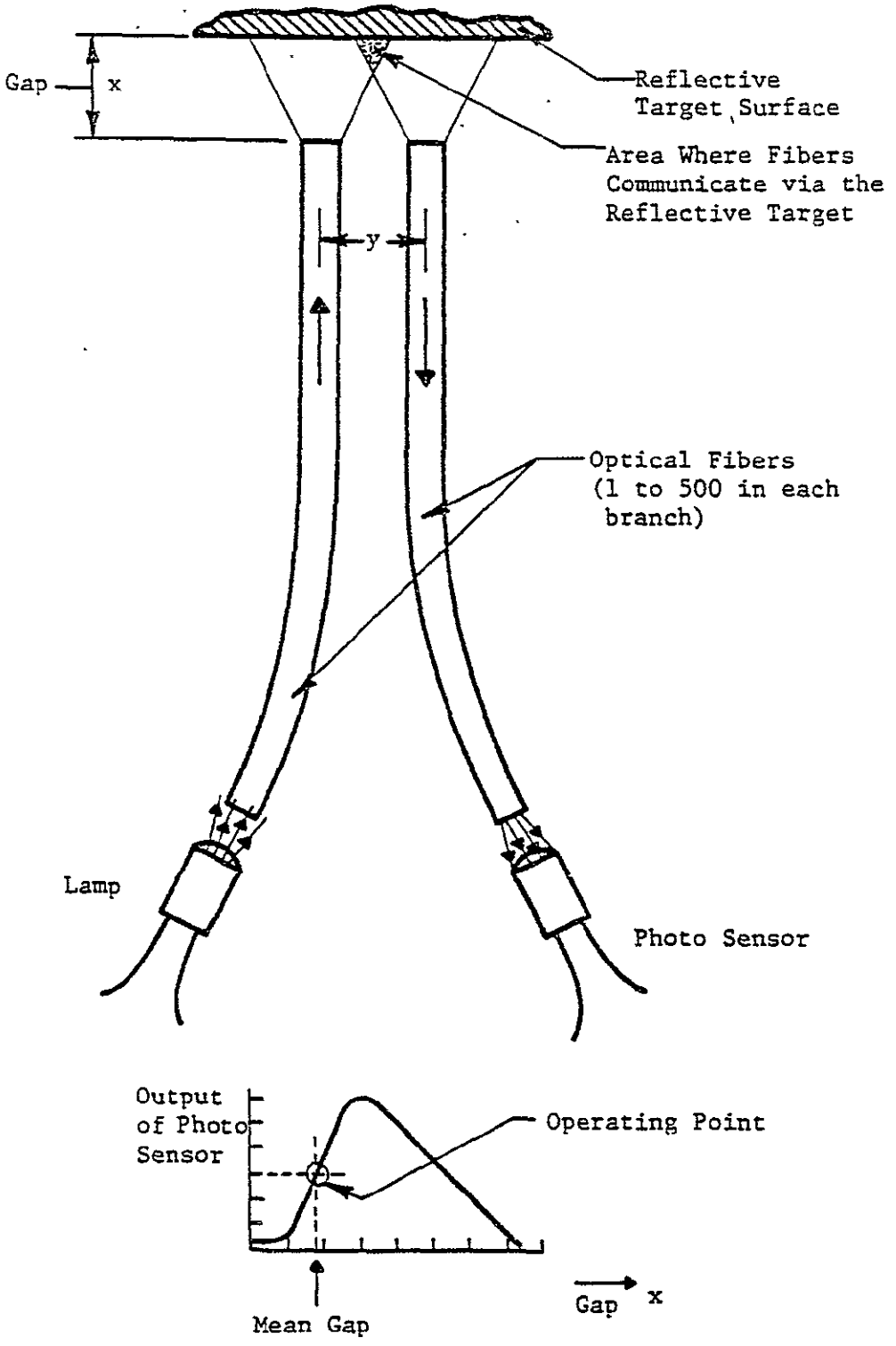

Fig. 2 Fiber Optic Proximity Probe, Principle of Operation and Response Curve

82837

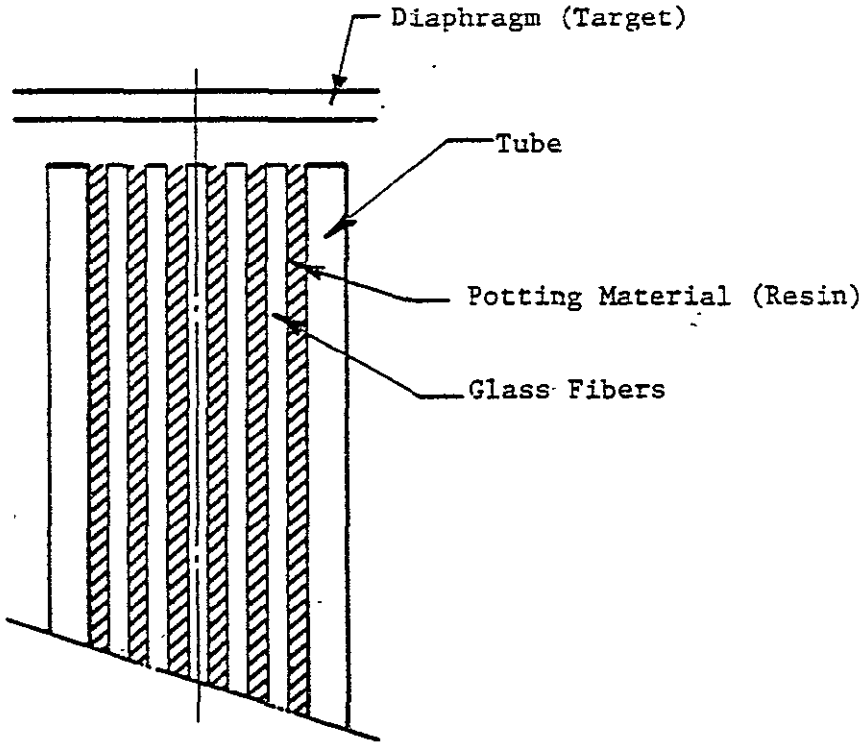

Fig. 3 Fiber Optic Proximity Sensor Section

82838

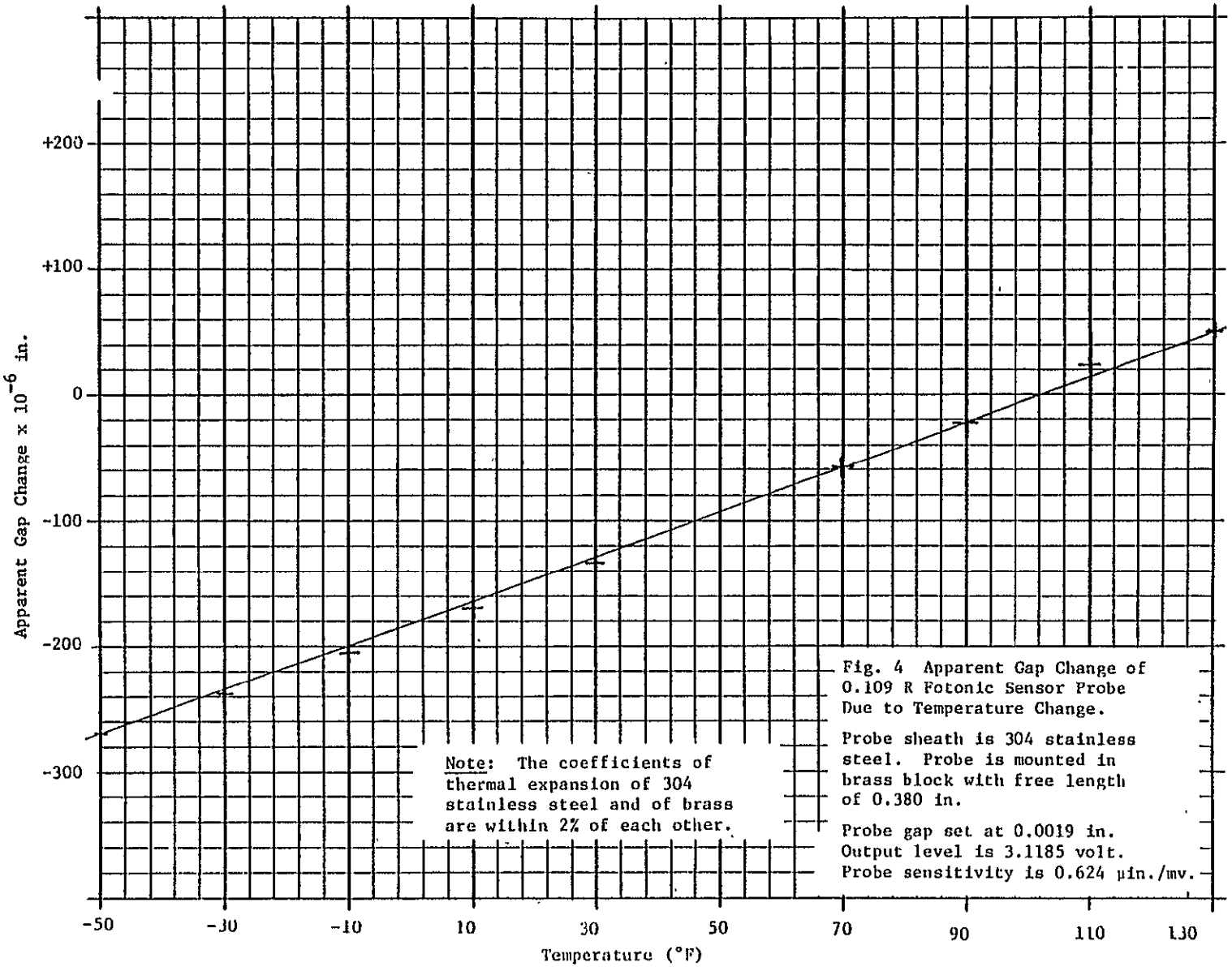

Fig. 4 Apparent Gap Change of 0.109 R Fotonic Sensor Probe Due to Temperature Change.

Probe sheath is 304 stainless steel. Probe is mounted in brass block with free length of 0.380 in.

Probe gap set at 0.0019 in. Output level is 3.1185 volt. Probe sensitivity is 0.624 µin./mv.

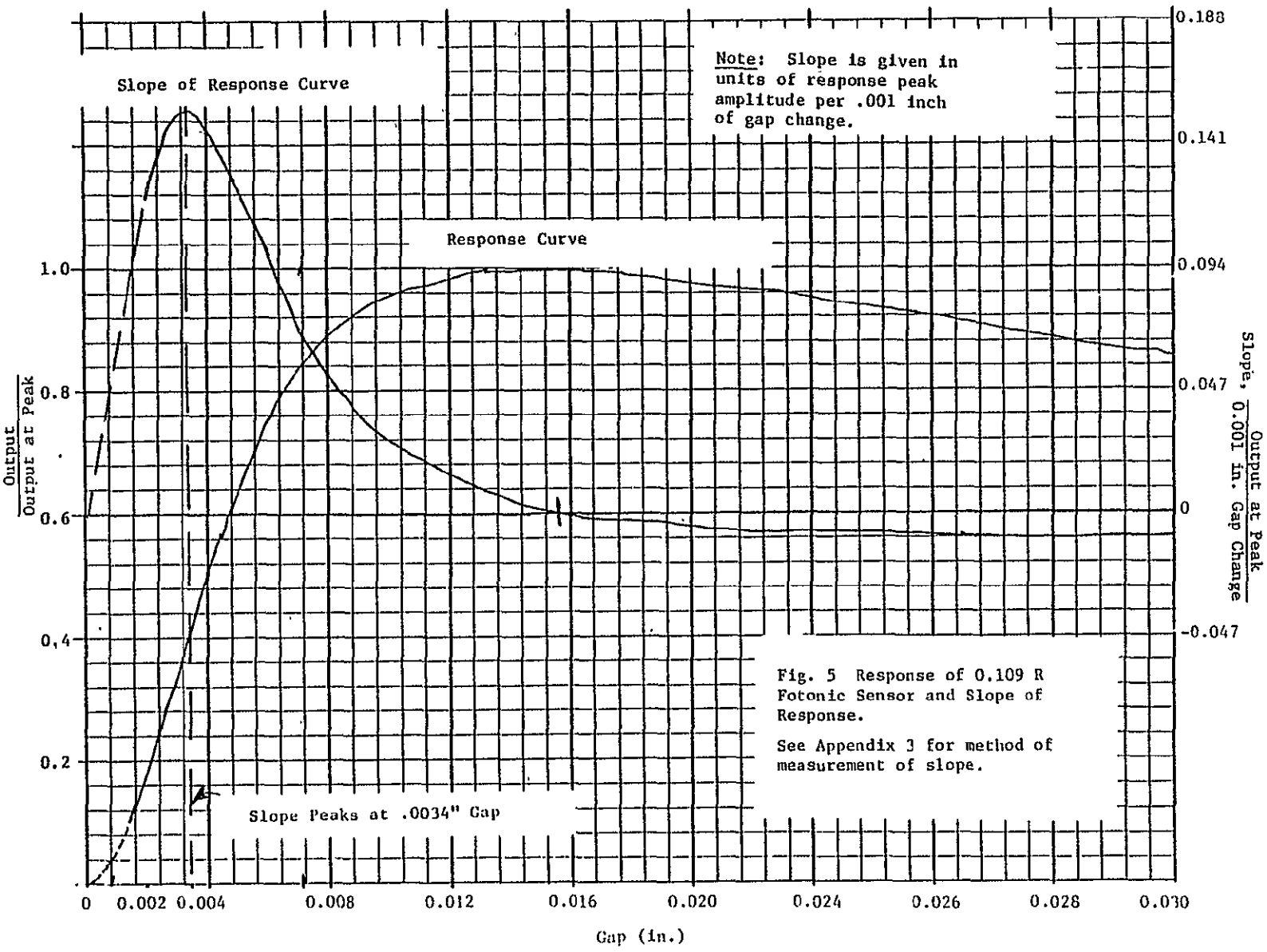

Fig. 5 Response of 0.109 R Fotonic Sensor and Slope of Response.

See Appendix 3 for method of measurement of slope.

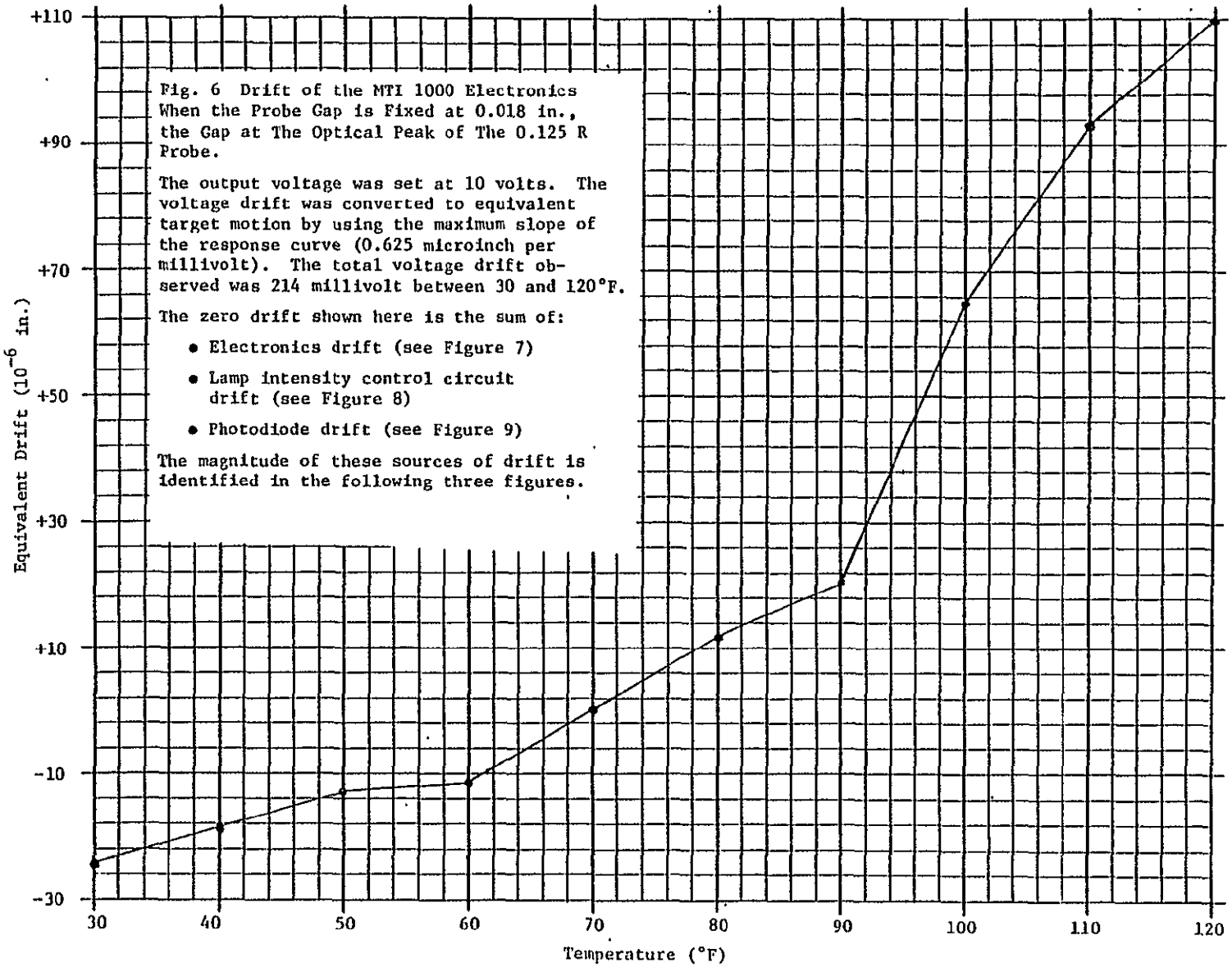

Fig. 6 Drift of the MTI 1000 Electronics When the Probe Gap is Fixed at 0.018 in., the Gap at The Optical Peak of The 0.125 R Probe.

The output voltage was set at 10 volts. The voltage drift was converted to equivalent target motion by using the maximum slope of the response curve (0.625 microinch per millivolt). The total voltage drift observed was 214 millivolt between 30 and 120°F.

The zero drift shown here is the sum of:

- Electronics drift (see Figure 7)
- Lamp intensity control circuit drift (see Figure 8)
- Photodiode drift (see Figure 9)

The magnitude of these sources of drift is identified in the following three figures.

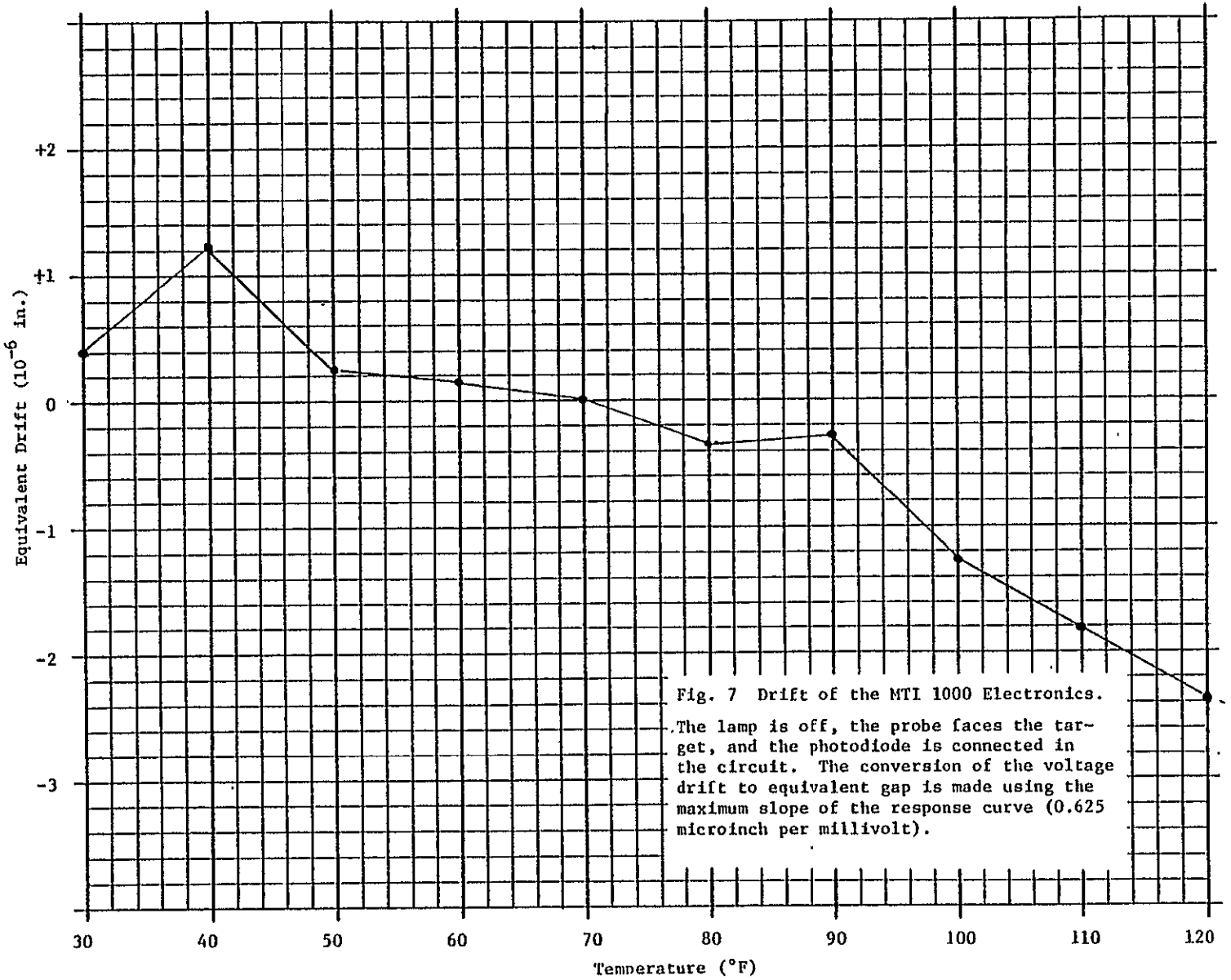

Fig. 7 Drift of the MTI 1000 Electronics. The lamp is off, the probe faces the target, and the photodiode is connected in the circuit. The conversion of the voltage drift to equivalent gap is made using the maximum slope of the response curve (0.625 microinch per millivolt).

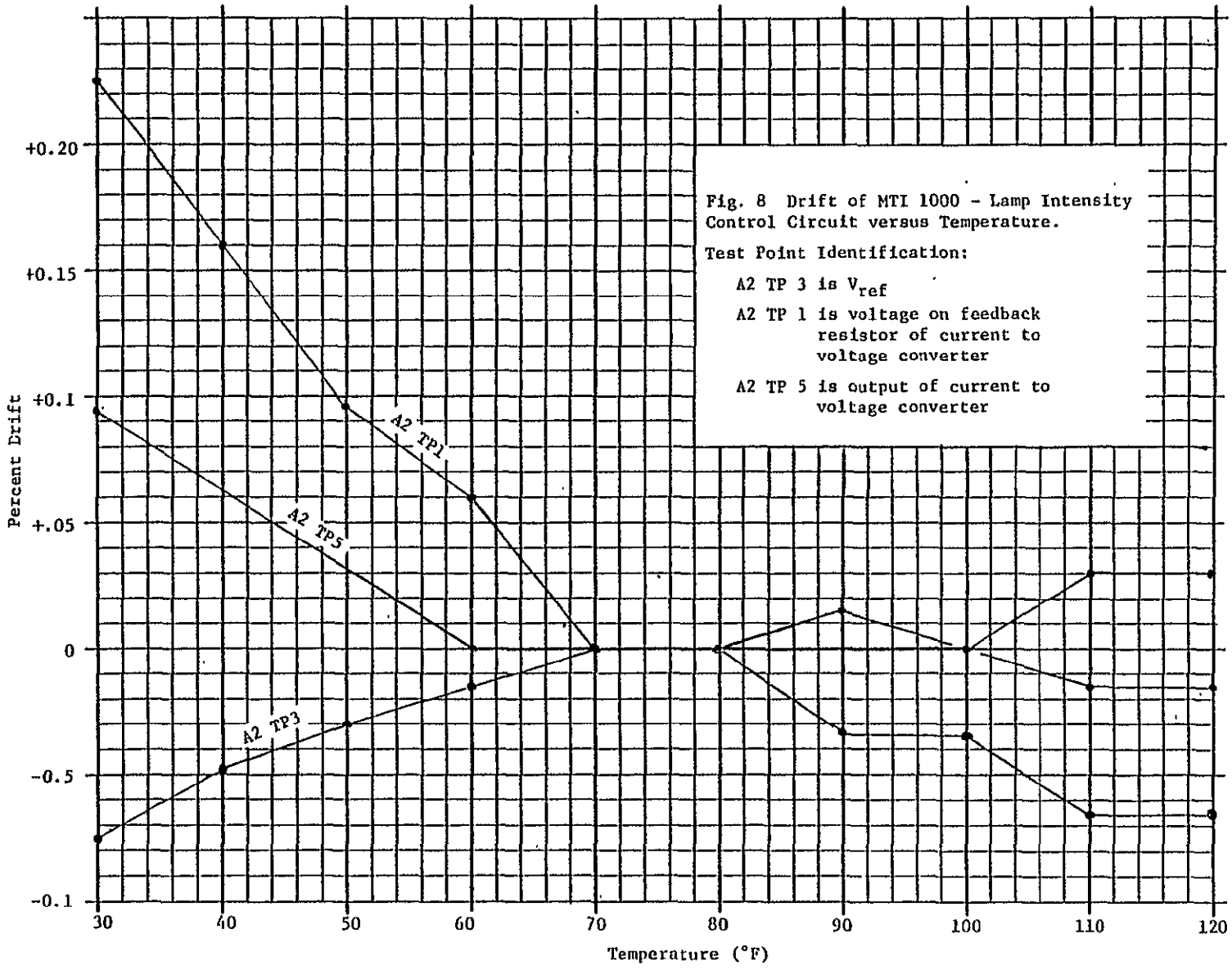

Fig. 8 Drift of MTI 1000 - Lamp Intensity Control Circuit versus Temperature.

Test Point Identification:

A2 TP 3 is V_{ref}

A2 TP 1 is voltage on feedback resistor of current to voltage converter

A2 TP 5 is output of current to voltage converter

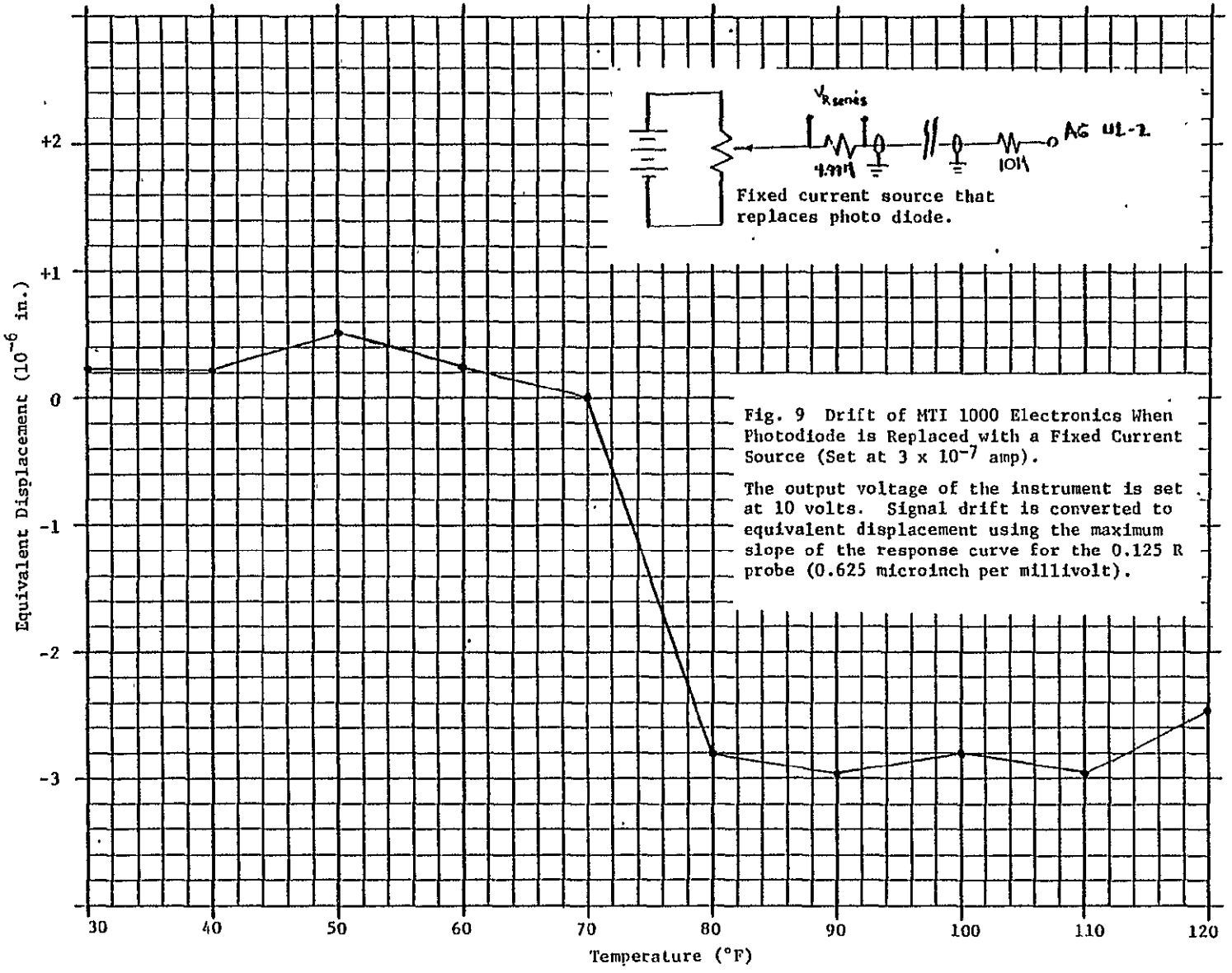

Fig. 9 Drift of MTI 1000 Electronics When Photodiode is Replaced with a Fixed Current Source (Set at 3×10^{-7} amp).

The output voltage of the instrument is set at 10 volts. Signal drift is converted to equivalent displacement using the maximum slope of the response curve for the 0.125 R probe (0.625 microinch per millivolt).

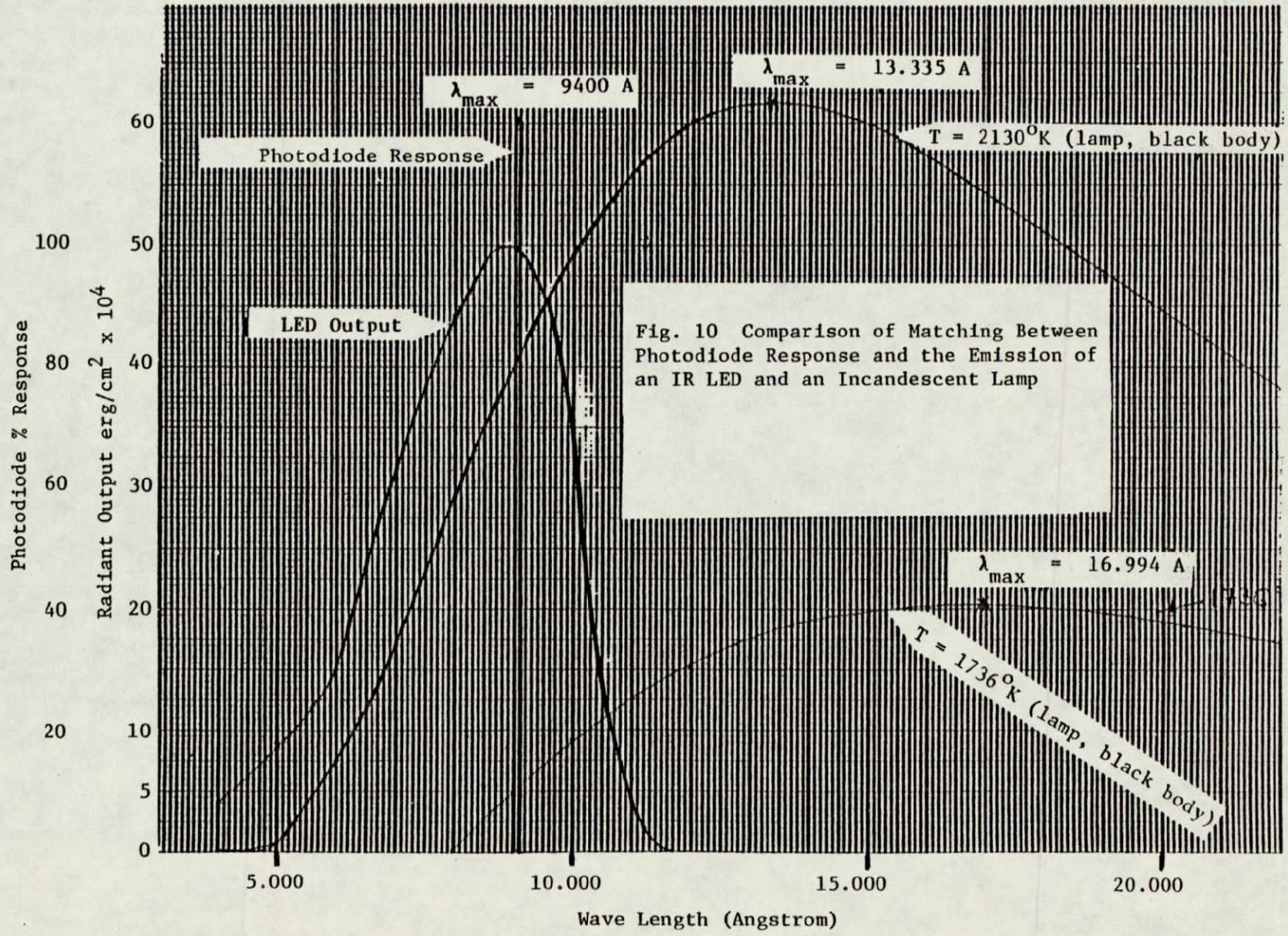

Fig. 10 Comparison of Matching Between Photodiode Response and the Emission of an IR LED and an Incandescent Lamp

2.1. Optical-to-Electrical Conversion Module (2)*

This module, a layout of which is shown in Figure 17, provides the mechanical coupling of the fiber optics to the LEDs and photodiodes. It produces voltages proportional to the LED intensities and the received light intensities.

The fiber optics and opto-electrical elements are brought together in a two-piece aluminum lamp block. The block is made in two sections to facilitate assembly and is not intended as a disconnect. See Figures 15 and 16.

The electrical half of the block carries four photodiodes and two infrared LEDs. Two of the photodiodes monitor the intensity of the LEDs and two detect the light returning to the unit via the receiving fibers of the optical probe. The six electro-optical devices are installed in 0.25-in. diameter holes and insulated from the block by plastic bushings. The devices are mechanically referenced to the optical axis by the shoulders on the LEDs and photodiodes. The position of the devices is maintained by a plate which acts against the cases through an insulating sheet. Figure 18 shows a concept sketch of a section through the receptacle assembly. The detailed drawings of this assembly are provided in Drawing No. SK-C-8473 and SK-C-8474 located in the pocket at the end of this report.

The fiber optic terminations are carried by the second half of the block. In order to prevent undesirable scattering of light, the metal ferrules which carry the fibers mate tightly with the holes which receive them in the electro-optical section of the block. An O-ring seals the connection against contaminants, which could degrade the optical coupling.

The block halves are held and locked together by three #8 screws and three tapered pins through the flange. The #8 clearance holes are tapped for #10-32 screws, in order to allow the block sections to be driven apart.

---

*Numbers in parentheses identify the blocks shown on Figure 12.

Four current-to-voltage converters constitute the electronics portion of this module. These converters utilize Burr Brown OPA 102 BM low noise, low offset voltage operational amplifiers and Dale-type UAR low-temperature-coefficient resistors.

The uncompensated output of the pressure transducer (raw signal) is available from the second channel in this block at the jack marked "Displacement Output" in Figure 12.

2.2 LED Intensity Control Circuit (3)

Two voltages, proportional to the intensity of the LEDs in the optical-to-electrical conversion module, are supplied to error amplifiers in this circuit. These amplifiers compare the voltages with fixed reference voltages and output an amplified version of the integral of the difference in the voltages.

This integrator approach ensures the long-term stability of LED intensities. The magnitude of the lamp intensity is set by adjusting the reference voltage using fixed trim resistors, as shown in Figure 12.

2.3 Displacement Signal Amplifier (4)

This circuit provides a gain of 20 to the diaphragm displacement analog voltage produced by the optical-electrical conversion module. In order to implement a fixed-output offset and compensate for thermally induced offset drift, the first stage also acts as a summing amplifier.

2.4 Temperature Signal Amplifier (5)

This circuit provides an overall gain of 20 to the transducer temperature analog voltage produced by the optical-electrical conversion module. The output of the inverting (gain of 10) first stage is applied to the input summing junction of the displacement signal amplifier, to compensate for thermal offset drift in the transducer. To ensure smooth compensation and to prevent vibrations of the temperature probe from disrupting the output, this

stage limits the bandwidth of the temperature signal to 100 Hz. The final output of this circuit is applied to the multiplying input of the multifunction module, which compensates for thermal shifts in transducer diaphragm compliance.

2.5 Multifunction Module (6)

This device provides the transfer function

$$\frac{10}{9} V_y \left(\frac{V_z}{V_x}\right)^m$$

where:

V_y = transducer diaphragm compliance

V_z = transducer diaphragm displacement

V_x = 1

m = a selected exponent which provides optimum linearization of the transducer output.

The inputs to this device are scaled in such a way that the output will be 10 Vdc at zero pressure and approximately 1 Vdc at full-scale pressure.

2.6 Offset Amplifier (7)

This inverting stage offsets the output voltage to 0 Vdc at zero pressure and produces an output of +5 Vdc at full-scale pressure.

2.7 Scaling Amplifier (8)

This circuit uses a Burr Brown OPA 102 BM low noise, low offset voltage operational amplifier to buffer an attenuated version of the 5V output for the 30-MV full-scale output.

2.8 Output Voltage Active Clamp (9)

This circuit clamps the outputs to +5V and +30 MV in order to avoid potential damage to external circuitry in the event of over pressure. The clamp voltage may be varied easily to meet actual system requirements.

2.9 Voltage Reference (10)

This circuit provides a precision, stable +10 Vdc voltage for use by the LED intensity control circuit, the various offset networks, and the active clamp.

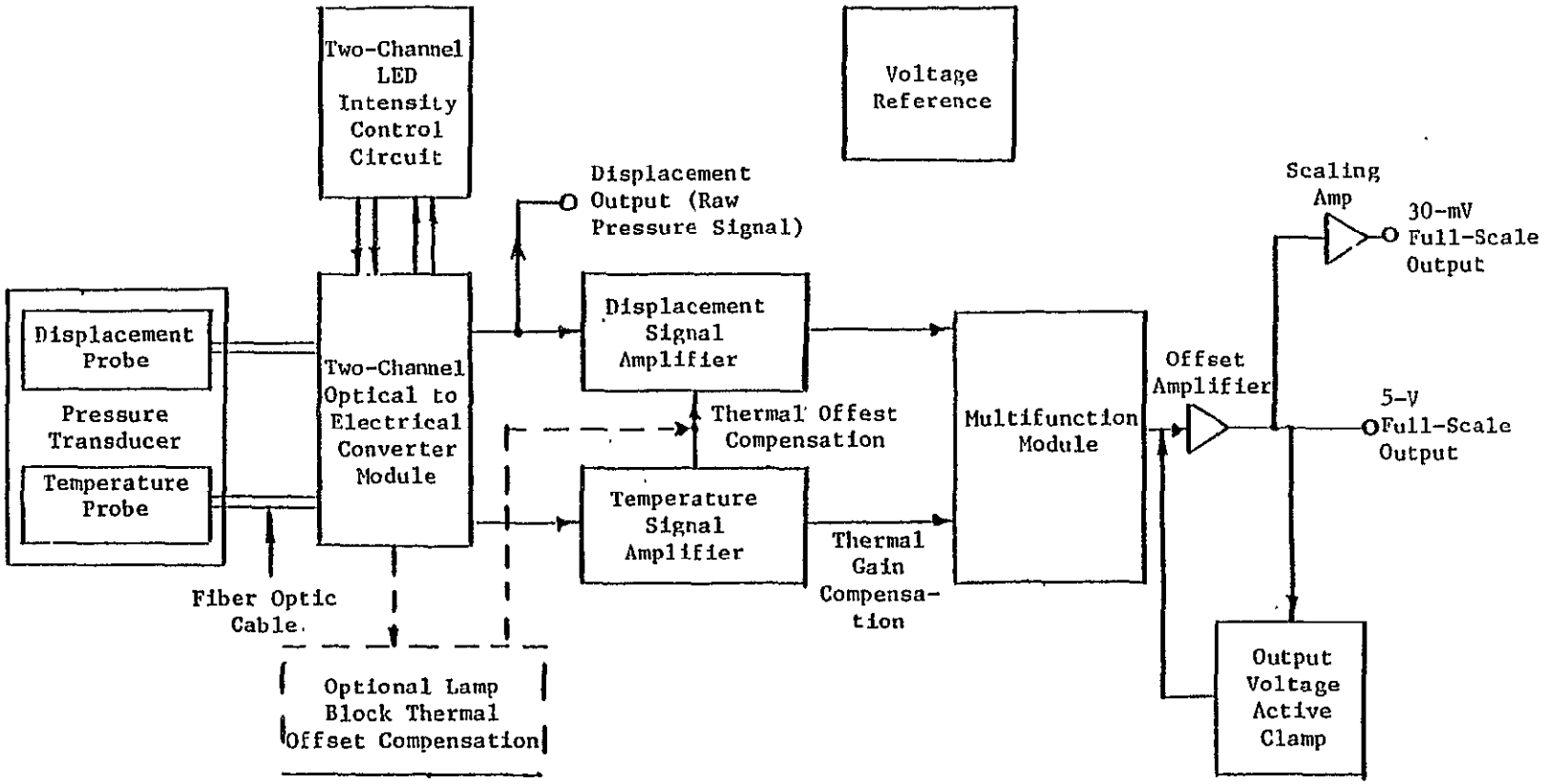

Fig. 11 Fiber Optic Pressure Transducer Block Diagram

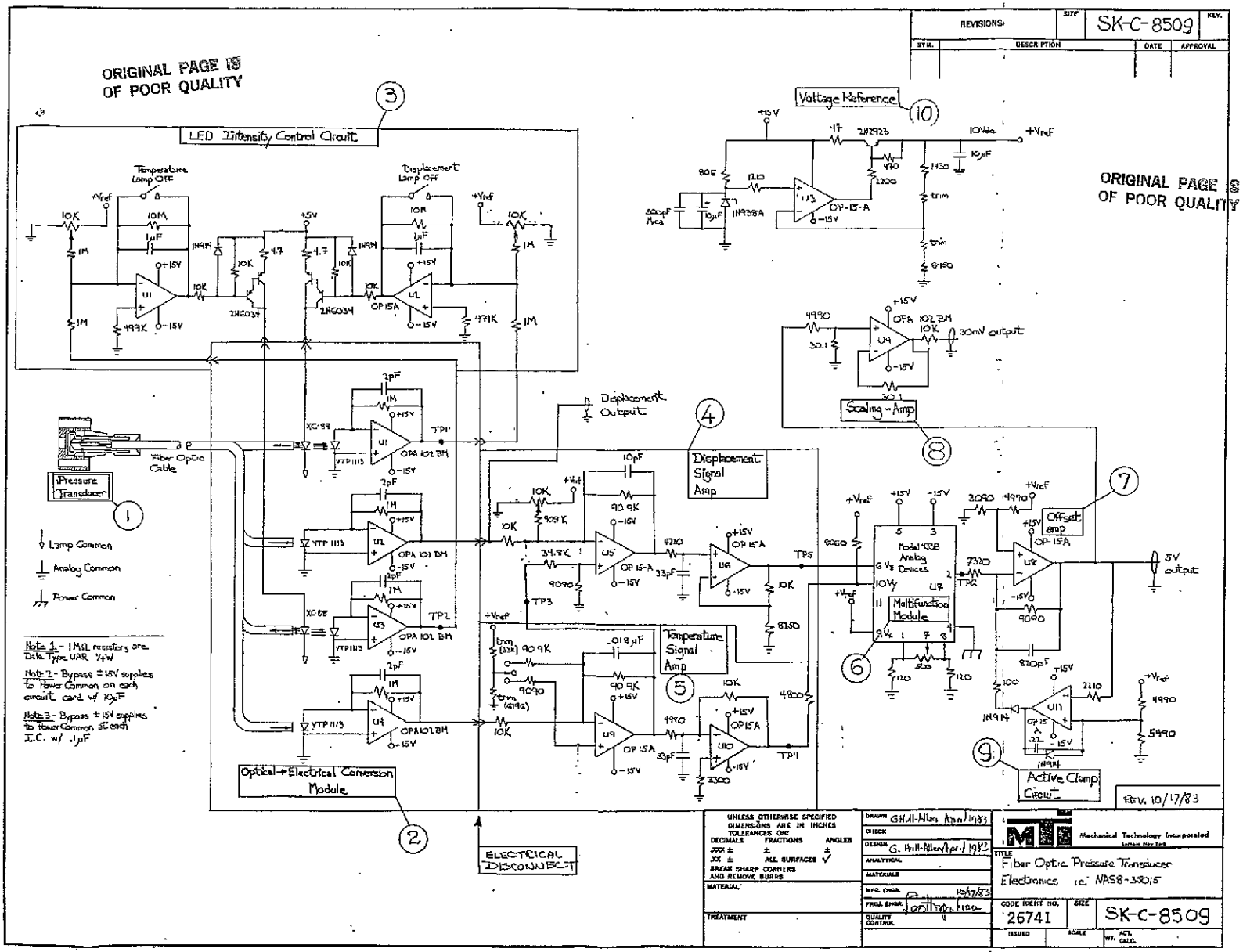

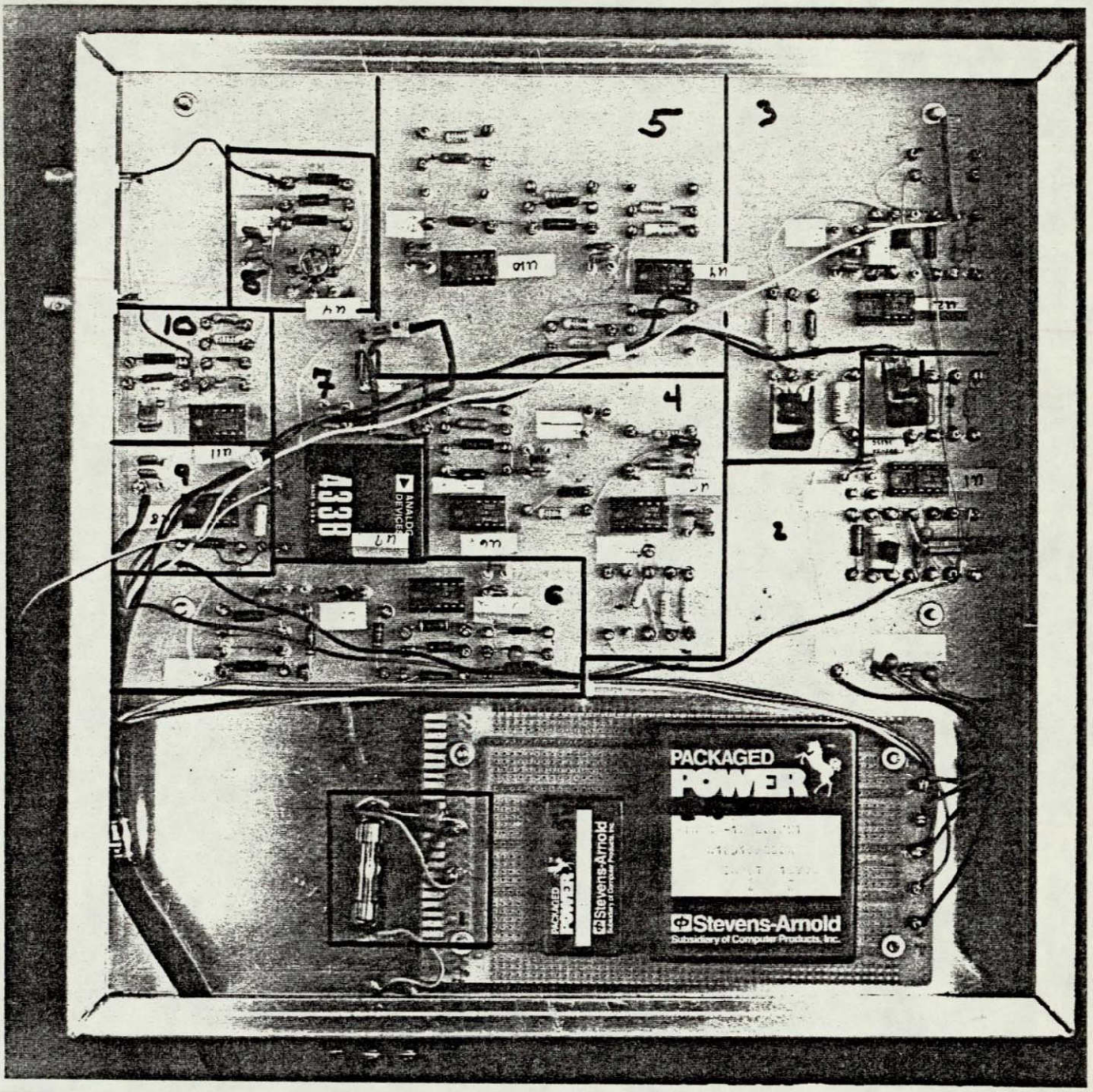

Fig. 13 Breadboard Electronics of Fiber Optic Pressure Transducer

1. Input Fuse/Reverse Protection Diode
2. Temperature LED Control
3. Displacement LED Control
4. Displacement Signal Amp
5. Temperature Signal Amp
6. Voltage Reference
7. Multifunction Module
8. 30 mV Output Amp
9. 5 V Output Amp
10. Active Clamp

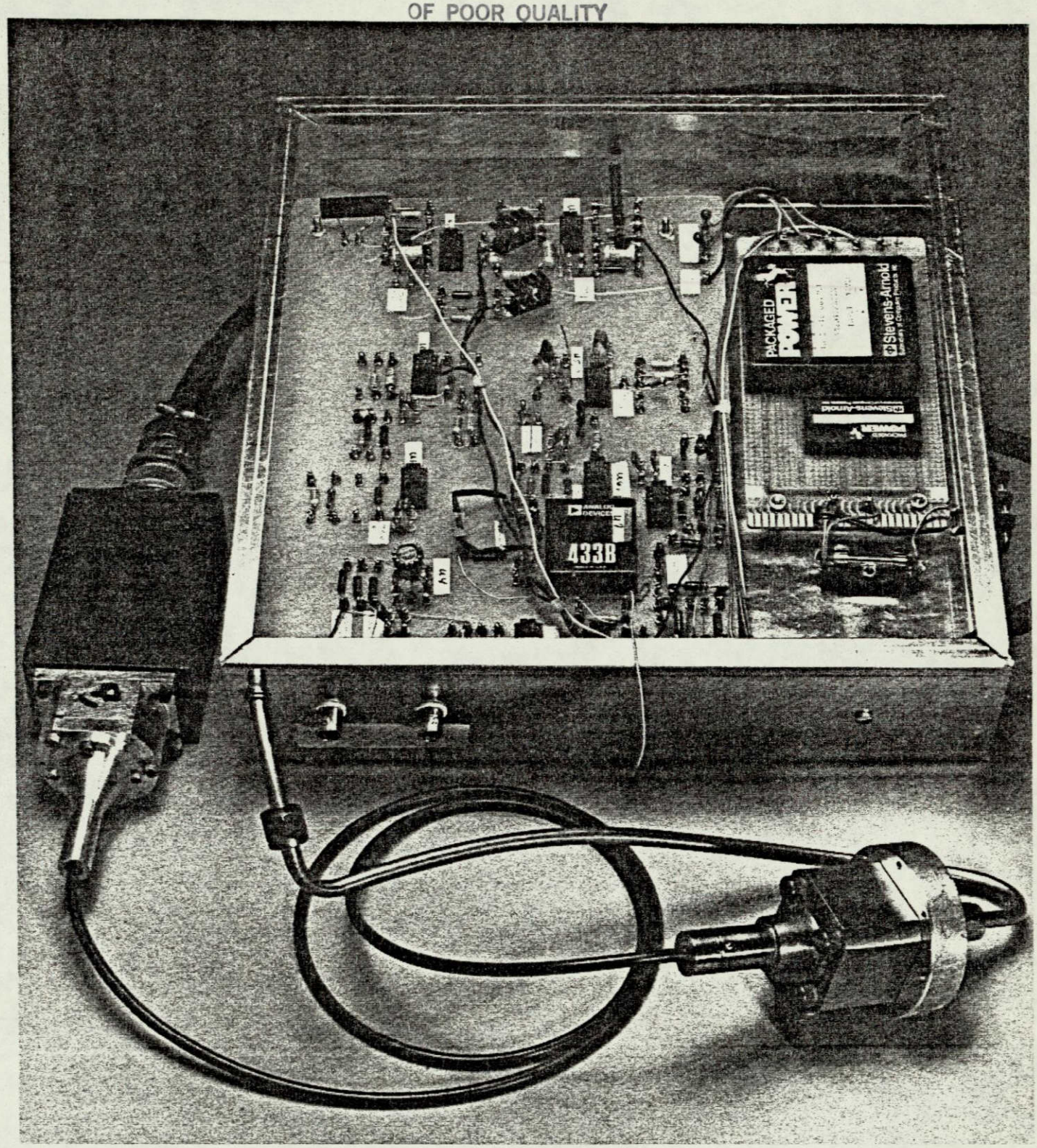

Fig. 14 Fiber Optic Pressure Transducer Breadboard

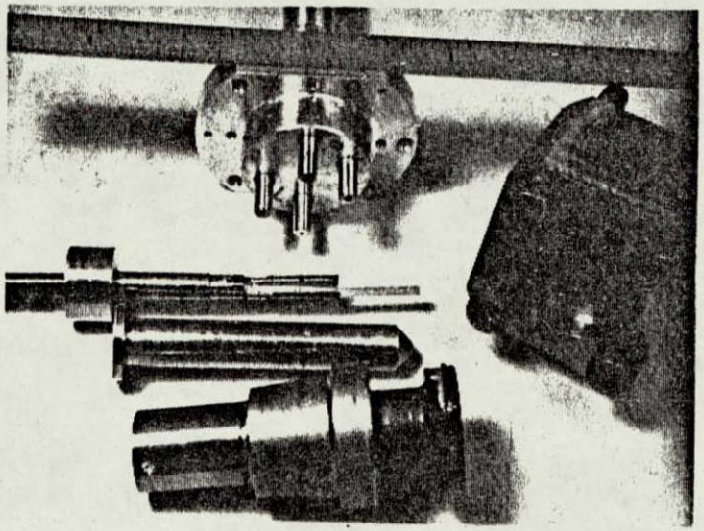

Fig. 15 Transducer Parts During Assembly. In center is temperature probe on retaining clip, and larger fiber bundle for pressure sensing. Below that are fiber probe body and diaphragm/support tube inside transition piece. On the right is the flange.

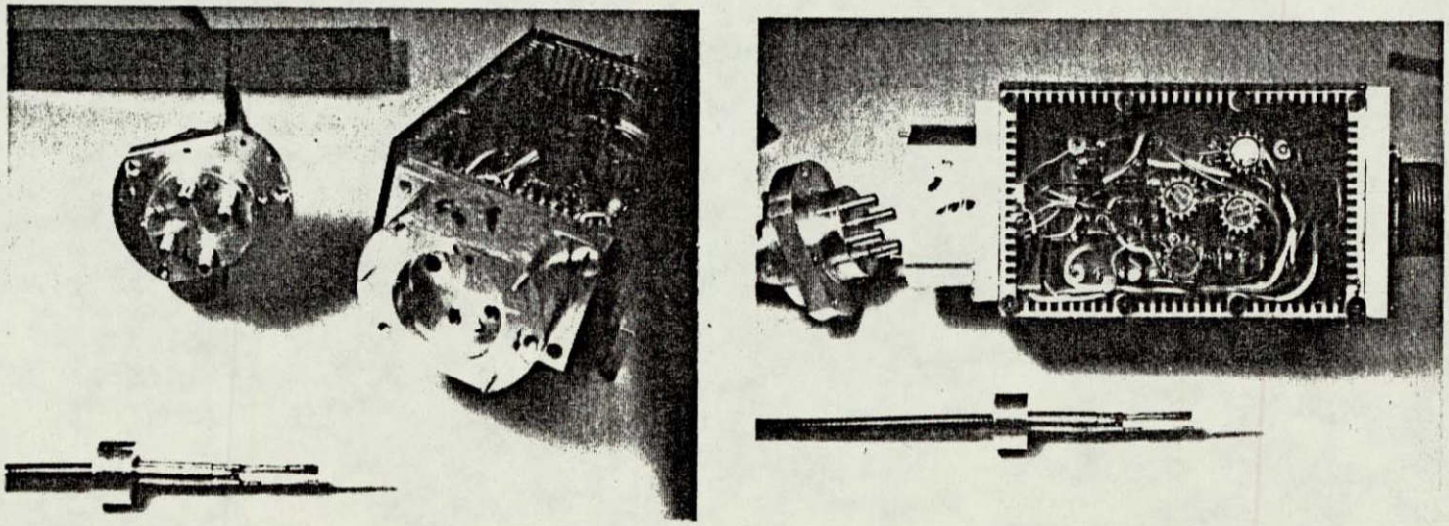

Fig. 16 Two Views of Opto-Electronic Package, Fiber Optic Connector, and Probe Pair (During Assembly)

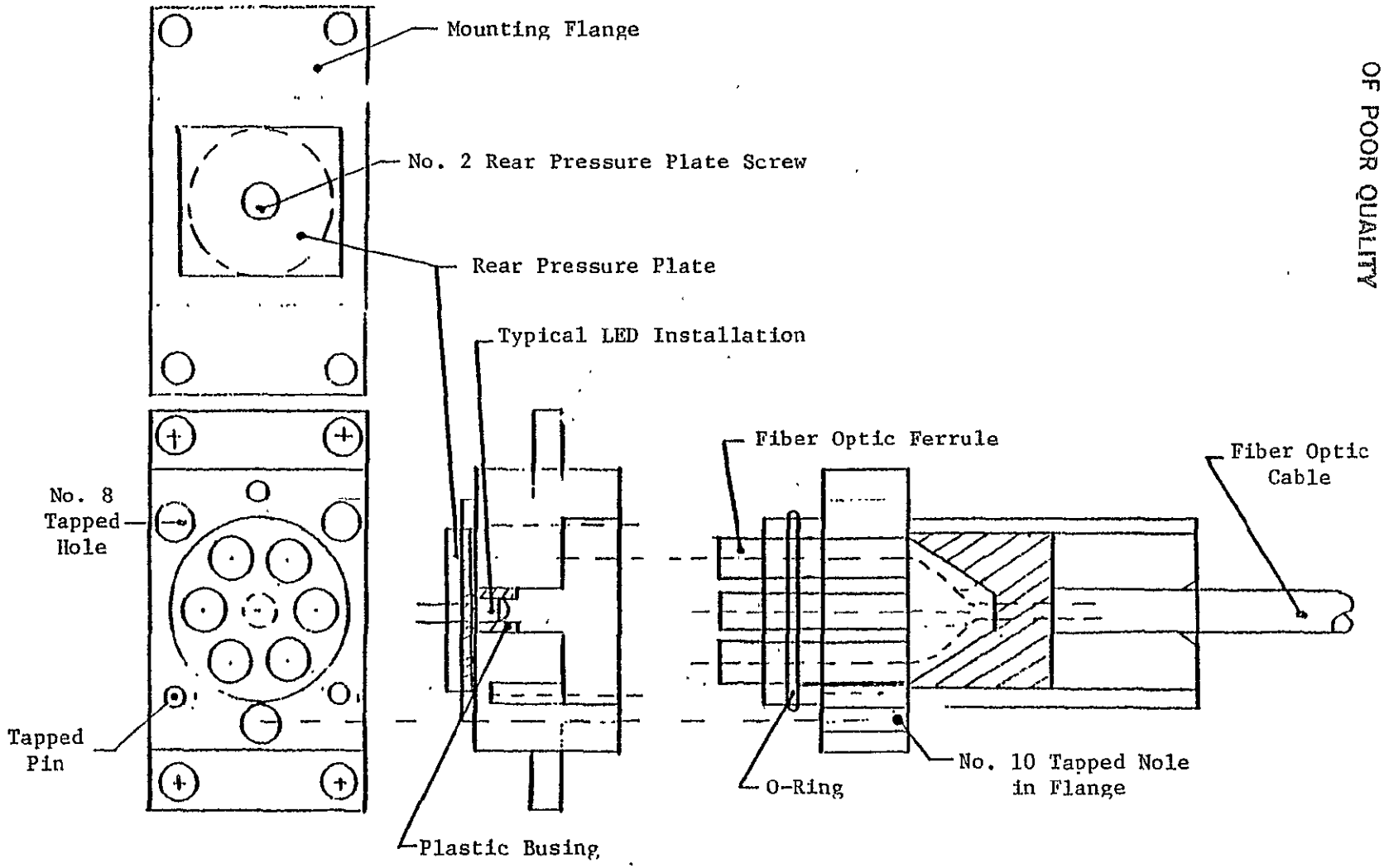

Fig. 18 Fiber Optic Pressure Transducer Lamp Block Concept

3.0 FUNCTIONAL TESTING OF BREADBOARD SYSTEM

The functional testing of the breadboard components and system included the following:

- Test of the breadboard electronics, using standard fiber optics probes
- Test of the fiber optic probes during transducer fabrication, using a commercial fiber optic readout (MTI-KD45)
- Test and pressure calibration of the completed system.

The purpose of these tests was to:

- Identify and eliminate fabrication errors
- Assure correct functioning of all subassemblies
- Qualify system before delivery.

Some of the system data taken during cryogenic and hot tests is reported in Appendix 7, Table A7-1. The displacement calibration of the pressure sensing fiber optic probe is given in Figure A7-9. Figure 19 shows the slope of the system response to pressure without linearization or temperature compensation. It also shows the effectiveness of the linearization in the tabulation of system output, including linearization. Appendix 10 summarizes the pressure calibration test data recorded at NASA-MSFC.

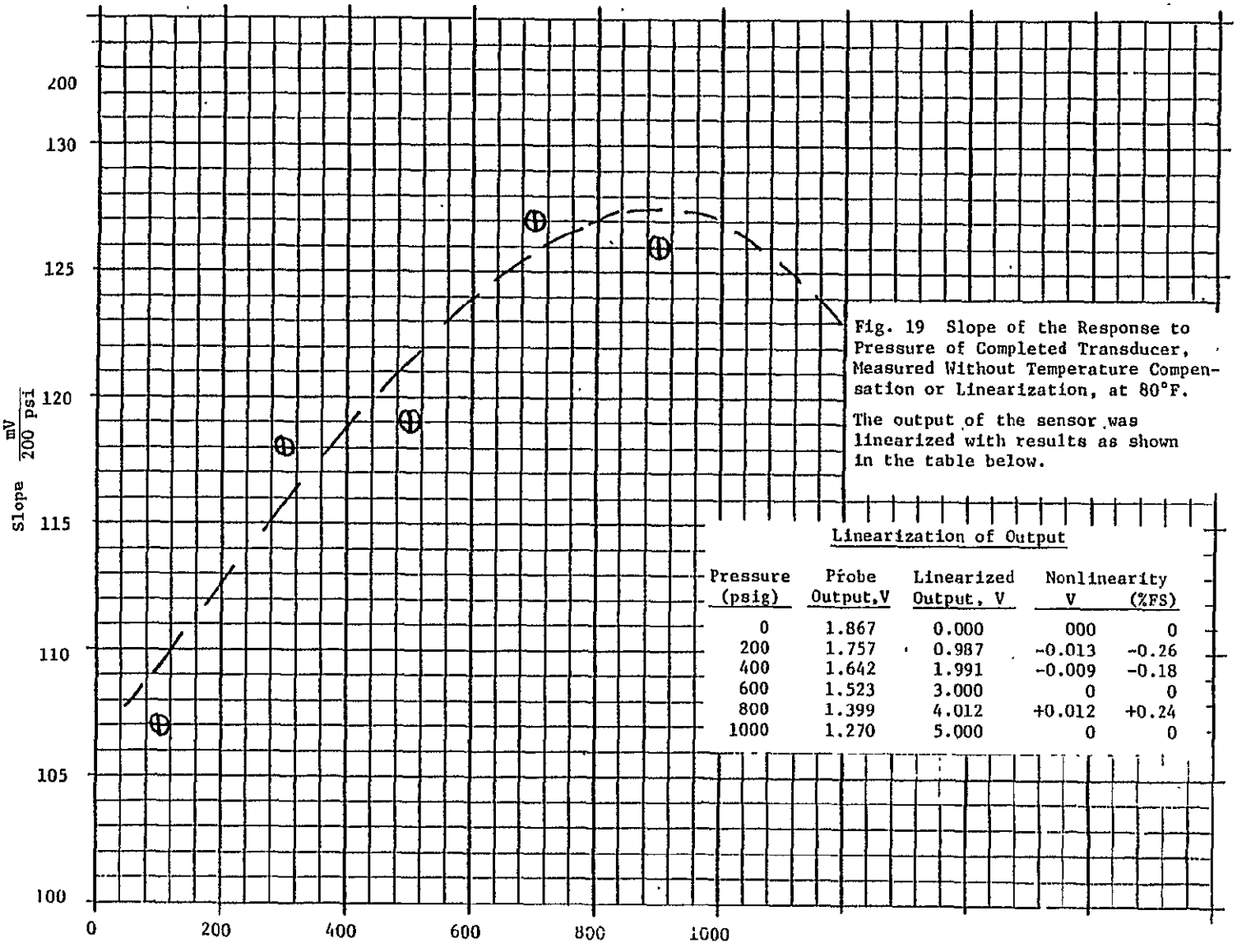

Fig. 19 Slope of the Response to Pressure of Completed Transducer, Measured Without Temperature Compensation or Linearization, at 80°F.

The output of the sensor was linearized with results as shown in the table below.

Linearization of Output

Pressure (psig)	Probe Output, V	Linearized Output, V	Nonlinearity V	Nonlinearity (%FS)
0	1.867	0.000	000	0
200	1.757	0.987	-0.013	-0.26
400	1.642	1.991	-0.009	-0.18
600	1.523	3.000	0	0
800	1.399	4.012	+0.012	+0.24
1000	1.270	5.000	0	0

4.0 PRINCIPAL PROBLEMS AND RECOMMENDATIONS

The system performance obtained with the breadboard is very encouraging, but a number of areas require more development work before a prototype system can be made. Some of the problem areas, listed in the order of importance, are the following:

1. Thermal hysteresis of the fiber optic bundle termination
2. Condensation of air inside the transducer
3. Response of fiber optic temperature sensor
4. Effect of bending of fiber bundle on cross talk between the illuminating and sensing fibers
5. Effect of temperature on breadboard electronics zero and gain
6. Ruggedness of cable sheath

1. Thermal Hysteresis

Items 1 and 2 are the most critical problems. Both will require considerable effort before solutions are found. The very wide operating temperature range and the nonlinear effects on material properties of the cryogenic operating temperatures create difficult problems. In the breadboard transducer design, no special effort was made to avoid thermal hysteresis, because it had not been observed in the thermal tests made earlier in the program. The probe design used the shortest possible sheath length for the fiber bundle at the sensing end, but no special provisions were made to lock the bundle to the sheath. There are concepts that will enhance the bond between the bundle and the sheath. Also, resins other than the one used in the breadboard probe may give better performance.

2. Condensation of Air

The breadboard transducer is not hermetically sealed. The sealing problem is similar to the bonding problem. To obtain an effective seal around 500 to 1000 glass fibers within a short length is difficult. The area of the seal cannot be exposed to bending stresses because fiber breakage would result. Thus, the use of a seal would substantially add to the present length of the transducer.

The potting agent, used to make the probes will provide a seal around the fibers, but it cannot be expected to be hermetic. In the design in Figure 2, if the radial gap between parts 3 and 4 were sealed, the sensing gap would be protected against condensation for a limited time. The temperature sensor is, at present, vented to the atmosphere inside the transducer to avoid a pressure differential when the temperature changes. If the vent were omitted, the temperature sensor would also be protected from condensation for some time.

The leakage rate through the fiber optic probes must be established experimentally. The permissible leakage rate would depend upon the internal surface area of the cavity into which the oxygen and nitrogen flow, and the permissible fluid film thickness as fluid forms on the wall and in the gap. As the transducer cools down, the diaphragm will be coldest, because it is in contact with the cryogenic liquid. Therefore the diaphragm will attract the oxygen and later the nitrogen, as the temperature drops below the boiling points of those gasses. The oxygen and nitrogen may leak through the seal in gaseous or liquid form, depending upon the temperature at the ambient side of the seal. The mass leakage rate may be independent of whether the liquids or the gases pass through the seal. To answer these questions, an experimental evaluation of seal leakage must be made on a realistic physical and operational model of the transducer. For a film thickness of 0.001 in., the total liquid volume on the walls of the diaphragm cavity is on the order of 0.01 cm^3 ($\simeq$ 10 standard cc of gaseous oxygen). If this volume had leaked into the cavity in eight hours, the leakage rate would have been 10 $cm^3/30{,}000$ sec = 3×10^{-4} cc/sec. The leakage rate through a hermetic seal using helium is usually specified at rates that are three to four decades lower than the number found above.* It seems, therefore, that the sealing quality needed to avoid condensation can be several decades poorer than what is usual for hermetic instrument envelopes.

The cavity volume of the temperature sensor is very small, and the permissible rate would be much lower than for the diaphragm cavity. However, the

---

*These rates are based on the level of resolution of commercial leak detectors (i.e., helium mass spectrometers).

temperature probe is not likely to reach the liquid oxygen temperature, as it is about one-half inch removed from the diaphragm. In addition to oxygen, water vapor and CO_2 could migrate to the gaps, but their partial pressures are very low, and hence flow rates would be two to three decades below that of oxygen.

The items listed as numbers 3 through 6 all must be looked at, but they do not represent difficult development problems.

3. Temperature Response of Probe

The fiber optic temperature sensor will have a nonlinear response at cryogenic temperatures, which must be matched to the nonlinear zero drift of the pressure sensing fiber probe. No detailed experiments were made to obtain these two responses to temperature, because of the hysteresis and non-repeatability present in the breadboard transducer. The temperature compensation of the breadboard system removes 70-80% of the temperature-induced drift that otherwise would occur in the output. It is probably possible to improve the compensation effectiveness.

4. Effect of Bending of Fiber Bundle on Response

Bending of the fiber bundle caused a 1 to 2% shift. This shift disappeared immediately when the cable was allowed to resume its original shape. To eliminate this cross talk, the illuminating fibers must be separated optically from the receiving fibers. This will require a slightly larger cable sheath than used in the breadboard.

5. Temperature Effects on Electronics

The temperature effect on the breadboard electronics is expected to be very low, but experimental confirmation must be obtained.

6. Cable Sheath

The present cable is not suitable for cryogenic use, and it lacks the necessary armor. It must be redesigned to meet prototype requirements for strength and flexibility. Fiber breakage, which can occur when the fibers are buckled in the sheath, must be avoided through proper design and fabrication. Appendix 5 discusses the effect of fiber breakage on probe output.

APPENDIX 1

DESIGN METHODOLOGY FOR DIAPHRAGM TYPE PRESSURE TRANSDUCERS*

In the design of a diaphragm type pressure transducer, a compromise is sought between key items in the performance specifications and the physical and performance limitations set by the type of transducer design that is used.

To aid in the trade-off between performance and design parameters, their relationships are given in a design table. The table is constructed in the following paragraphs. The equations for stress, deflection and resonant frequency of a clamped diaphragm under uniform pressure are as follows (see Ref. 1-1, 1-2):

Maximum bending stress (at edge) $$\sigma = K_1 q \left(\frac{a}{t}\right)^2 \qquad 1\text{-}1$$

Deflection $$w = K_2 q \frac{a^4}{t^3} \qquad 1\text{-}2$$

Resonant Frequency $$f = K_3 \frac{t}{a^2} \qquad 1\text{-}3$$

Eliminating q between (1-1) and (1-2) gives: $$\frac{\sigma}{w} = \frac{K_1}{K_2} \frac{t}{a^2} \qquad 1\text{-}4$$

Eliminating $(\frac{t}{a^2})$ between (1-3) and (1-4) gives: $$f = \frac{K_2 K_3}{K_1} \frac{\sigma}{w} \qquad 1\text{-}5$$

Eliminating t between Eq. (1-1) and Eq. (1-2) results in: $$q = \frac{K_2^2}{K_1^3} \sigma^3 \frac{a^2}{w} \qquad 1\text{-}6$$

Rewriting Eq. (1-4) to isolate t gives: $$t = \frac{K_2}{K_1} \sigma \frac{a^2}{w} \qquad 1\text{-}7$$

Ref. 1-1 Timoshenko, Theory of Plates and Shells, 2nd Edition, Pg. 55, Eq. (e), p. 56, Eq. (f).

Ref. 1-2 J.P. Den Hartog, Mechanical Vibrations, 2nd Edition, 6th Impr. Pg. 432, Eq. 25.

*The material in this Appendix was taken from MTI 75TR57 LMFBR Sodium Pressure Sensor Study, L. Hoogenboom, Argonne National Laboratory, Subcontract 31-109-38-3119, July 1975. Therefore, the cases used in illustrations of the use of the design method, are only concerned with very high temperature transducers. The design method can be extended to any type of diaphragm based pressure sensor, whether for high temperature or cryogenic service.

Symbols used in these formulas are:

a = diaphragm radius

t = diaphragm thickness

q = pressure

$K_1 = \frac{3}{4}$

$K_2 = \frac{3}{16} \frac{1 - \nu^2}{E}$

$K_3 = .47 \sqrt{\frac{E}{(1 - \nu^2)\rho}}$

E = modulus of elasticity

ρ = density

ν = Poisson's ratio

The equations 1-1, 1-2, and 1-3 contain 6 parameters (σ, q, a, t, w, f). The modulus of elasticity and density appearing in the ratio $\frac{E}{\rho}$ are not included as variables.

Of the six parameters, three must be chosen and then the other three are found using equations 1-1, 1-2, and 1-3.

The equations can be used to judge the effect of a parameter change on transducer performance or specifications. Or inversely, if a change in specifications is desired, the formulas show how the change can be obtained. As there is generally a compromise in transducer dimensions and performance, the equations show in a convenient form how the best balance can be struck. Some examples of the use of the equations are given in Table 1-1. In the table, "x" indicates the parameter(s) that stay fixed. The "K" indicates the factor by which the other parameters must change to let the parameters marked "x" remain constant. The first line in the table shows an example where the diameter is changed by a factor K and how this change affects thickness t and pressure q for fixed σ, w and f. The next lines only show the multipliers without the symbols for the parameters involved. Design data on the existing MTI transducer design (using 347 SS) are given on line 12. The table is incomplete because f is not treated as a design input parameter. The reason is, that f most likely will satisfy the transducer specifications anyway, and carrying f as an input parameter would make the table considerably longer and less easy to use.

By using the formulas, the design can, for example, be adapted to other pressure ranges within the same temperature range. Or if a thicker diaphragm is desired, the increase in diameter for fixed deflection, stress and pressure range can be calculated. Certain design inputs related to material properties are, of course, needed. Also consideration of sources of noise and drift will enter in the choice of overall dimensions. For example, the minimum full scale deflection for a 1/2" diameter transducer should be at least 500 μin. if a Wayne-Kerr capacitance proximity probe is used to measure the deflection. The reason is that the dimensions of the proximity probe for a 500 μin. range are the smallest that can be made with sufficient accuracy. Also, the axial thermal drift in the capacitance proximity probe structure over a 1000°F range is in the order of 50 μin. For a probe with 500 μin. range, thermal drift is 10% of full scale, which is acceptable. It is desirable to use a larger range probe with a smaller percentage thermal drift, even though the thermal zero drift is very reproducible.

PRESSURE AND TEMPERATURE LIMITS OF EXISTING DESIGN, USING 347 SS

The present design was made for application to the film pressure measurement (120 psi at 1000°F) in sodium bearings. Minimum size (diameter) was desired. Therefore, a 1/2 inch diameter diaphragm was chosen. For the pressure range desired and the stress limit imposed by the use of 347 SS, the resulting deflection and probe range were very small (.0005 inch at 120 psi). A larger deflection range is desirable, and as will appear below, is possible for a larger diameter diaphragm with higher permissible stress.

The diaphragm design data presented above are used here to determine the pressure limit of the present proven design. The limit is derived for the following inputs:

1. diaphragm diameter range

   $.430 < 2a < .860$ inch

   (maximum transducer diameter is about 1.0 inch for 2a = .860 inch).

2. diaphragm thickness limits

   $.010 \text{ inch} < t < .2a$

3. $\sigma_{max} = 10{,}000$ psi

4. maximum temperature is 1200°F

5. deflection .0003 inch.

The maximum pressure for which this design is adequate within the limits set above is determined by converting the numbers in line 12 of the table to those for a design with maximum q. Inspecting the table, it can be seen at line 2 that for a fixed stress (σ = 10 kpsi) and fixed deflection (w = .0003) inch) the q can be increased by a factor of K^2 if the diameter is increased by a factor of K, and the thickness by a factor of K^2. The maximum increase in diameter above that listed in line 12 and allowed within the limits for 2a is a factor of:

$$K = \frac{.860}{.430} = 2.0$$

The maximum pressure range is then found by multiplying the q listed in line 12 by K^2:

$$q_{max} = (2)^2 \times 75 = \underline{300 \text{ psi}}$$

The thickness of this diapragm will be:

$$t = (2)^2 \times .016 = .064 \text{ inch } (< \tfrac{1}{2} a = .215 \text{ inch})$$

These dimensions are entered on line 13 of the table. It appears from this calculation that the present design can serve the pressure range of 300 psi given in the specifications on page 1.

EXPANSION OF PRESSURE AND TEMPERATURE LIMITS OF THE EXISTING DESIGN

Inspecting the diaphragm design table, it can be seen that to obtain pressure over-range, the most effective change is that of the allowable stress (and with it the thickness) as shown in line 6. This will require the use of a different diaphragm alloy. The choice of diaphragm material is limited by the thermal expansion dictated by the use of 304 SS in the transducer body and proximity probe. There is no alloy that matches 304 SS within $10^{-6}/^{\circ}F$, which is the value required to avoid excessive weld or operating stresses, and thermal zero shift. It may, therefore, become necessary to construct the transducer body and the integral cable from another alloy than the customary 304 SS. For example, a combination of an Inconel 600 proximity probe and transducer body with an Inconel X-750 diaphragm would have acceptable thermal compatibility.

If this material is used, the permissable stress would be considerably higher. It would be typically 18 kpsi at 1400°F, 35 kpsi at 1300°F and 55 kpsi at 1200°F.

By introducing a stronger material, the higher permissible stress level can be traded against two other parameters:

1. Pressure range q, by increasing it from 300 to 500 psi to obtain over-range.

2. Full scale deflection, by increasing it from .0003 inch to .003 inch.

First, line 9 in Table 1-1 is used to increase the pressure range of line 13 by a factor of 1.67. The result is shown in line 14. The stress level is increased to only 16.7 kpsi, which allows safe operation at up to 1400°F. Then line 10 is used to increase the deflection of line 14 by a factor of 10. The result is shown in line 15. The stress level is now up to 55 kpsi, the maximum permissible at 1200°F.

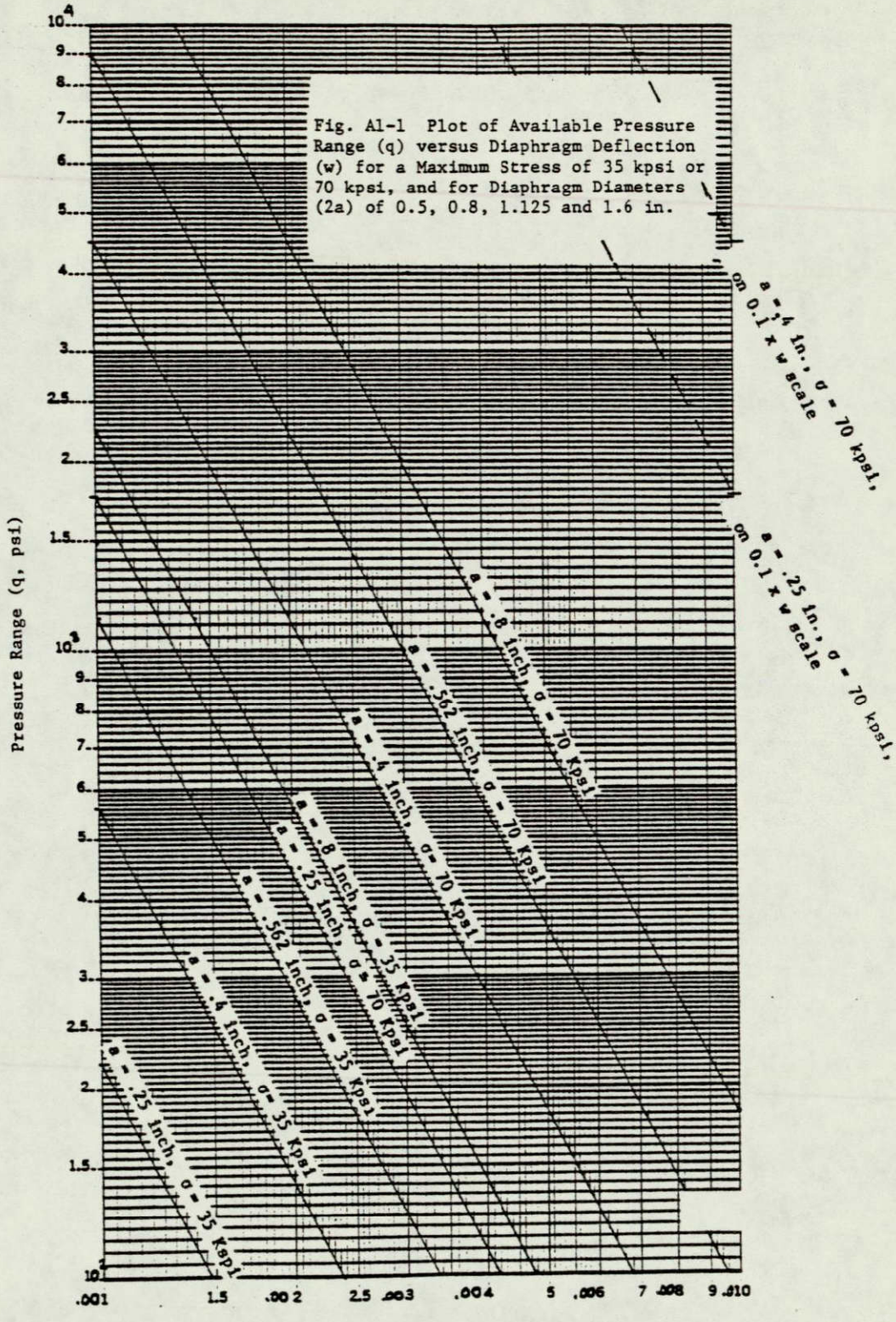

Fig. A1-1 Plot of Available Pressure Range (q) versus Diaphragm Deflection (w) for a Maximum Stress of 35 kpsi or 70 kpsi, and for Diaphragm Diameters (2a) of 0.5, 0.8, 1.125 and 1.6 in.

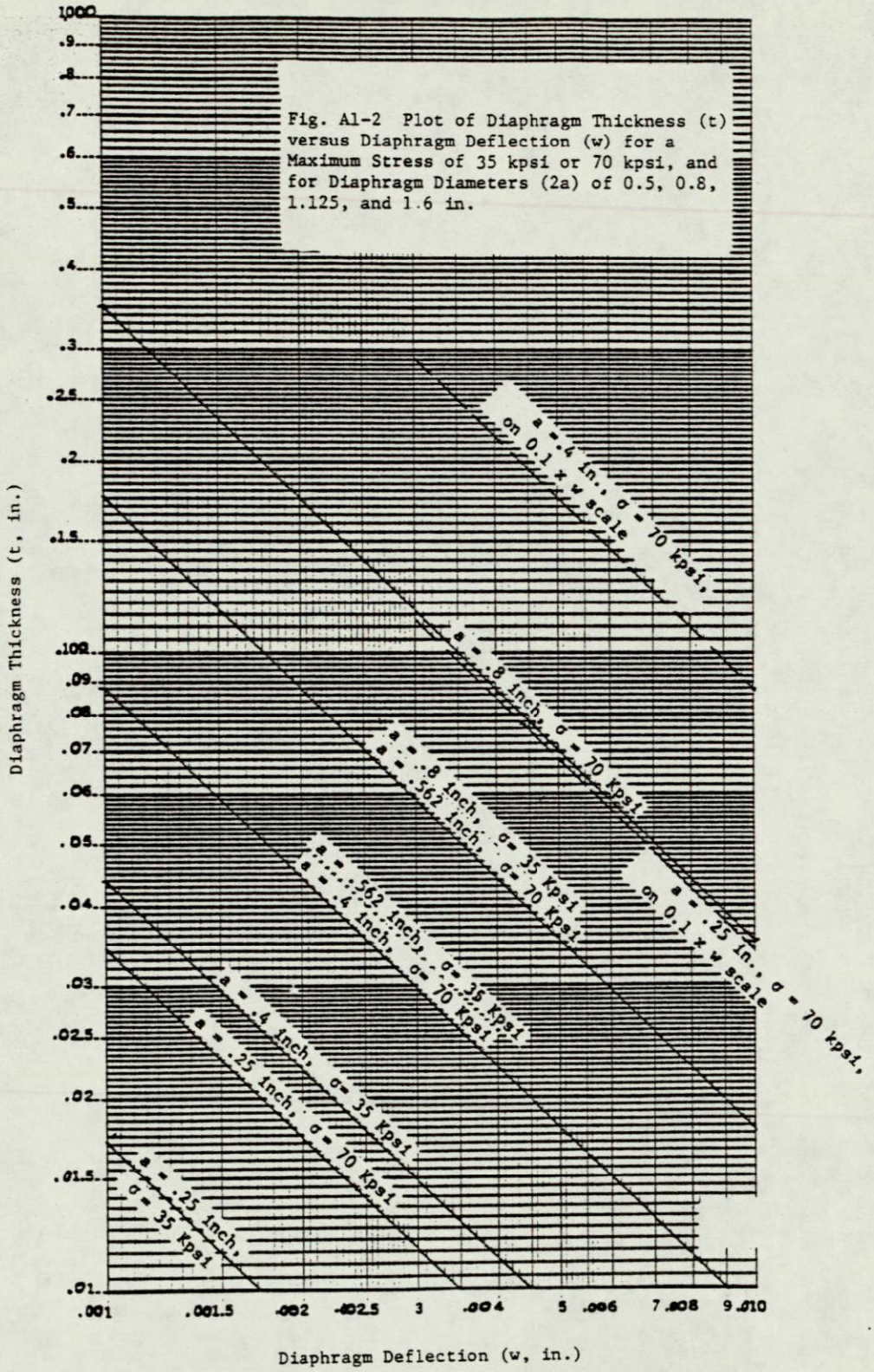

Fig. A1-2 Plot of Diaphragm Thickness (t) versus Diaphragm Deflection (w) for a Maximum Stress of 35 kpsi or 70 kpsi, and for Diaphragm Diameters (2a) of 0.5, 0.8, 1.125, and 1.6 in.

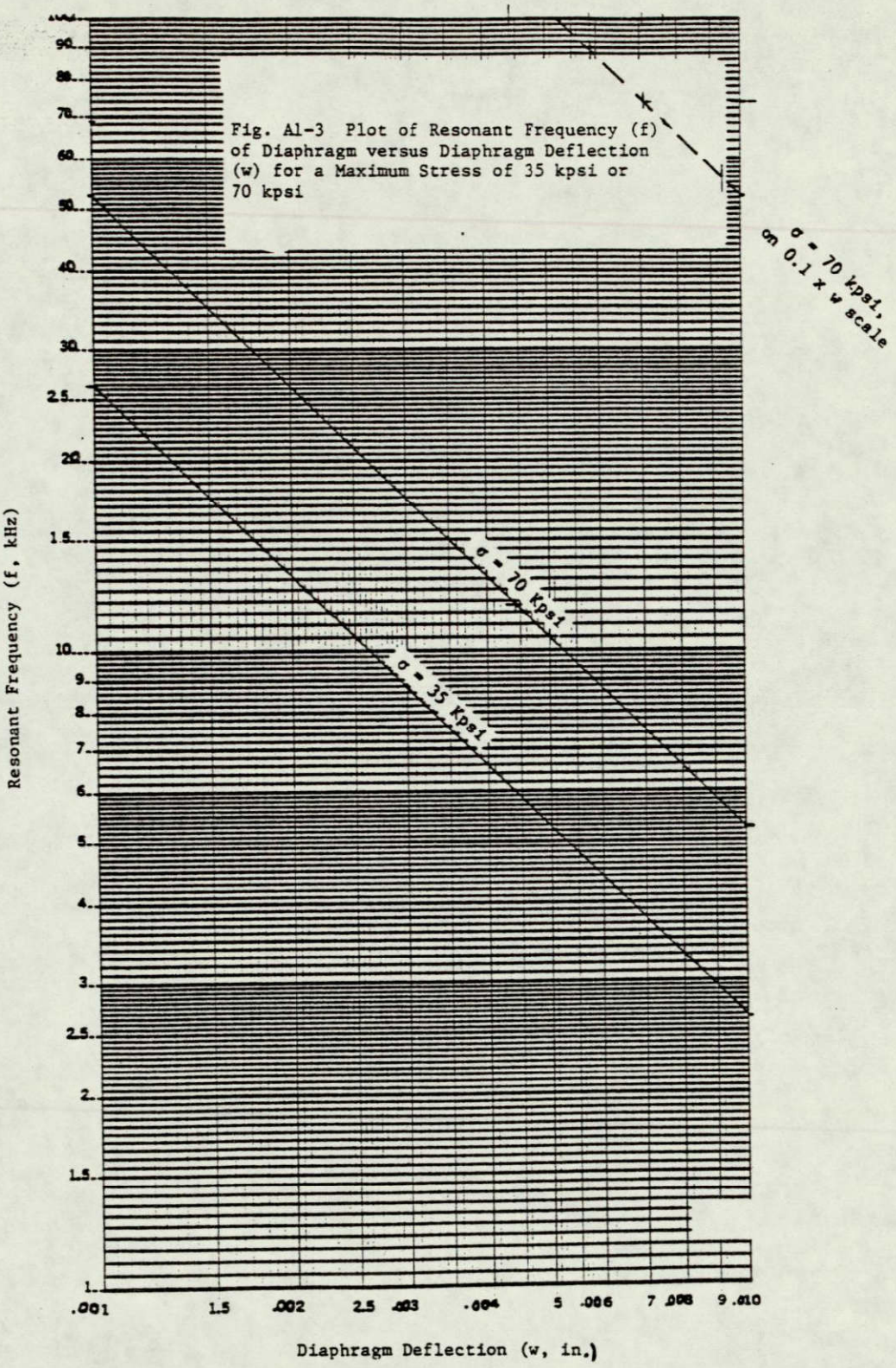

Fig. A1-3 Plot of Resonant Frequency (f) of Diaphragm versus Diaphragm Deflection (w) for a Maximum Stress of 35 kpsi or 70 kpsi

APPENDIX 2

LINEARITY AND LINEAR RANGE

Summary:

The non-linearity limit given in the pressure sensor specifications is converted into an allowable slope variation of the Fotonic Sensor. The actual performance of a single .065R probe is such that it is judged unacceptable for pressure sensor service.

A set of sensors in push-pull would eliminate or soften the limitation, but would do so only if the mean gap for each of the sensors were controlled very rigidly.

In general, the non-linear component of a sensor response can be expressed as an exponential of the input variable. In the following a rigorous definition of linear range and linearity are given, based on a sensor response as given in equations (2-1) and (2-2):

$$E_s(x) = K_1 x + K_2 x^2 \qquad (2\text{-}1)$$

$$\frac{\partial E_s}{\partial x} = K_1 + 2K_2 x \qquad (2\text{-}2)$$

If the displacement range (x_1) and the maximum deviation $\Delta E(x_p)$ of $E_s(x)$ from a straight line through E=0 and $E = E_s(x_1)$ are given, the allowable non-linear content (K_2x^2) and mean slope variation (K_2x_1) can be calculated, as is done in the following. Figures A2-1 and A2-2 illustrate the mathematical approach. The straight line connecting E=0 and $E = E_s(x_1)$ is given by:

$$E_\ell(x) = \frac{E_s(x_1)}{x_1} x \qquad (2\text{-}3)$$

where: $$E_s(x_1) = K_1 x_1 + K_2 x_1^2 \qquad (2\text{-}2a)$$

The maximum deviation $\Delta E(x_p)$ is found by calculating the extreme value of:

$$\Delta E(x) = E_\ell - E_s = \left[\frac{E_s(x_1)}{x_1} - K_1\right] x - K_2 x^2 \qquad (2\text{-}4)$$

Substituting eq(2-2a) in eq(2-4) results in:

$$\Delta E(x) = K_2 x(x_1 - x) \qquad (2\text{-}4a)$$

The maximum value $\Delta E(x_p)$ is found for $x=x_p$ and x_p follows from:

$$\frac{\partial \Delta E}{\partial x} = K_2(x_1 - 2x_p) = 0$$

$$x_p = \tfrac{1}{2}x_1$$

The maximum value for $\Delta E(x)$:

$$\Delta E(x_p) = \frac{K_2}{4} x_1^2$$

If the maximum deviation is given as a fraction of full scale $\alpha E_s(x_1)$, then:

$$\frac{\Delta E(x_p)}{E_s(x_1)} = \frac{K_2}{4} x_1^2 \frac{1}{K_1 x_1 + K_2 x_1^2} \leq \alpha \qquad (2\text{-}5)$$

The maximum non-linear content in eq(2-2) (as a fraction of the linear content) is formed by rewriting eq(2-5), separating K_1 and K_2:

$$\text{Non linear slope fraction} = \frac{K_2 x_1}{K_1} \leq \frac{\alpha}{0.25 - \alpha} \approx 4\alpha \qquad (2\text{-}6)$$

If the response curve has an inflection point at $x = 1/2\ x_1$, then the same procedure described above is followed except that only one half of the response curve is considered at a time, as is illustrated in figures A2-3 and A2-4. In this instance the slope curve has a roof shape. The permissable slope variation in figure A2-3 for a given maximum deviation $\Delta E(xp)$ is derived as follows:

$$\Delta E(x) = \frac{E_s(x_1)}{x_1} x - E_s(x) = (K_1 + \tfrac{1}{2}K_2 x_1)x - K_1 x - K_2 x^2 = K_2(\tfrac{1}{2}x_1 - x)x$$

$$\Delta E(x) = K_2(\tfrac{1}{2}x_1 - x)x \qquad (2\text{-}7)$$

The peak value for eq(2-7) occurs for a value $x = x_p$ found from:

$$\frac{\partial \Delta E}{\partial x} = K_2(\tfrac{1}{2}x_1 - 2x_p) = 0$$

$$x_p = 1/4\ x_1$$

The maximum deviation is:

$$\Delta E(x_p) = \frac{1}{16} K_2 x_1^2$$

Expressed as a fraction of full scale voltage $E_s(x_1)$ (see formula at top of figure A2-3):

$$\frac{E(x_p)}{E_s(x_1)} = \frac{1}{16} K_2 x_1^2 \frac{1}{(K_1 + \frac{1}{2}K_2 x_1)x_1} \leq \alpha \qquad (2\text{-}8)$$

Separating K_1 and K_2 in eq(2-8) gives the non-linear fraction in the slope (in the interval $0 \quad x \quad \frac{1}{2}x_1$):

$$\text{non-linear fraction in slope} = \frac{1}{2} \frac{K_2 x_1}{K_1} \leq \frac{\alpha}{.125 - \alpha} \cong 8\alpha \qquad (2\text{-}9)$$

Equations (2-6) and (2-9) show the allowable slope excursion for the two response models used. The target specification for the pressure sensor shows a non-linearity of 0.15% of F.S. ($\alpha = .0015$). The allowable slope excursions are .6% and 1.2% respectively. To assure that the response curve meets this target, the measurement of response slope of the proximity sensor and pressure sensor must be made with about ten times greater accuracy (about 0.1% of mean slope).

Linearity of Fotonic Sensor:

The Fotonic Sensor response peaks at a gap of about .013 inch, and has a peak slope at about .0035 inch gap. The peak slope occurs over a very narrow range, actually at only one point of the response curve (an inflection point), around which the slope varies symmetrically, similar to the diagram in Figure A2-4.

The range over which the .065R probe has a symmetric slope variation of less than ±1.2% is roughly .0006 inch, at a stand-off of .0035 inch. If the stand-off is varied by a small amount from .0035 inch, then the slope variation becomes anti-symmetric and steeper, and the displacement range over which the slope variation is less than ±.6% is even much smaller than .0006 inch. The very narrow range, and the sensitivity of slope to the actual gap that is evident, make the regular Fontonic Sensor probe unsuitable for the pressure sensor application if it is used single sided. If two sensors could be used in push-pull, the linearization obtainable would certainly help. The fact remains however that the precise mean gap for each sensor would have to be set and controlled with very high precision to assure that both sensors operate with exactly the same non-linear content (of opposed sign). This is so because of the steep slope gradients of the random probes on the front slope. If instead the back slope is used, the non-linear content is much reduced, but signal levels are also down by a factor of 15-20, and thus the zero drift (due to electronics limitations) may become a performance limiting factor.

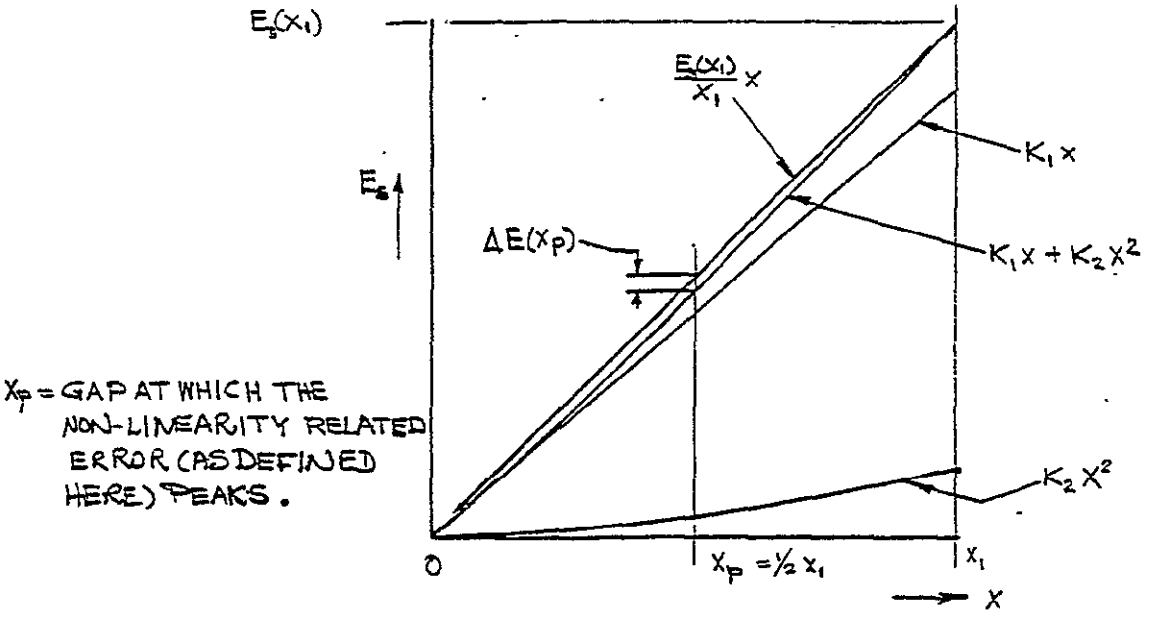

Fig. A2-1 Linear and Nonlinear Components of Sensor Response

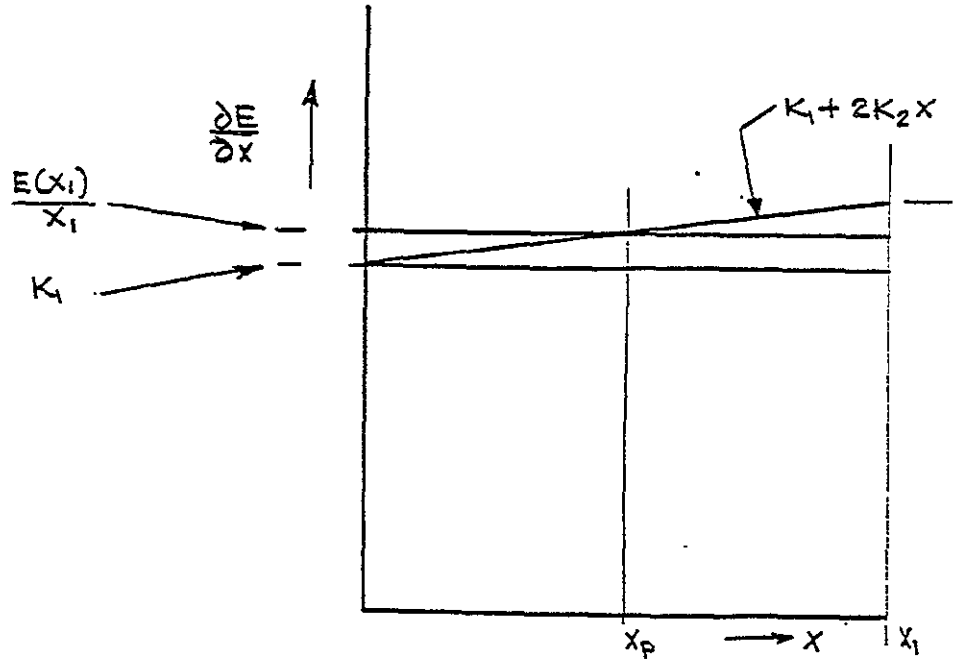

Fig. A2-2 Slope of Linear and Nonlinear Components of Sensor Response

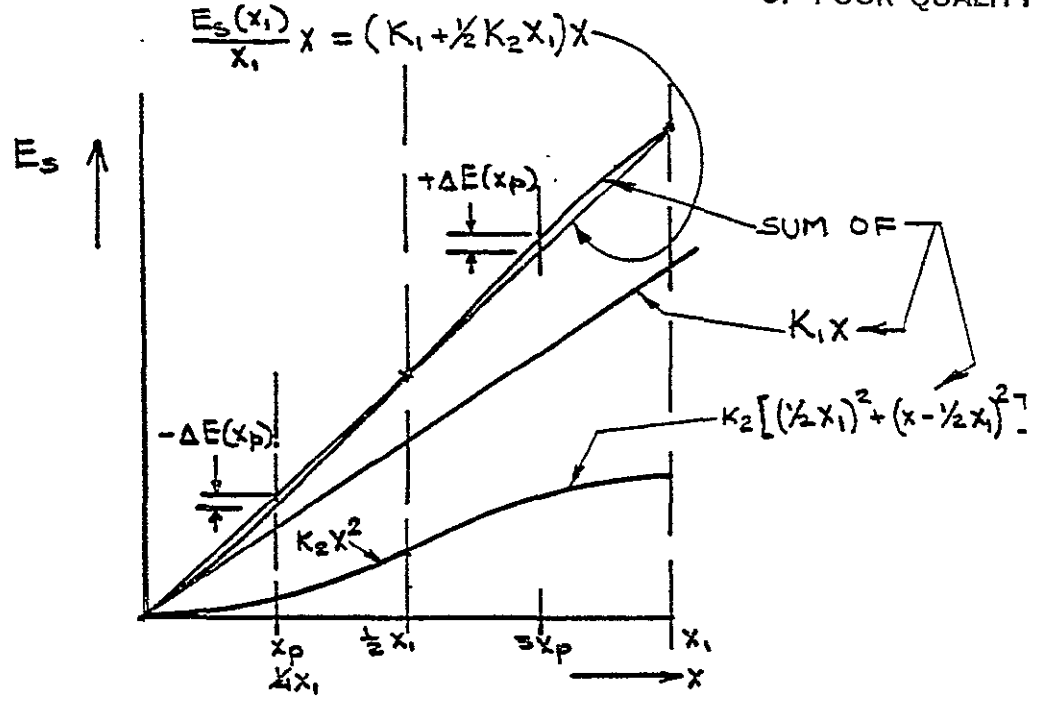

Fig. A2-3 Linear and Nonlinear Components of Sensor Response with Inflection Point at Mid-Scale

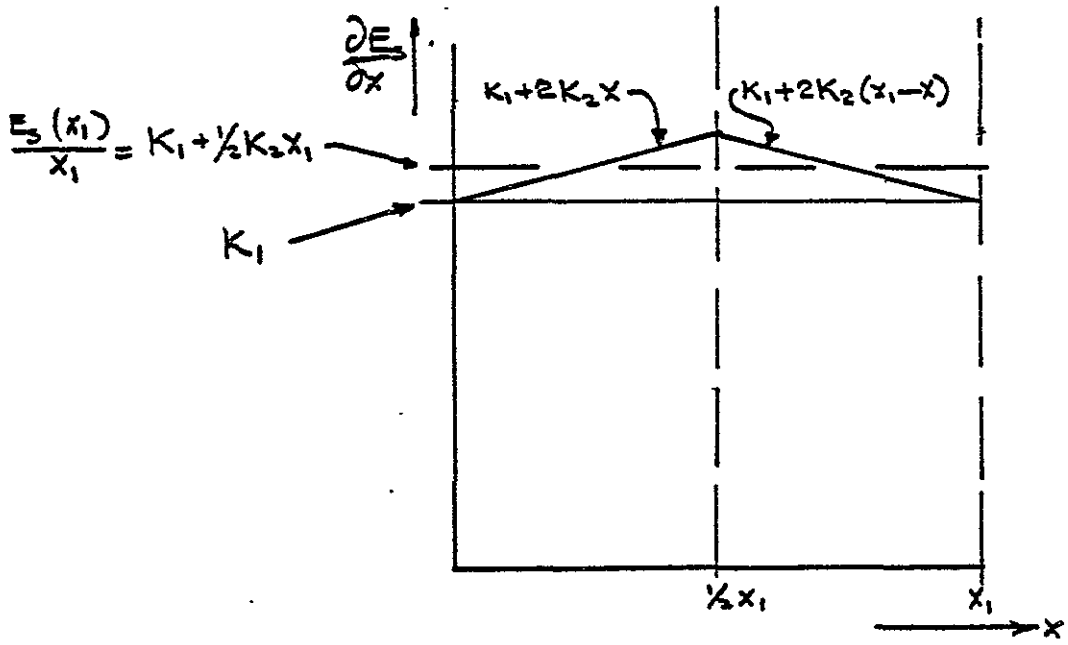

Fig. A2-4 Slope of Linear and Nonlinear Components of Sensor Response with Inflection Point Mid-Scale

APPENDIX 3

PRECISE MEASUREMENT OF SLOPE OF SENSOR RESPONSE

To qualify the linearity of the developmental sensor (first the proximity sensor and then the completed pressure sensor) requires that precise incremental calibrations are made. If the slope of the proximity sensor response is to be measured with a resolution of ± .1% to ± .2%, then the resolution of the calibrating equipment must be at least double that (.05% to .1%). If increments of 10% of full scale are used, the calibration data must have an accuracy of .005% to .01% of full scale.

To obtain data with this level of resolution is a formidable problem. In the following the actually available levels of measurement accuracy are examined. Two basically different calibration methods are explored. One method consists of changing the input (gap) in precise steps, and by measuring the resulting output voltage change. The other method uses a continually vibrating target, which results in a continous alternating signal from the probe, which is converted to a steady state signal by a precision phase sensitive detector. The output of the phase sensitive detector is proportional to the slope of the response curve. By integrating the slope curve, the gap response can be obtained. Integration of the slope data can be done numerically or after obtaining an analytical expression for the slope curve.

Errors in the first (stepped) calibration method are over a period of 5 - 10 minutes:

Gap Error (accuracy)

* With standard large (4" diameter) micrometer (for example Brown & Sharpe No. 296-10)	± .000050/over 1" range ± .000004/over 1/8" range*
* With Mitutoyo model 521-106	± .000010/over .050 range
* Fixture effects, thermal, mechanical (estimated)	± .000005/over ± 1° F or due to ± 1 g vibration
* Probe effects, thermal, mechanical	± .000005/ ± 1° F, ± 1 g

Electrical Error:

* Digital voltmeter (0.1% to .02%)	± .002 volt (10 volt range)
* Instrument error (Fotonic Sensor) ± 10 volt range, estimated.	± .001 volt/ 1° F
* As mentioned in a phone conversation by Brown and Sharpe	

Errors in the slope based calibration over a period of 15-60 seconds are:

Gap Error:

* Dither motion amplitude control, closed loop, for dither motion less than .001 inch	± (0.1% to .02%)
* Detector error	< ± .02%
* Digital voltmeter for ± 10 volt range	± .002 volt
* Plotter error (linearity and dead-band)	± .2%
* Plotter dead-band (estimated)	± .02 inch
* Resolution of plotter used with 100% off-set and expanded scale	± .1%

From the listings given above, the overall accuracy of the two methods can be evaluated.

Stepped Calibration Method Error:

The gap error (dx) is ± .00002 inch

The signal error (dE) is ±.02% of full scale.

Dithered Calibration Method (Slope Based Method) Error:

Input motion error	± (0.1 to .02) % of amplitude
Output Voltage	± .02% of F.S. (for digital voltmeter)
Output Voltage	± .1% of F.S. (for plotter)

Using the analysis given in Figure A3-1, the slope error with the stepped calibration method is:

$$\varepsilon = \pm \frac{2}{\alpha} \left(\frac{dE}{E_1} + \frac{dx}{x_1}\right)$$

Where E_1 and x_1 are full scale values of signal output and gap change.

Following are some numerical examples using the errors for gap (x) and signal (E) as given above. Figure A3-2 illustrates the calculations geometrically. The numbers used are:

- Full scale gap change (x_1) is .001 inch and .005 inch.
- Full scale voltage: E_1 = 10 volts
- The gap error dx = $\pm$ 20 x 10^{-6} inch.
- The voltage error dE = $\pm$ .02% of F.S.
- Gap increments: α = 0.1 (i.e., 10% of full scale)

With these, the slope error becomes:

$$\frac{2}{0.1}\left(.0002 + \frac{20 \times 10^{-6}}{.005}\right) < \varepsilon < \frac{2}{0.1}\left(.0002 + \frac{20 \times 10^{-6}}{.001}\right)$$

$$.084 < \varepsilon < .404$$

The slope errors range between 8% for a gap range of .005 inch to 40% for a gap range of .001 inch. If the step size is increased to 20% of F.S., the error is cut in half, but the non-linearity data is less precise.

If the dithered calibration method is used, the slope error is equal to the sum of the motion error and read-out error, ranging between a total of $\pm$ .02 to $\pm$ .2%. When the dithered method is used, the static gap measurement accuracy can be relatively poor without affecting results. An essential requirement when using the dithered target is that the dither excursion is kept constant, preferably in a servo loop. Figures A3-3 and A3-4 illustrate the direct slope measurement method that was used to obtain the slope data described elsewhere in this report. See Figure 4.

Integration of Slope Data:

When directly taken slope data, with a resolution/accuracy of .01% to 0.1% is available, and if a good fit ($\pm$ .02% to $\pm$ 0.2%) can be obtained of this data to a simple linear equation, integration of the slope equation will result in a response equation of the same accuracy. That is, if the slope is accurate to $\pm$ 0.2%, then the maximum error is $\pm$ 0.2% of reading.

When the response curve is obtained through the customary stepped calibration, and if the gap accuracy is $\pm$ 20 micro-inch, and if the gap range is .001 inch or .005 inch F.S., then the maximum error is from $\pm$ 2% to $\pm$ 0.4%.*

The conclusion is that directly taken slope data can be expected to result in a more accurate calibration than obtained with a step wise calibration, particularly so if the displacement range is very narrow.

* Under the assumption that electronic errors are negligible.

$$\text{Slope} = \tan\varphi = \frac{\Delta E}{\Delta x}\left[\frac{1 \mp 2\frac{dE}{\Delta E}}{1 \pm 2\frac{dx}{\Delta x}}\right]$$

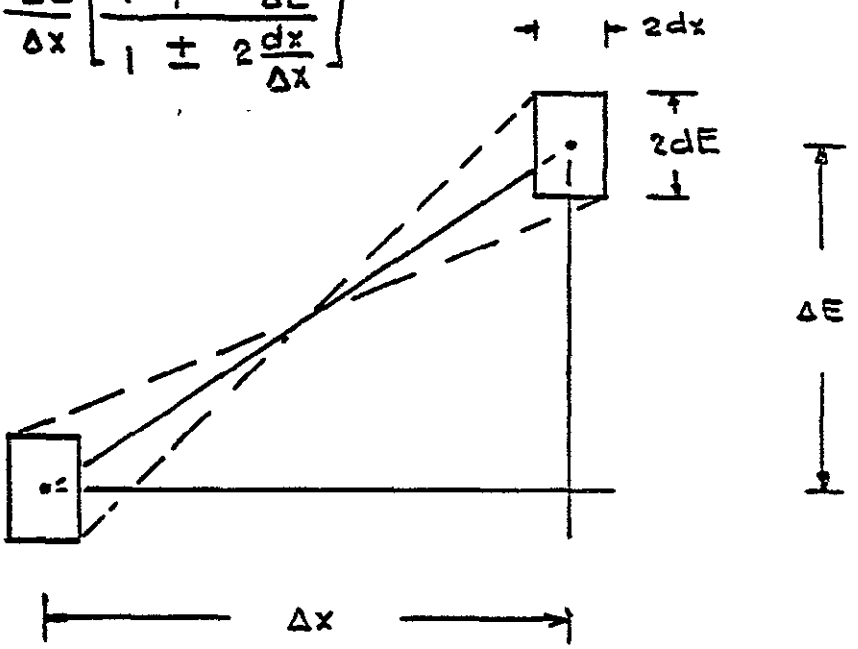

SLOPE:

$$\tan\varphi \cong \frac{\Delta E}{\Delta x}\left[1 \pm 2\left(\frac{dE}{\Delta E} + \frac{dx}{\Delta x}\right) + 4\,\frac{dE}{\Delta E}\,\frac{dx}{\Delta x}\right] = \frac{\Delta E}{\Delta x}\,(1+\varepsilon)$$

$$\varepsilon \cong \pm 2\left(\frac{dE}{\Delta E} + \frac{dx}{\Delta x}\right) = \pm\frac{e}{\alpha}\left(\frac{dE}{E_1} + \frac{dx}{x_1}\right)$$

Fig. A3-1 Slope of Error (E) as Function of Measurement Errors (dE, dx) and Step Size (α, Fraction of FS Values E, and x_1)

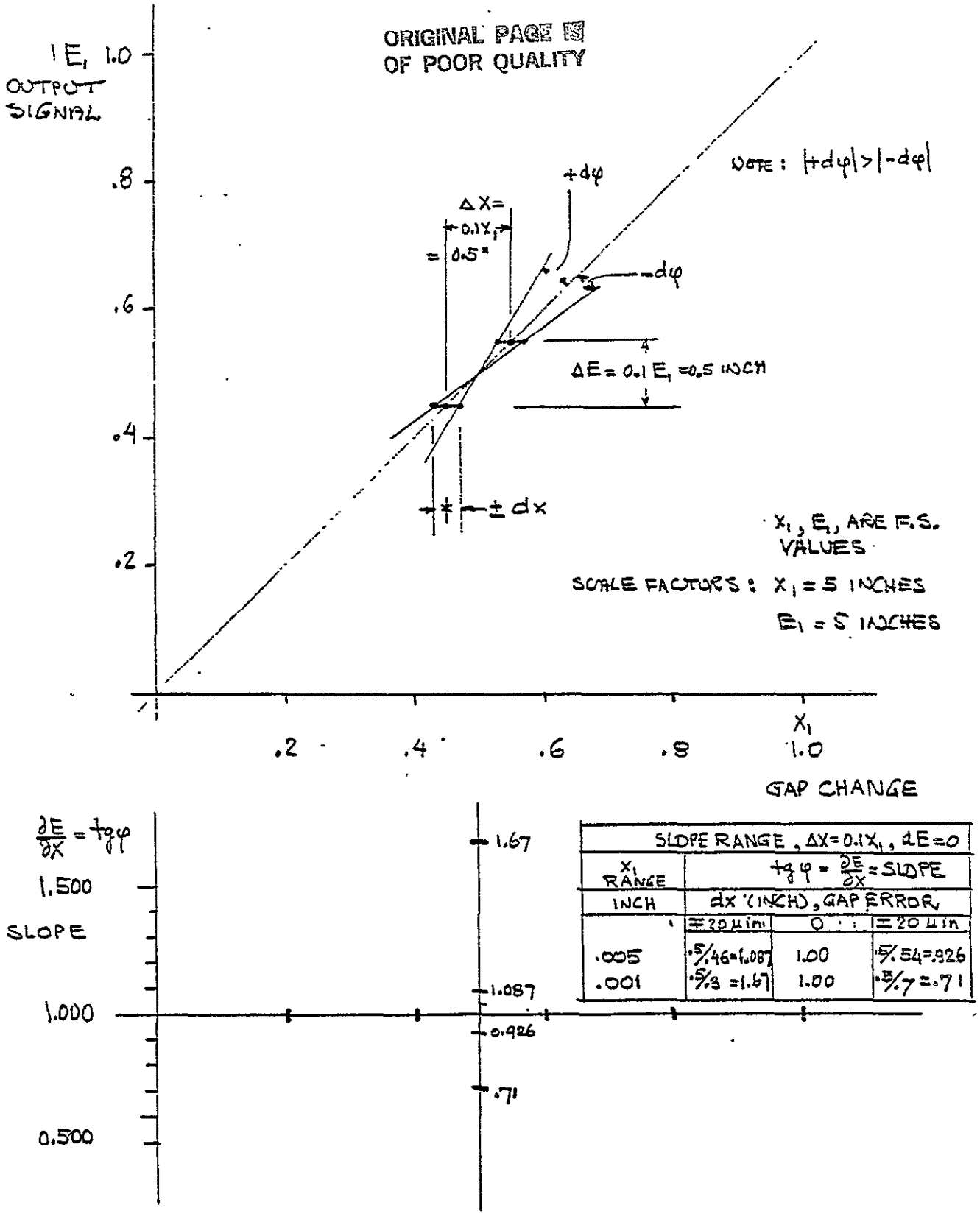

SLOPE RANGE, ΔX = 0.1X1, dE = 0			
X1 RANGE	tgφ = ∂E/∂X = SLOPE		
INCH	dx (INCH), GAP ERROR		
	±20 μin	0	±20 μin
.005	.5/.46 = 1.087	1.00	.5/.54 = .926
.001	.5/3 = 1.67	1.00	.5/.7 = .71

Fig. A3-2 Slope Variability for 20 μin. Gap Error Gap Range of 0.001 in. or 0.005 in. FS, and 10% FS Step Size

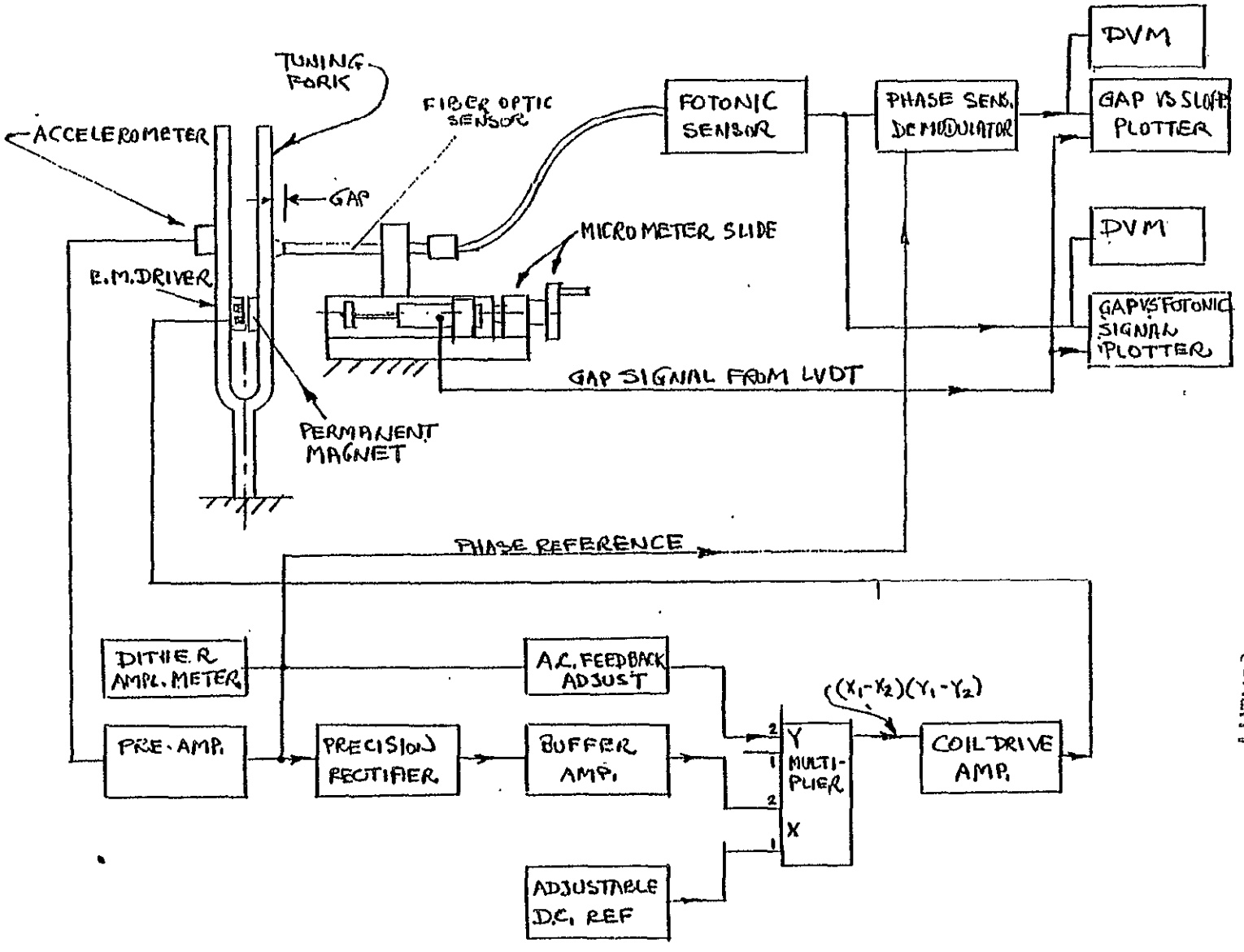

Fig. A3-3 Direct Measurement of Slope of Response Curve Using a Dithered Target

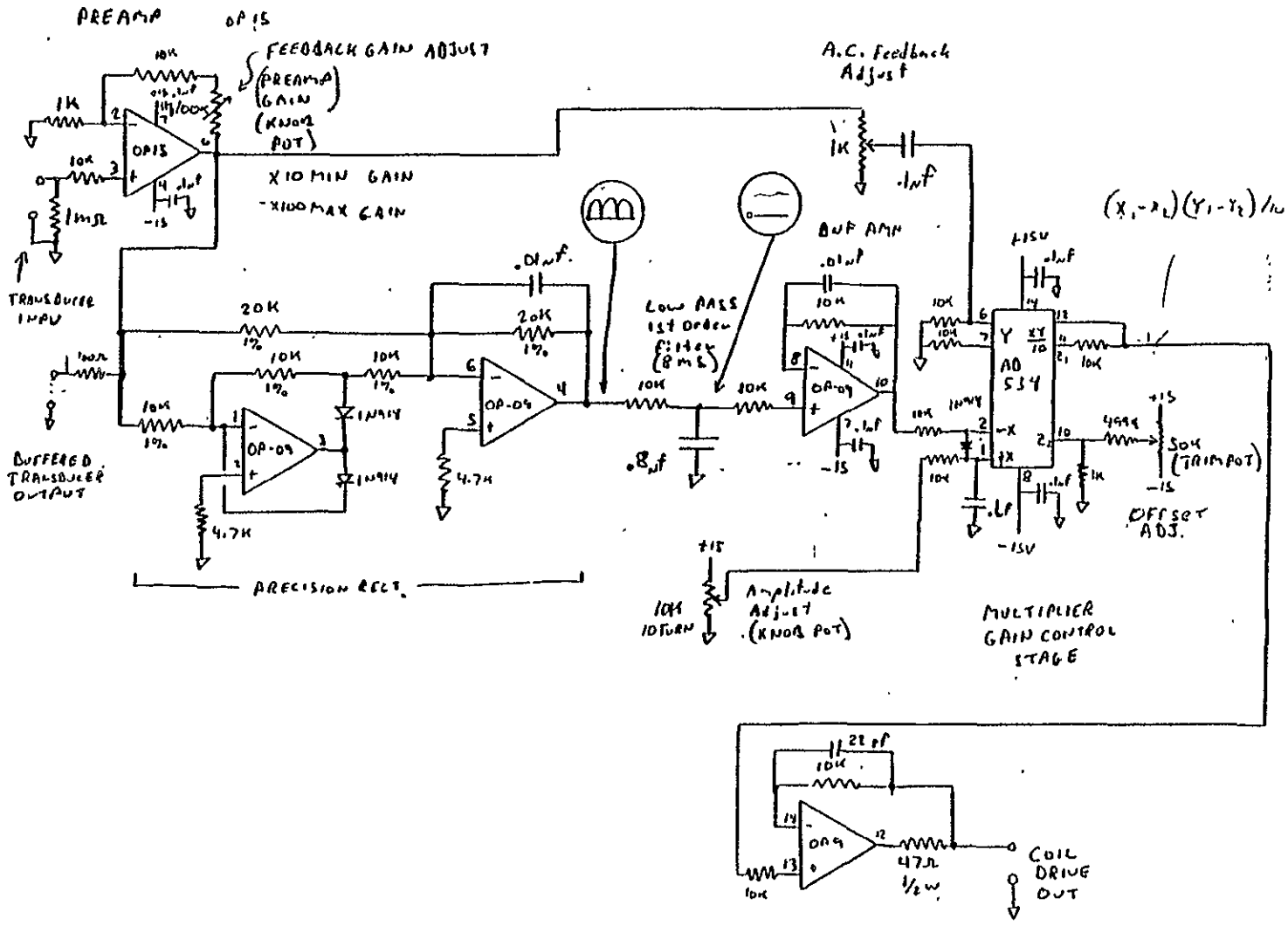

Fig. A3-4 Servo Amplifier for Resonant Target Control

APPENDIX 4

THERMAL TIME CONSTANT OF FIBER OPTIC PROBE

When a fiber optic probe is exposed to a change in temperature, there will be a time lag between the change in temperature at the outside diameter and the temperature of the center fiber. The transient response of a cylinder to a step change in temperature is such that when the dimensionless time (the Fourier number) reaches a value of 1, the difference in temperature between outer diameter and center is less than 4% of the step size. The Fourier number is:

$$N_{Fo} = \frac{\alpha}{L^2} t \qquad (3\text{-}1)$$

α = thermal diffusivity (cm^2/sec)

L = radius of cylinder (cm)

t = time (sec)

The thermal diffusivity is:

$$\alpha = \frac{k}{\delta C_p} \qquad (3\text{-}2)$$

k = thermal conductivity

δ = density

C_p = specific heat

For glass the diffusivity is (3-6) x 10^{-3} cm^2/sec. For a glass fiber bundle of .090 inch diameter (radius ≈ 0.1 cm), the Fourier number is:

$$N_{Fo} = \frac{6 \times 10^{-3} cm^2/sec}{0.01\ cm^2} = 0.6t/sec$$

The N_{Fo} reaches a value of 1.0 when t = 1.6 seconds. Thus, when the surface of the fiber bundle is exposed to a step change in temperature of Δt, the temperature at the center of the bundle will change by 0.96 ΔT in 1.6 seconds. At t = 1.6 seconds, the fiber bundle will have less than a 4% of ΔT temperature difference between outside and center.

If the fiber probe is separated from the metal tube surrounding it by .002 inch of gas, the thermal resistance of this gas film will cause additional delay. The length of the delay can be estimated from the product of the film resistance and the thermal capacity of the bundle section. The heat conduction (k) of air at $0^{o}C$ is 6×10^{-5} cal/cm sec ^{o}C, and the thermal capacity (c) of glass is 0.6 to 1.2 cal/cm^3 ^{o}C. For a cylinder the resistance of the film is:

$$R_f = \frac{t_1}{k\pi dh} \qquad (3\text{-}3)$$

The thermal capacitance is:

$$C_{th} = \pi d^2 hc \qquad (3\text{-}4)$$

Symbols used are:

t_1 = film thickness (cm)

d = cylinder diameter (cm)

h = cylinder height (cm)

k = heat conductivity of gas (cal/cm sec^{o}C)

c = heat capacity of glass (cal/cm^3 ^{o}C)

The product of resistance and capacitance is:

$$R_f C_{th} = \frac{t_1}{k\pi dh} \pi d^2 hc = \frac{t_1 dc}{k} \qquad (3\text{-}5)$$

For d = 0.2 cm, t_1 = .005 cm (0.002 inch), k = 6×10^{-5} cal/cm (air at $0^{o}C$), C = 1.2 cal/cm^3 ^{o}C, the RC time (constant) becomes:

$$R_f C_{th} = \frac{.005 \text{ cm} \times 0.2 \text{ cm} \times 1.2 \text{ cal/cm}^3\,^{o}C}{6 \times 10^{-5} \text{ cal/cm sec}\,^{o}C} = 20 \text{ seconds}$$

This result means that when the metal tube surrounding the sensor is exposed to a step change ΔT that the glass temperature will change as $(1-e^{-t/RC})\ \Delta T$ where t is the time elapsed. Thus for $t = 3RC$ (= 1 minute), the glass temperature is $(1 - e^{-3})\ \Delta T = .95\ \Delta T$.

The two results obtained show that when the film of gas is placed in a series with the glass cylinder that the film resistance controls the thermal response delay of the probe. If practical, the film resistance could be reduced by inserting a resilient conductive layer (thin foil rolled into tube). The overall response improvement that would be obtained is proportional to the reduction in film resistance.

APPENDIX 5

EFFECT OF FIBER BREAKAGE ON PROBE OUTPUT

Summary:

The first order effect of fiber breakage on a random fiber optic proximity probe is a proportional reduction in signal. Due to the relatively large probe output at zero pressure, the effect of fiber breakage can be large, unless the probe output at zero pressure at the last calibration is stored together with the output sensitivity due to pressure. These two pieces of information permit full data correction for the effect of fiber breakage.

Discussion and Analysis of Problem:

If a random probe is made with N fibers, then the total signal is the sum of the signals from 1/2N receiving fibers. The signal level from each fiber at a given gap depends somewhat on the position of the fiber in the probe face. Fibers at the edge receive on the average only one-half as much light as fibers near the center of the probe. If it is assumed, however, that each receiving fiber collects the same amount of light, then it follows that the effect on signal level of fiber breakage (in either branch of the probe) is proportional to the number of fibers broken. Thus, the effect of broken fibers as a percentage of the total is the same as that of, for example, target reflectivity. The effect of fiber breakage (percentage) on pressure sensor output is multiplied by a factor made up of full scale displacement, probe output at zero pressure and proximity probe sensitivity as illustrated in Figure A5-1. In this figure, the fiber probe response is shown as a straight line, with a slope equal to E_w/q, volt/psi, as obtained in the last calibration before fiber breakage occurred. Due to a fiber breakage fraction (α), that slope changes by a factor of $(1-\alpha)$. The change in output from E_o (the latest zero reference available) due to a pressure (p) is shown in Eq. (A5-1). If a new zero pressure reference $(1-\alpha)E_o$, was made available since fiber breakage occurred, then the change in output due to a pressure p is given by Eq. (A5-2). If the original zero pressure reference (E_o) and the new zero pressure reference, $(1-\alpha)E_o$, are both available, then $(1-\alpha)$ can be calculated. With $(1-\alpha)$ available, a full correction for fiber breakage can be made. In Eq. (A5-1) the error due to fiber breakage is made up of two parts, a fixed part ($+\alpha E_o$) and a pressure dependent part

$$(-\alpha p \frac{E_w}{q}).$$

For low pressures, the error as a percentage of full scale will be largest. The full scale output change (E_w) is 10% to 20% of the output (E_o) at zero pressure. Thus, if fiber breakage is 1%, the equivalent pressure signal error percentage is multiplied with the

ratio E_o/E_w (a factor of 5 to 10). This is the worst case. If instead of using E_o as the zero pressure reference the $(1-\alpha)E_o$ level is used, the error in the percentage pressure signal is equal to the fiber breakage percentage. This is obviously a much more desirable signal processing approach. If, in addition, both E_o and $(1-\alpha)E_o$ are available for signal interpretation, then a full correction for fiber breakage can be made.

The corrections for fiber breakage require the same procedure as the one that would be needed for any other source of signal attenuation, such as target reflectivity changes. The assumption made in all this is that the gap between probe and target remains fixed to ± 1 micro inch.

The experience with the smallest MTI probes, which contain only seven fibers, either grouped as six around one (CTI probe) or three fibers next to four (half and half probe), has been that fiber breakage is very uncommon. Only if the sheath is kinked sharply, a fiber can break.

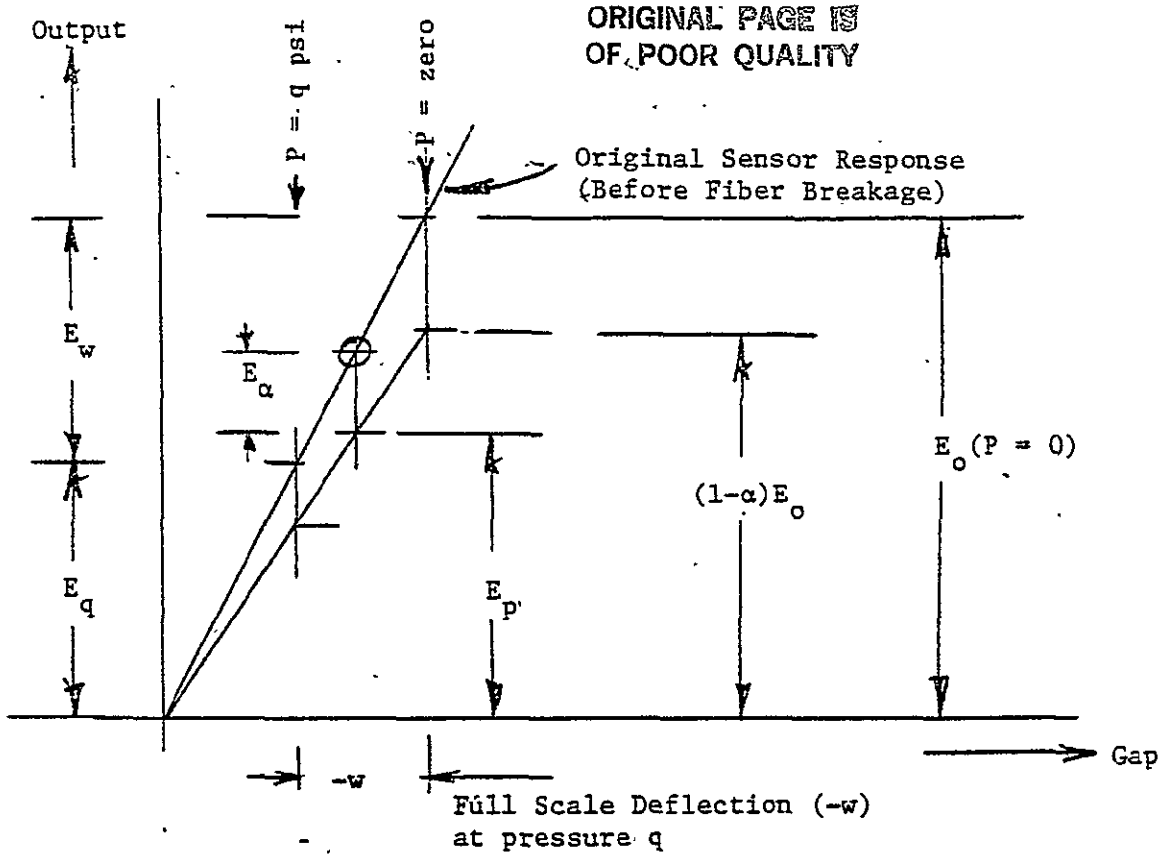

FIGURE A5-1 EFFECT OF FIBER BREAKAGE ON SYSTEM OUTPUT

Total Number of Fibers in Random Probe = N

Fibers Broken Since Last Calibration = αM

E_α = Absolute Error at Pressure P

E_W = 10% to 20 °F E_o

Sensor Output:

$$E_p = (1 - \alpha)\left(E_o - p\frac{E_w}{q}\right)$$

1. System output if original E_o is used as zero pressure reference:

$$E_o - E_p = \alpha E_o + (1 - \alpha)\, p\frac{E_w}{q} \qquad \text{(A5-1)}$$

2. If a new zero reference $(1 - \alpha)\, E_o$ is available, system output will be:

$$(1 - \alpha)\, E_o - E_p = (1 - \alpha)\, p\frac{E_w}{q} \qquad \text{(A5-2)}$$

3. If $(1 - \alpha)\, E_p$ and E_o are both available $(1 - \alpha)$ can be calculated and a full correction for fiber breakage can be made.

L. Hoogenboom
April 1983

APPENDIX 6

SCOPE OF WORK AND SPECIFICATIONS

SCOPE OF WORK

OBJECTIVE

The objective of this research is to determine feasibility of methods capable of providing pressure measurements on the Space Shuttle Main Engine. The intent is to demonstrate the feasibility of pressure sensor development whereby the conversion of the sensing element behavior to an electrical signal can be performed with a modular concept, i.e., the electrical conversion module would be common for all pressure ranges and temperature environments. With this concept it is intended that the sensing element design would revert to a simple mechanical design. For example, pressure ranges could be changed by changing only mechanical design parameters such as diaphragm thickness. The objective is to define and demonstrate new methods to advance the state-of-the-art of pressure sensors in terms of reliability, accuracy, and ease of manufacture for SSME application.

A. Performance

The following performance characteristics are design goals for this investigation and will be considered end item specification for future R&D for prototype development.

1. Full Scale Pressure - Various ranges up to 9,000 psig.
2. Linearity - Within 0.15 percent FS or better.
3. Hysteresis - 0.1 percent FS or better.
4. Non-Repeatability - 0.05 percent FS.
5. Non-Return to Zero - 0.05 percent FS Maximum.
6. Thermal Sensitivity - 0.005 percent FS/degree F.
7. Thermal Zero Shift - 0.005 percent FS/degree F.
8. Thermal Gradient - Sensor shall operate within error band when exposed to a temperature gradient of 165° F. across sensor.
9. Rated Overload - PSIA, PSIG, PSIS: Overload of two and one-half times the rated pressure will not cause permanent damage and 1.5 times will not cause permanent change of residual zero output or calibration curve.
10. Zero Balance - Within plus or minus 0.25 percent FS or better at ambient temperature (77° F.) and atmospheric pressure.
11. Response - Two types: i.e. 0-300 hz and 0-20,000 hz
12. Electrical to Pressure Calibration - Capability shall be provided as specified for electrical to pressure calibration at 20% and 80% full scale correlation shall be 0.1% full scale.
13. Static Pressure Rating - Two times rated pressure.
14. Voltage output: 30 mv; Total Error Band - 1% referenced to 77°F calibratic
15. Excitation - 10 volts

B. Environmental

The following environmental specifications are given to indicate conditions that will have to be met in final adaptation to Space Shuttle Main Engine applications The Laboratory model does not have to meet these conditions.

1. Vibrational Environment - The transducer shall be capable of operating within the Error Band at any temperature within the range of minus 65F to plus 165F while exposed to the following vibrational environment:

Sinusoidal Sweep Amplitudes

10 Hz @ 20 g peak
20 Hz @ 80 g peak
36 Hz @ 80 g peak
44 Hz @ 120 g peak
170 Hz @ 120 g peak
315 Hz @ 400 g peak
2000 Hz @ 400 g peak

Steady-State Random Vibration Amplitudes

20 to 125 Hz @ 0.10 $(g\ rms)^2/Hz$

125 to 200 Hz @ +4.4 db/octave

200 to 265 Hz @ 0.20 $(g\ rms)^2/Hz$

265 to 300 Hz @ +18.3 db/octave

300 to 360 Hz @ 0.34 $(g\ rms)^2/Hz$

360 to 400 Hz @ +19.5 db/octave

400 to 1325 Hz @ 0.6 $(g\ rms)^2/Hz$

1325 to 1750 Hz @ +11.5 db/octave

1750 to 2000 Hz @ 1.8 $(g\ rms)^2/Hz$

Random Composite Reference Level = 39.53 g rms

Superimposed Steady-State Sinuoids

Sinusoidal dwells for 6.5 Hrs.
7.7 g rms at 600 Hz (RPL)
4.0 g rms at 500 Hz
6.5 g rms at 2000 Hz

Sinusoidal sweep for 1.0 hours

7.7 g rms from 350 Hz (MPL) to 620 Hz (FPL) to 350 Hz at 270 Hz/min.

6.5 g rms from 1400 Hz (MPL) to 2000 Hz (FPL) to 1400 Hz (MPL) at 600 Hz/min.

Composite Reference Level = 52.2 g rms

II. Statement of Work

The contractor shall perform for MSFC the following related research program:

Task A. Provide a method or methods which offer promise for conducting a feasibility demonstration.

Task B. Develop, through accomplishing the following reviews, laboratory or breadboard hardware capable of demonstrating the feasibility of the method and to define problems which will be encountered in pursuit of prototype sensors and demonstration hardware for Space Shuttle main engine test firings:

1. *Preliminary Design Review at MSFC

   Furnish the design concept along with adequate design criteria, schematics, etc., so that approval of the design concept can be accomplished.

2. *Critical Design Review at MSFC

   Furnish necessary engineering drawings and data to allow critique of design and necessary changes required to accomplish the objective of the Scope of Work.

3. *Final Design Review at MSFC

   Furnish final design drawings incorporating any changes specified in the Critical Design Review. Drawings shall be in sufficient detail for fabrication of the breadboard. Final approval for fabrication will be given based on this review.

*Engineering data and drawings shall be furnished to MSFC ten (10) working days prior to review meetings at MSFC.

4. Laboratory Demonstration at MSFC

   Provide a laboratory demonstration of delivered demonstration hardware.

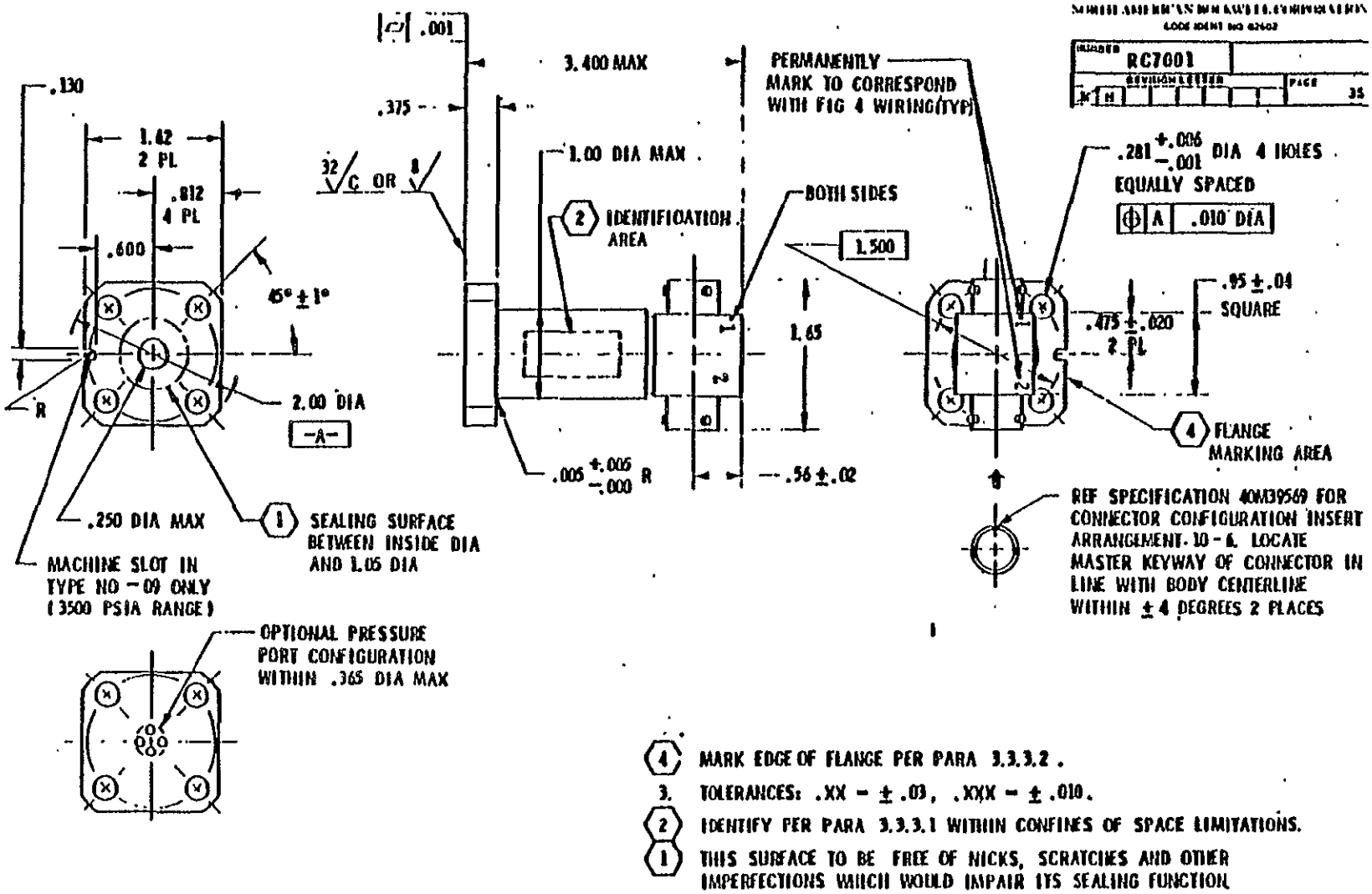

Fig. 1 Bayonet Connector Configuration

5. Final Report Draft Review at MSFC

   Provide a final report at the completion of the contract which complies with the content requirements described in Attachment "A". Reports Requirements paragraph B. A draft of this report shall be made available for review ten (10) working days prior to review meetings at MSFC. MSFC will provide review comments and suggested changes to the report within ten (10) days. The contractor shall within an additional ten (10) days update and finalize the report and provide it to MSFC prior to the completion of the contract period. The report shall be provided in accordance with Attachment "A" Reports Requirements Paragraph D.

Specifications Assembled from References 1 and 2 (See Footnote (1))

Input data for the group of pressure transducers is summarized as follows: (Transducer only except where cable or electronics is mentioned).

1. Pressure range (2):0 - 300 to 0-9000 psia in seven ranges.(psig, psia, psis)

2. Overload (5):2½ times rated pressure (psig, psia, psis) will not cause permanent damage; 1½ times rated pressure will not cause change of residual zero output or calibration curve.

3. Proof Pressure (3):* 1.5 X full scale pressure with zero shift less than ¼% of full scale.

   * 5 X full scale pressure or 20.000 psi, applied to pressure cavity, for structural purposes only, for transducers with overrange protection.

4. Burst Pressure (3):* 3 X full scale pressure or 20.000 psi, whichever is smaller.

   * 7.5 X full scale pressure or 20.000 psi for sensor with overrange protection.

5. Normal temperature range (5): -65°F to 165°F.

6. Operative temperature limits (4): -452°F to 450°F.

7. Temperature range (electronics)(4): -50°F to +125°F operational

   non-operational. -80°F to +200°F

8. Non-linearity: $\pm$.15% of F.S. (maximum deviation from straight line through terminal points of response).

9. Hysteresis: < 0.1% F.S.

10. Non-repeatability: < .05% F.S.

11. Non-return to zero: < .05% F.S.

12. Sensitivity shift due to temperature: < .5%/100°F

13. Zero shift due to temperature: < 0.5%/100°F

14. Gradient Effect: < 0.5%/165°F across axial length of sensor

15. Zero off-set: < $\pm$ 1/4% of F.S. at 77°F and atmospheric pressure

16. Dynamic Response: 0-300 Hz
    0-20.000 Hz

17. Life: 8 hours M.T.B.F. based on 60 pressure cycles

18. Dimensional Envelope (present): 3 x 3 x 3.5 $in.^3$, 12 oz. weight.

19. Accuracy requirement is applicable to static and dynamic pressure load.

20. Lead Length: 15 feet maximum.

21. Pressure sensor is flush mounted on pressure part and is not exposed to flow.

---

(1) Ref. 1, Rockwell International Corp., Rocketdyne Div., Procurement Spec. No. RC7001, dd 25 March 1980.
Ref. 2, RFP8-1-2-EC-25722, Exhibit Am and Amendment 2.

(2) Ref. (1), p. 31.

(3) Ref. (1), p. 6.

(4) Ref. (2), Amendment 2.

(5) Ref. (1), Exhibit A.

APPENDIX 7

THERMAL DIFFERENTIAL EXPANSION AND THERMAL HYSTERESIS IN FIBER OPTIC PROBES

In a typical fiber optic proximity probe, a bundle of glass fibers is fixed inside a metal envelope with a resin adhesive. When the probe temperature is changed, thermal stresses develop as a result of differential thermal expansion or contraction. When the probe is held in a test fixture that is made of the same metal throughout (the same as that of the probe envelope), the probe will produce an output when exposed to a changing temperature. Over a narrow temperature range, the change in probe output will be proportional to temperature change, and the output will follow the temperature without hysteresis. Over a wider temperature range, the probe output may show a variable sensitivity to temperature and also hysteresis.

The thermal stresses that develop in the probe act radially and lengthwise. The radial stresses when they are positive (tensile) load the bonds between fibers and envelope directly. If the radial stresses are negative (compressive) they enhance axial coupling through friction. The lengthwise stresses are concentrated at the ends of the envelope bore where the fibers exit or terminate. Bond failure starts at the ends of the bonded length and progresses from there inwards. Figures A7-1 and A7-2 illustrate what relative thermally induced motion can be expected between the fiber bundle and the envelope. In Figure A7-1 the resin collar shown prevents the bundle from moving into the envelope. As a result, when heating the probe, all the differential thermal motion will become concentrated at end sensing end. In Figure A7-2, probe cooling will result in bundle extension beyond the metal envelope at both ends. The axial thermal behavior of the probe is a function of bond strength and differential expansion magnitude. The length over which the fibers are (or have become) unbonded from the metal decides the free fiber length and hence the thermally induced output. In some epxeriments with standard probes the apparent unbonded length of fibers was typically 2-3 bundle diameters long.

In a preliminary experiment, the data shown in Figure 4 was obtained with a standard probe of MTI manufacture and of unknown age and history of use. The results in Figure 4 show a nearly linear effect of temperature on zero drift. The differential thermal expansion between glass and 304 stainless steel is (4 to 5) x $10^{-6}/^{\circ}F$. The apparent gap change due to temperature in Figure 4 is +1.8 x 10^{-6} inch/$100^{\circ}F$. Assuming that the face of the probe remains flat, the unbonded fiber bundle length (ℓ_u) follows from:

$$\ell_u = \frac{180 \times 10^{-6} \text{ inch}/100^{\circ}F}{(4 \text{ to } 5) \times 10^{-6}/^{\circ}F} = \frac{1.8}{(4 \text{ to } 5)} = (.45 \text{ to } .36) \text{ inch}$$

The remainder of the fiber bundle remained bonded to the stainless steel tube in spite of thermal stresses. If these tests had been extended over a wider temperature range, a greater length of unbonded fibers could be expected.

Following this test, temperature tests were made on a group of standard fiber optic probes. This group of probes was ordered special from Fiber Optics Technology of Pomfret, CT to evaluate the effect of probe size, fiber size and type of resin on thermal zero drift. The probes were made with the standard 3" long tube of 304 stainless steel with smooth bore. The tube sections used are 1/8 x .09 bore and 1/16 x .045 bore. Probes were made with two fiber sizes (.002 inch and .001 inch diameter) and two epoxy resins. The tubes are packed with fibers, which are bonded (potted) over a length of 1/2 - 1 inch. As the tubes have smooth bores without step or grooves, no locking of the bundle against axial motion (other than through the resin bond or through friction) can occur.

The probes were numbered #1 through #5 and they are identified by the following data:

Probe #	Size (O.D.) Inch	Fiber Bundle Dia. - Inch	Fiber Size Inch	Maximum Use Temperature ^{o}F	Resin Type EPO-TEK
1	.065	.045	.001	600	CF6
2	.065	.045	.002	450	353
3	.065	.045	.002	600	CF6
4	.125	.09	.001	600	CF6
5	.125	.09	.002	450	353

The data taken is plotted in Figures A7-3 to A7-9. In Figures A7-3 to A7-7 data is shown for tests in which the oven temperature is raised and dropped in a short time, typically 5-10 minutes. The probes show a considerable amount of lag in response between the heating and cooling parts of a cycle. At the end of the cycle shown in Figure A7-3, the loop closes, and there is no residual zero shift (hysteresis). The two negative data points were taken 16 hours after the last positive point was recorded. In subsequent cycles (listed with Figure A7-3) there is virtually no permanent zero shift for this probe. To evaluate the effects of a lag in the probe response, probe #1 was tested again at low heating rates. The data for these tests is shown in Figures A7-8 and A7-9. The lower curve is data taken with the probe placed in a hot oven. The upper curve is data for the probe heated slowly by raising the oven temperature gradually. The horizontal distance between the two curves is 5 to 10 degrees F, and the vertical distance is 25 to 30 micro-inch. The heating rate for the top curve is about $4^{o}F$/ minute and for the bottom curve it is $24^{o}F$/minute. The rapid

heating along the bottom curve caused a delayed thermal response between:

1. The thermocouple (which was pressed against the outside of the brass block with a spring clip) and the brass target block.

2. The brass block and the sheath.

3. The sheath and the inner core of the probe.

Initially, the thermocouple may have read a slightly higher temperature than the brass block, which then would cause deparation of the two curves. At the end of the test, when the heat flow into the brass block virtually stopped, the curve separation should have disappeared, but at the end the curves are still separated by 4-5 degrees F.

Thus it seems unlikely that the block temperature was logging the thermocouple reading. Along the lower curve, the time needed by the block to reach the oven temperature (156°F) was about 9 minutes. For this heating rate, the maximum temperature difference along the free length of the probe was calculated to be less than 4°F. The maximum mean temperature difference between the free probe length and the block was about 2 degrees. Thus the differential expansion between probe and block would not be more than 2 degrees F x 0.38 inch x 10^{-5}/°F = 7.6 x 10^{-6} inch.

The maximum calculated radial temperature difference in the probe itself is less than 0.5 degree F during the test along the lower curve. This temperature difference cannot generate a significant differential expansion effect and therefore no probe drift. The conclusion is that a major part (>75%) of the zero drift response observed must be attributed to a mechanical cause. It evidently takes some time for the probe to fully respond to the thermal differential expansion effects within the glass-resin-metal composite. When the heating rate is sufficiently slow, then the thermal stresses relax as fully as possible and thermal drift is maximum. The time needed for relaxation and the degree of relaxation are probably a strong function of temperature. At cryogenic temperatures, the resin will be harder, and relaxation and additional drift will be less.

In the finished pressure sensor, thermal cycling between room temperature and -150°C and room temperature and +80°C produced permanent gap changes of 20-60 micro inch. Figures A7-1 and A7-2 illustrate the action of temperature on this type of probe. The bonded length in this sensor is 0.32 inch. The differential expansion for glass versus Inconel 600 is (4 to 5) x 10^{-6}/°C, which results in about 120-150 micro inch/100°C of potential differential movement (increased gap) when raising the sensor temperature. At cryogenic temperatures the differential thermal expansion is only a fraction of that at room temperature and above, and the displacement effects can occur at either end of the probe length, and are probably cut in half because of that. Therefore probe heating will result

in much greater zero drift and in thermal hysteresis. Probe cooling will produce effects which are much smaller, that is after the first cooling cycle, when residual hysteresis effects of the preceding heating cycle have been shaken down. In the first experiments with the pressure sensor, it was cooled down and very little thermal effect was observed. Only after the first heating cycle did permanent zero shift appear. Once the fiber bundle has shifted into the probe, there is no mechanism that will automatically move it back (forward) again. At various points in the thermal experiments with the pressure transducer, it was tapped in an effort to disturb the fiber bundle. The tapping had no effect on the probe output. When the fiber cable exiting from the transducer was moved and bent, it also was not possible to produce a permanent zero shift.

In retrospect, it seems that the probe construction should have avoided the resin collar and should have provided positive locking action at the tip of the probe. Before accepting this conclusion, experiments must be made to isolate the cause of zero shift as observed, over a wide temperature range. In these experiments, probes made with a variety of resins and fiber and envelope surface preparation (including micro blasting of fibers and grooving the envelope) must be used. In these experiments, the envelope length and bore diameter must be the same as those used in the pressure sensor and the resin flow must be controlled to avoid the (probably) undesired collar and its effects.

Table A7-1 lists the results of the temperature tests made on the completed sensor at MTI. These tests were made to obtain the basic performance data of the sensor. The zero shift at room temperature referenced to the first test point ranges from +11.4% to -14.1%. The positive zero shift (gap decrease) relates to exposure to low temperatures. The largest negative zero shift (gap increase) occurred after the first exposure to high temperature followed by a cryogenic test. The variations in response slope range from -4.5% to +4%. The transition from a minus slope change to a plus slope change occurred at the same test point at which the zero shift reversed sign.

Zero shifts measured at room temperature may have been caused by shifts in the position of the fibers. When the fibers shift position, the deflection due to a 1000 psi pressure excursion is also shifted on the probe response curve. The response curve of the probe is shown in Figure A7-10. The nominal range over which the 1000 psi related deflection occurs, is from a gap of .0054 inch down to .0035 inch. This gap range is centered to the right of the point of maximum slope. To see this more clearly, Figure 5 is helpful. It shows a very sharp peak for the slope. The data in Figure 5 is for a slightly different probe, and the peak occurs at a slightly smaller gap, than would be found for Figure A7-10 if a precise slope plot had been made. When the probe gap (at zero pressure) shifts down, the response to 1000 psi increases, as the maximum slope range of the response curve moves closer to the center of the operating gap range. When the probe gap (at zero pressure) shifts up, the response to a 1000 psi load decreases. This did not happen in the tests reported in Table A7-1. Actually the reverse happened. The conclusion is, therefore, that the final gap obtained after the probe was welded, shifted down such that the maximum slope range of the curve became located to the <u>right</u> of the 1000 psi gap interval.

The slope curve in Figure 5 normalized to 1.00 at the peak can be approximated to the left side of the peak with

$$\text{Slope} = S = 1 - \left(\frac{x}{.0034} - 1\right)^2 \qquad (1)$$

x = gap

Eq. (1) shows a peak at $x = .0034$ inch and passes through zero at $x = 0$.

Id Eq. (1) is used to obtain a response curve and if the asymmetry around $x = .0034$ inch of the actual slope curve is ignored, the response becomes:

$$\int s\,dx = x - \frac{1}{3}\left(\frac{x}{.0034} - 1\right)^3 .0034 + C_1 \qquad (2)$$

In the pressure sensor the gap set before welding, was such that between zero and 1000 psi, the gap change would be located slightly to the right of the peak of the response slope. This was done to assure that the linearization module could perform correctly. This module can only linearize response curvature of a fixed sign. Therefore, the pressure response was not allowed to cross the inflection point of the proximity probe.

Actually, after welding, a gap reduction was suspected, and was confirmed by the test results shown in Table A7-1. The gap reduction caused the transducer to operate past the inflection point of the proximity response. Eq. (2) is useful in illustrating what happened. The change in output when the gap changes from (.0034 + .001) to (.0034 - .001) is:

$$.0044 - \left(\frac{1}{3}\ \frac{.0044}{.0034} - 1\right)^3 .0034 - .0024 + \frac{1}{3}\left(\frac{.0024}{.0034} - 1\right)^3 .0034 =$$

$$.002 + \left(-.00002884 - .00002884\right) = .002 - .00005767$$

The non-linear content in this output is the second term, which is 2.9% of the linear part. If the .002 inch excursion used above is shifted to a smaller gap by .0005 inch, then the total output change becomes:

$$.0039 - \frac{1}{3}\left(\frac{.0039}{.0034} - 1\right)^3 .0034 - .0019 + \frac{1}{3}\left(\frac{.0019}{.0034} - 1\right)^3 .0034 =$$

$$.002 + \left(-.00000360 - .00009732\right) = .002 - .00010092$$

Now the non-linear content has increased to 5%, and the overall output is down by 2%. Changes of this magnitude in response are shown in Table A7-1, but they occur when zero shifts are only about .0002 inch instead of the .005 inch used in the example above. The trend as calculated is visible in the test data, but the actual magnitudes are not consistent with the model in Eq. (2). The physical differences between the probes represented in Figures 5 and A7-9 are very small and cannot be used to explain the discrepancy between the trend calculated with Eq. (2) and that shown in Table A7-1.

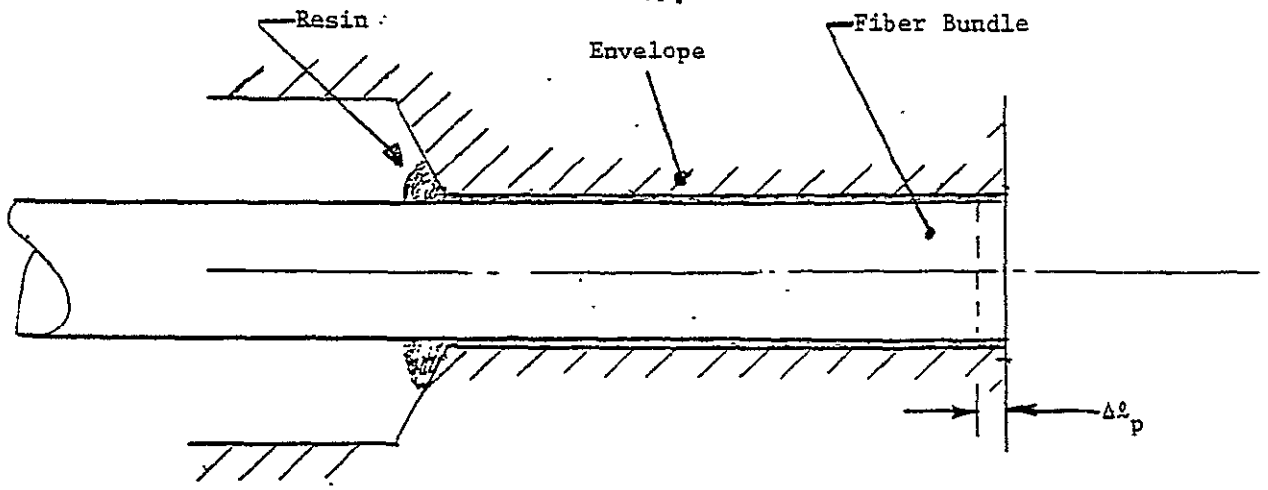

Fig. A7-1 Differential Expansion of Glass Fibers in Metal Envelope Above Room Temperature

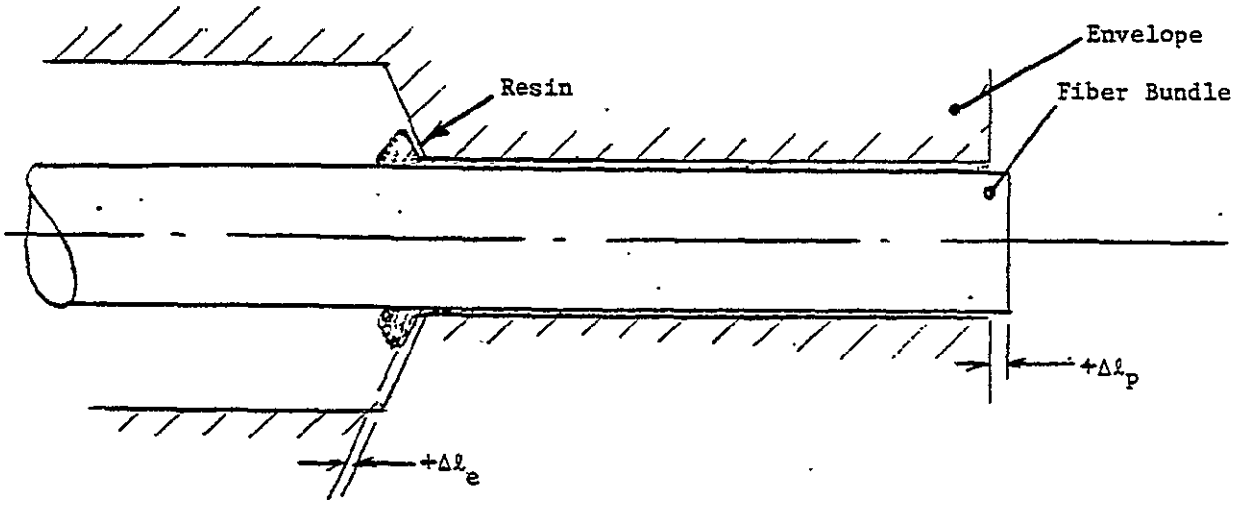

Fig. A7-2 Differential Expansion of Glass Fibers in Metal Envelope Below Room Temperature

Coefficients of Expansion (x 10^{-6}/°F):

Inconel 600	6.0 at -250°F
	6.3 at -200°F
	6.7 at -100°F
	5.8 at 70°F
	7.4 at 200°F
	7.7 at 400°F
Glass	5 to 6 80-500°F
304 Stainless Steel	10

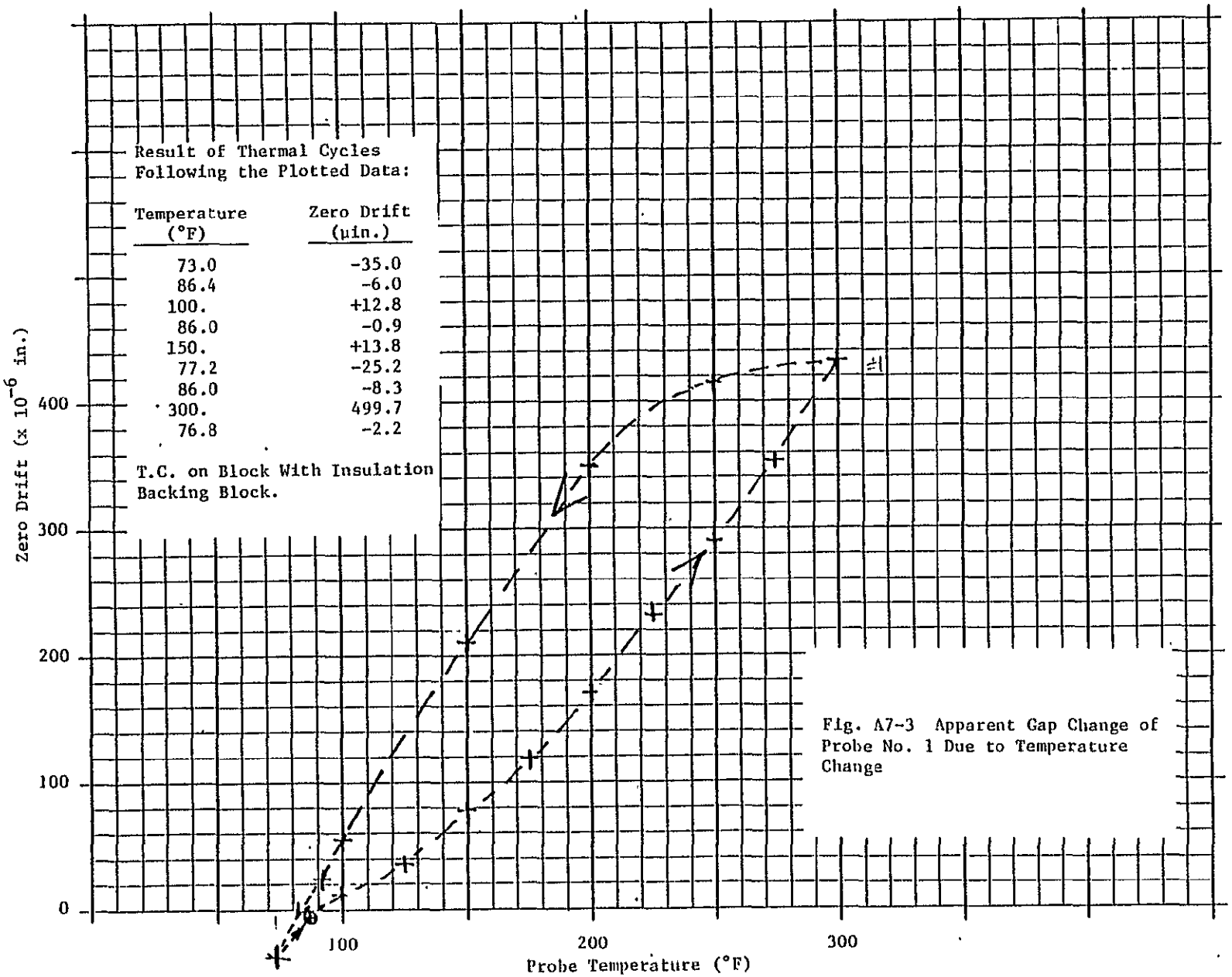

Fig. A7-3 Apparent Gap Change of Probe No. 1 Due to Temperature Change

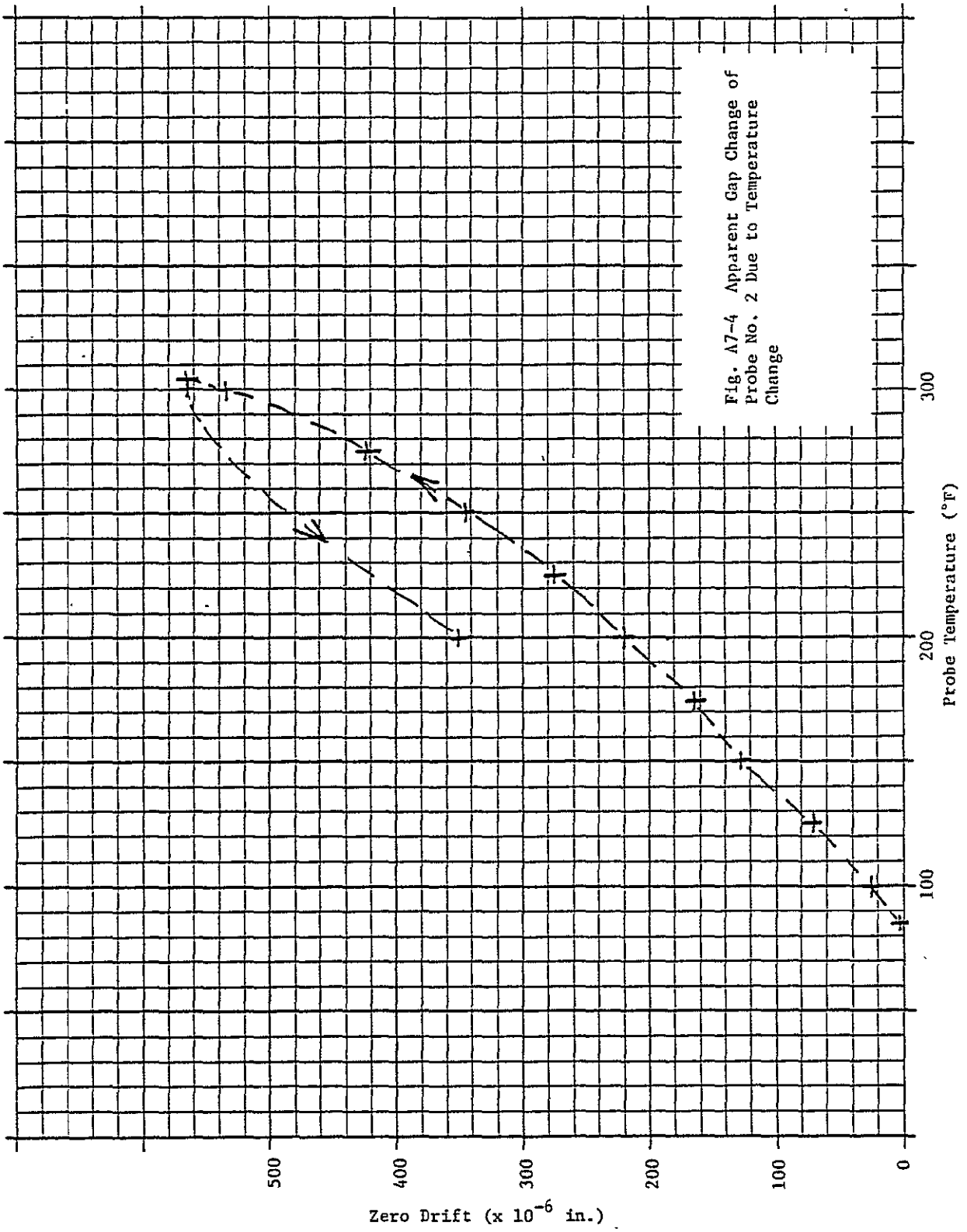

Fig. A7-4 Apparent Gap Change of Probe No. 2 Due to Temperature Change

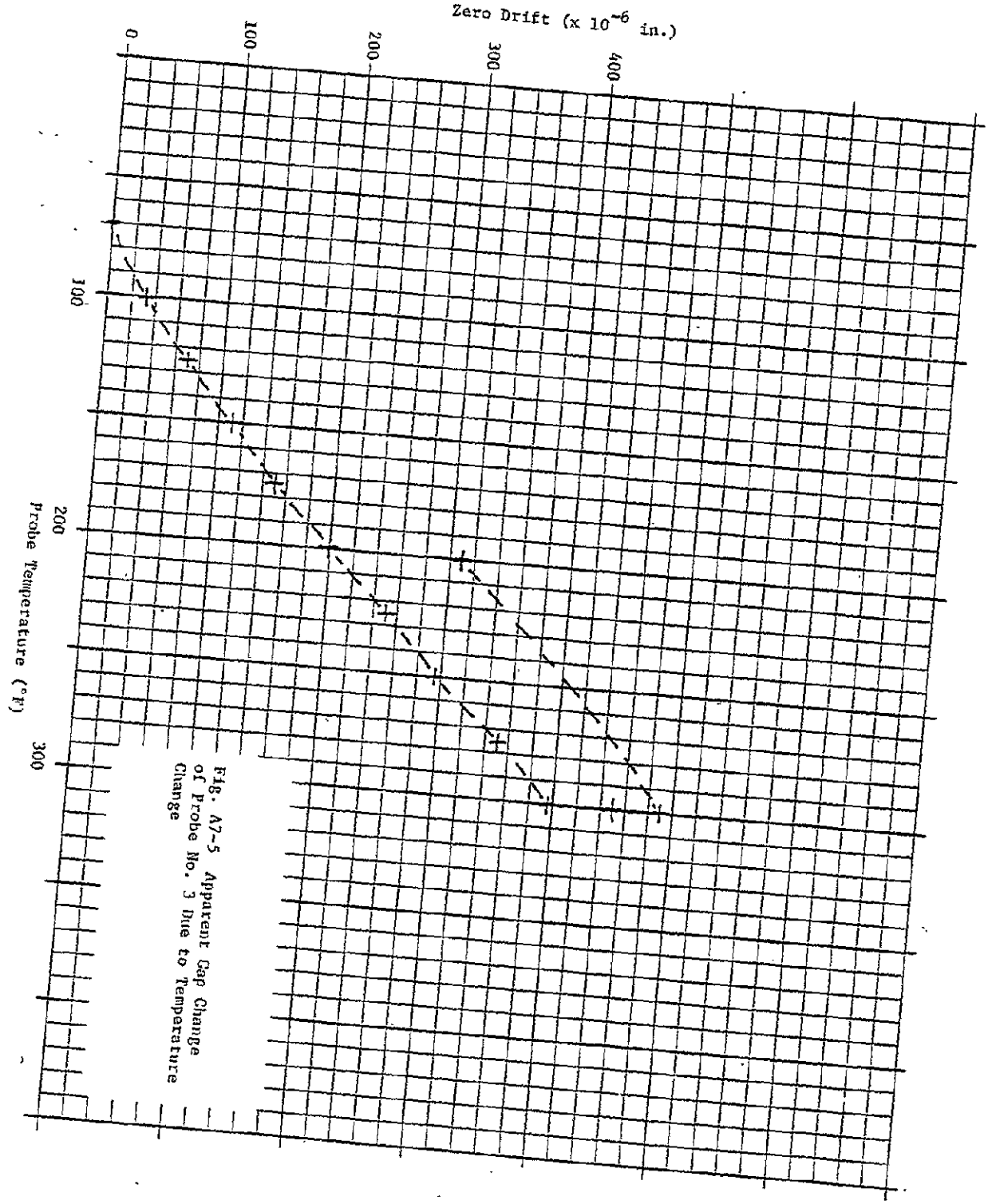

Fig. A7-5 Apparent Gap Change of Probe No. 3 Due to Temperature Change

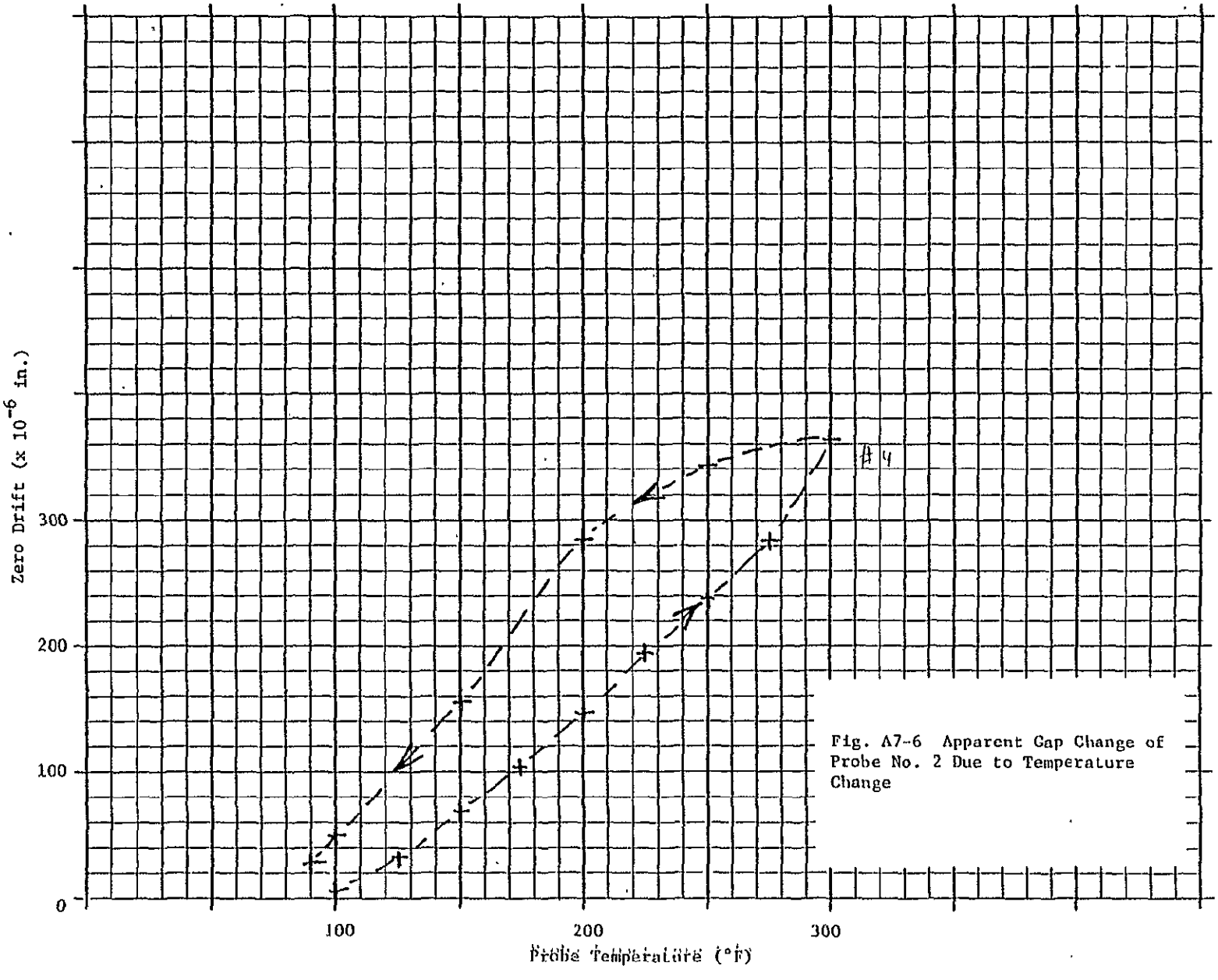

Fig. A7-6 Apparent Gap Change of Probe No. 2 Due to Temperature Change

Fig. A7-7 Apparent Gap Change of Probe No. 5 Due to Temperature Change

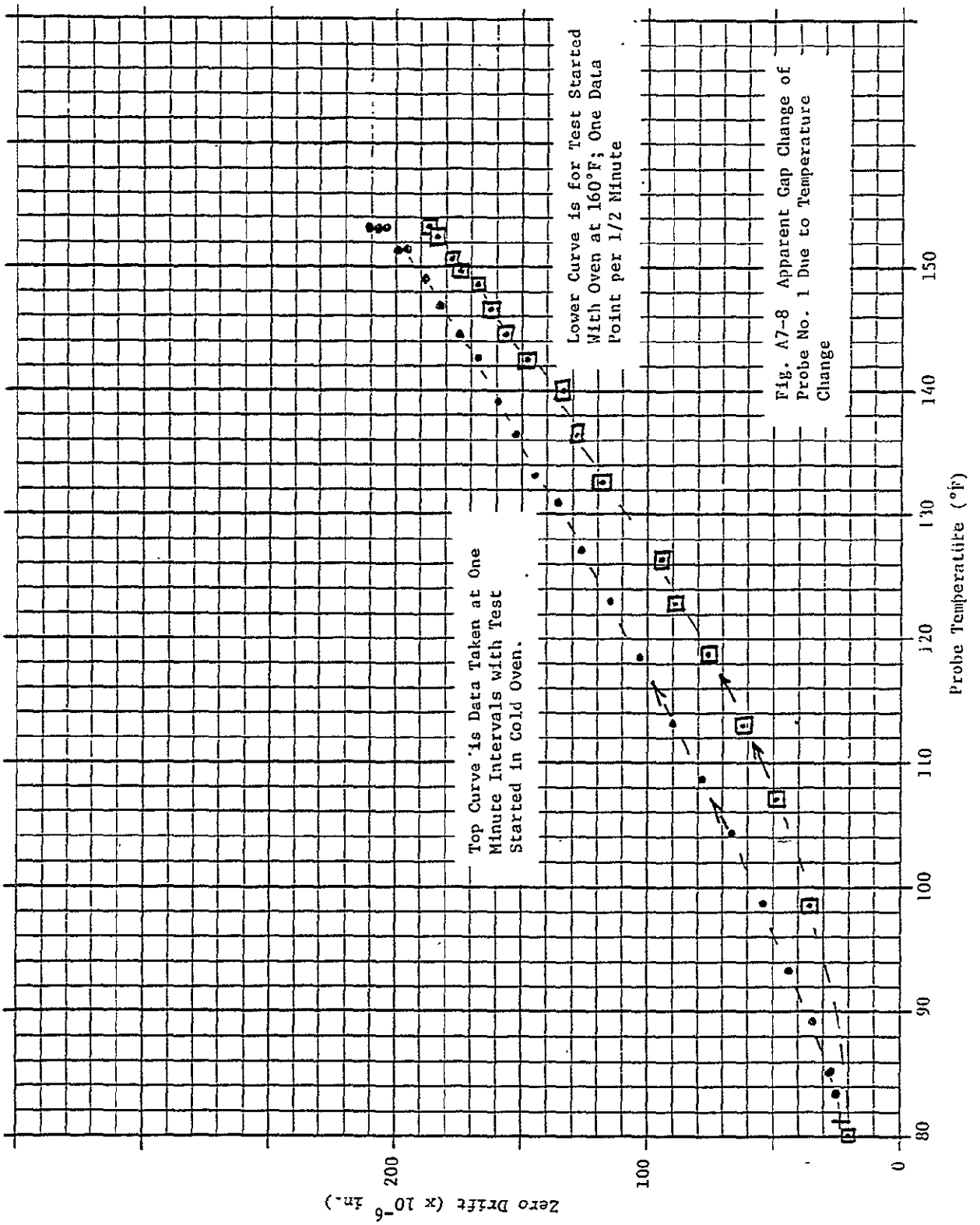

Fig. A7-8 Apparent Gap Change of Probe No. 1 Due to Temperature Change

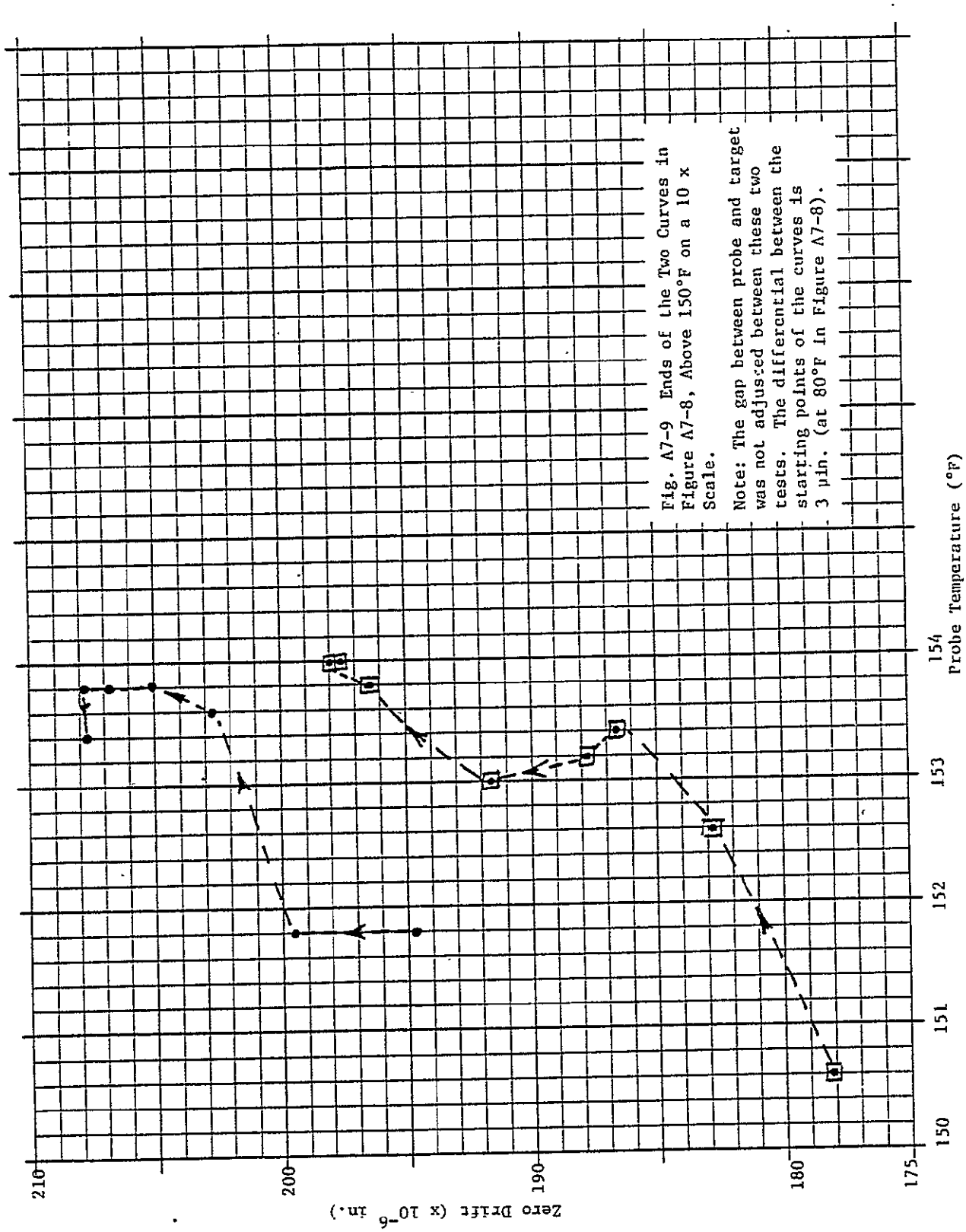

Fig. A7-9 Ends of the Two Curves in Figure A7-8, Above 150°F on a 10 x Scale.

Note: The gap between probe and target was not adjusted between these two tests. The differential between the starting points of the curves is 3 µin. (at 80°F in Figure A7-8).

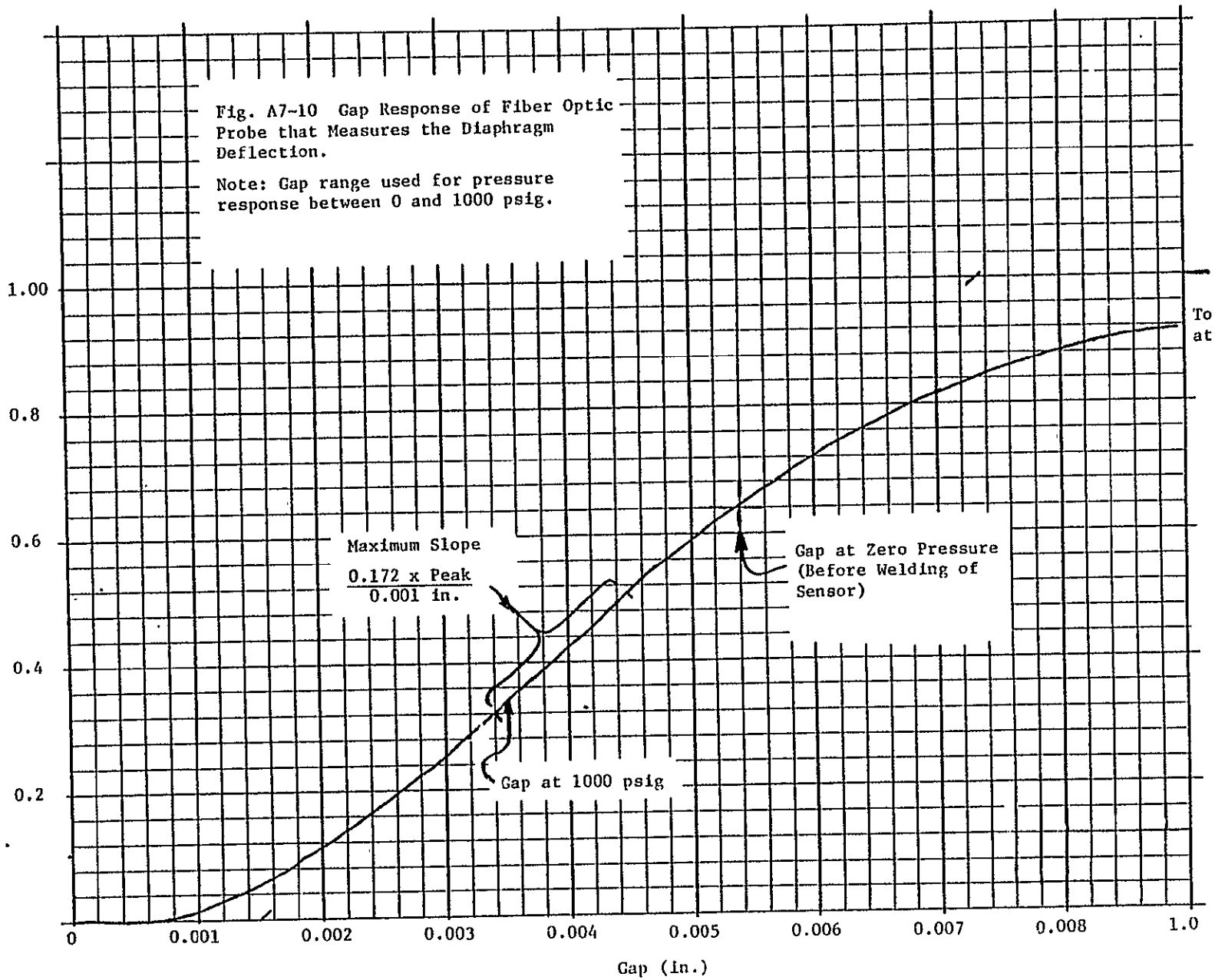

TABLE A7-1

ZERO SHIFT AND OUTPUT CHANGE OF PRESSURE SENSOR

DURING INITIAL TEMPERATURE TESTS

Date	Temperature	Probe Output		Output Change for 1000 psig	Zero Shift at R.T.		Response Change	Notes
		p = 0	p = 1000		%F.S.	Micro Inch	%F.S.	Temperature Cycle to:
10/3/83	RT	1.867	1.270	.597	--	0	0.0	
10/4/83	RT	1.799	1.219	.580	+11.4	-216	-2.8	
"	RT	1.799	1.220	.579	+11.4	-216	-3.0	
"	RT	1.800	1.221	.579	+11.2	-213	-3.0	-150°C
10/5/83	RT	1.808	1.227	.581	+ 9.9	-188	-2.7	
"	RT	1.807	1.226	.581	+10.1	-191	-2.7	
"	-186°C	1.860	1.288	.572	+ 1.2	- 22	-4.2	
		1.860	1.290	.570	+ 1.2	- 22	-4.5	
	RT	1.809			+ 9.7	-185		
10/6/83	RT	1.808			+ 9.9	-188		-100°C
10/6/83	RT	1.895	1.284	.611	- 4.7	+ 89	+ 2.3	- 80°C

Note: A positive zero shift indicates a decrease in gap.

TABLE A7-1 (continued

Date	Temperature	Probe Output		Output Change for 1000 psig	Zero Shift at R.T.		Response Change	Notes
		p = 0	p = 1000		%F.S.	Micro Inch	%F.S.	Temperature Cycle to:
10/6/83	RT	1.899			- 5.4	+102		+87°C
10/7/83	+7°C	1.922			- 9.2	+175		
	-165°C	1.951	1.345 +.005 -.003	.606 -.005 +.003	-14.1	+267	+0.7 +2.0	
	+134°C	1.911			- 7.4	+140		
	+ 84°C	1.902	1.282	.620	- 5.8	+111	+3.9	
	26°C	1.929	1.308	.621	-10.4	+197	+4.0	

Note: A negative zero shift indicates an increase in gap.

TABLE A7-2

TEMPERATURE EFFECT ON MODULUS

OF ELASTICITY OF INCONEL 718

Temperature		Modulus	% Change	% Change
^{o}F	^{o}C	psi		per $100^{o}C$
-308	-189	31.3	+5.0	+2.4
- 86	- 66	30.6	+2.7	+3.1
70	+ 21	29.8	0	0
147	+ 64	29.7	-0.3	-0.7
227	+108	29.3	-1.7	-1.95

from: Huntington Alloys Brochure, 2nd Ed., 1973

APPENDIX 8

EFFECT OF INCANDESCENT LAMP ON THERMAL DRIFT OF FOTONIC SENSOR

To appreciate the effect of the lamp, it is helpful to consider the interaction between the fiber probe's spacial non-uniformity at the sensing face and the highly non-uniform intensity distribution of the light from the lamp. Typically the fiber mixing in the random probe, consisting of 50% illuminating fibers and 50% receiving fibers, is far from uniform. Clusters of 2-25 fibers of one type in the sensing face occur. The most intense coupling occurs when an illuminating fiber is adjacent to a receiving fiber.

The illumination intensity of the lamp with integral condensor varies overall by a factor of four, as measured at the entrance to the illuminating bundle. From fiber to fiber the illumination intensity can vary by 15%. Thus if the filament in the lamp shifts one fiber diameter, the illumination of a fiber may change by 15%. If that fiber couples closely to 6 adjacent fibers (the maximum possible), the output of the 6 receiving fibers is changed by $\pm$15%. The 6 fibers are roughly 1% of the total number of receiving fibers. A $\pm$15% change in them results in a $\pm$.15% change in output level of the probe. This is comparable to the effect of a 90°F temperature change on the lamp control circuit, as shown in Figure 8. As calculated in the main text of this report, a 0.15% change in probe output level is equivalent to a gap change of 8 micro-inch.

When the lamp filament shifts one fiber diameter, the total number of fibers that is affected can be quite large. To couple the filament optically to the fiber bundle with good efficiency, the lamp filament is imaged on the fiber bundle by a condensing lens. The condensing lens is integral with the lamp. The filament image projected on the fibers shows three windings that can sweep across a total of 25-50 fibers in the illuminating bundle. If out of these fibers 10-20 are closely coupled to 6 receiving fibers, the probe output would change 1.5-3.0%, equivalent to 80-160 micro inches of gap change.

It was concluded that to avoid these drift problems, the incandescent lamp should be replaced by a light emitting diode (LED). The intensity distribution of the light emitting diode is such that the variation across a fiber bundle of .065 inch diameter illuminated by the diode is less than $\pm$5%. The light is emitted from a semiconductor junction, through a condensor lens integral with the diode case. The power dissipation of the light emitting diode is typically 10% of that of the incandescent lamp. The potential for temperature induced drift when using this light source, is much reduced, because of the rigidity of the diode structure and the very uniform light distribution.

Before the temperature induced drift of the incandescent source had been established, the sensitivity to vibration of this light source had caused concern. Until recently the light energy levels available from LED's, was so low that they could not be used as a substitute for an incandescent source.

The LED selected for the pressure sensor (EXCITON #XC88) produces a usable light energy that is 15% that of the customary incandescent source, (Gilway L1005) both at maximum allowable brightness. For this application, the brightness of the LED is amply sufficient, to obtain the desired signal levels. Only if the LED is used with fiber optic probes with very few fibers or with targets of poor reflectivity, will the lesser brightness become a limiting factor. Newer LED's are reported to have intensity levels comparable to those of an incandescent source of comparable aperture. The lack of aging of the LED and its greater overall reliability are additional features. It is expected that the LED will replace the incandescent light source in fiber optic proximity probes.

The problems present in the coupling of the light source to the input fibers and the potential for thermal drift are duplicated in the coupling of the receiving fibers to the photo diode. The thermal drift effects in the probe output ascribed solely to the incandescent source, actually may include some effects occurring at the transition from receiving fibers to photo diode. The potential for trouble at this point, however, does not seem to be high. The power dissipation of the photo diodes is very small, and the spacial distribution of the sensitivity of the diode is uniform to $\pm$10% across the input face (a lens).

The thermal drift characteristics of the breadboard pressure transducer electronics have not been evaluated as yet. This evaluation may become a task under a follow-on contract.

APPENDIX 9

SUMMARY OF THE INVESTIGATION OF MTI 1000 FOTONIC SENSOR IN SUPPORT OF THE DESIGN OF A FIBER OPTIC PRESSURE TRANSDUCER

Introduction:

The following material was presented in the preliminary design review at NASA-MSFC. It is reproduced here to document the rationale for some of the design decisions and to provide more descriptive circuit detail than could be given in the main part of this report.

Figure numbers in the following refer to figures used in the main test of the report.

The following items of analysis, design and experimentation will be discussed:

1. Analysis of existing circuitry and development of computer model to predict performance over a temperature range

2. Temperature testing of existing MTI 1000 hardware

3. Examination of parameters essential to successful use of an Infra-red LED illumination source

4. Analysis of the impact of electronics drifts on measurement of projected diaphragm displacements

5. Development of schemes to electronically compensate for:

    a) Changes in compliance of the transducer diaphragm with temperature

    b) Physical zero shift of the fiber optic proximity probe

    c) Non-linearity in the Fotonic Sensor response

6. Development of electronics block diagram.

Summary of Preliminary Design Analysis and Testing:

The analysis under item #1 was undertaken to determine which elements of the existing MTI 1000 Fotonic Sensor electronics exhibit sufficient stability to be utilized in this application and as an aid in making necessary improvements.

The temperature performance of the receiver/amplifier circuit was considered over the operational range of the OP-15 operational amplifiers ($30^{\circ}F$ to $120^{\circ}F$) used in the circuit.

The zero drift was predicted to be 1.4mV typical, 5.7 mV worst case and the full scale output voltage was predicted to be 29 mV typical and .74 V worst case. A major source of the full scale output drift, was found to be the temperature coefficient (50 ppm/$^{\circ}C$) of the feedback resistor in the receiver/amplifier current-to-voltage convertor. Selection of low temperature coefficient resistors (e.g., Vishay type H resistors with a temperature coefficient < 2.2 ppm/$^{\circ}C$) will significantly improve the stability of the circuit.

Based on the low predicted zero drift and the potential for great improvement in the gain drift, a decision was made to perform the testing under item #2. During this testing, gain drifts much larger than anticipated were observed (nearly 2% drift in the full scale output). In order to isolate the source(s) of the drift, a number of ancillary tests were run.

1. Test of lamp intensity over temperature

2. Test of gain stability with a fixed signal current ($\approx 3 \times 10^{-7}$ A) input to the receiver amplifier (i.e., optical elements eliminated from circuit) (Figure 9)

3. Test of lamp intensity control circuit drift (Figure 8)

4. Test of fiber optic probe mechanical drifts (Figure 4).

The results of these tests indicated that the electronics drifts of the receiver/amplifier are in line with the computer predictions (4.4 mV full scale drift and 4.5 mV zero drift from $30^{\circ}F$ to $120^{\circ}F$) and the lamp intensity control circuit drifts are less than .3%.

These elements are clearly not responsible for the 2% full scale drift. In research on Fotonic Sensor probes (Hoogenboom: Fiber Optic Blade Tip Clearance Sensor Investigation: MTI 82TR73) it has been suggested that fiber optic probes are sensitive to time varying light distributions over the probe's illuminating fibers. Therefore the light intensity profile of a Gilway L1005 lamp (which was used in the temperature testing) was mapped.

Due to the demonstrated electrical stability of the MTI 1000, it is hypothesized that changes in the mechanical alignment of the lamp, photodiodes, and fiber optic cable over temperature are responsible for the observed gain changes. In order to overcome these mechanical problems and potential problems arising from the motion of a lamp filament in a high vibration environment, it is proposed that an infrared light emitting diode be used as the Fotonic Sensor illumination source in a carefully engineered lamp/photodiode/fiber optic coupling block. Currently the coupling block utilizes set screws to locate the optical elements. The redesigned lamp block will overcome the shortcomings of the set screws by incorporating split clamps to hold the optical elements.

The investigation of LEDs under item #3 has led to an understanding of the following aspects of their use:

1. A high efficiency IR LED, such as the XCITON XC 88 FC, driven with 8 mA provides (with a reflective target) an illumination intensity at the receiver photodiode equivalent to that produced by the currently used incandescent lamp.

2. The emission wavelength of LEDs under consideration (890 nM) lies at the point of maximum sensitivity and minimum temperature coefficient of sensitivity of the receiver photodiodes (Vactec VTP 1). See Figure 10.

3. The direct relationship of LED current with output light intensity provides potential for more stable intensity control than an incandescent lamp, whose intensity is related to the sixth power of the lamp current and the fourth power of the lamp voltage.

In order to relate the results of the electronics stability evaluations to a diaphragm displacement measurement, the response of a standard MTI Fotonic Sensor probe has been selected as a reference. The probe selected is the 125R, which offers an excellent compromise between sensitivity and light intensity. Using the average front slope response of this probe (.624 μIn/mV), graphs of the apparent displacement drifts arising from the electronics offset and gain drifts have been generated (Figures 7 and 9). The magnitude of these drifts (< 4μIn over a range of 30°F to 120°F), has been deemed compatible with the 1 mil full pressure diaphragm displacement contemplated for the transducers (average drift - .004%/°F.

Testing of the fiber optic probe mechanical drifts revealed a highly linear motion of the sensor tip with respect to the sensor housing, over temperature (correlation coefficient of a line fit to the gap growth versus temperature data - 0.99995). If it should prove unfeasible to mechanically eliminate this drift, the temperature sensing circuitry intended to compensate for the changes in diaphragm compliance may also be used to compensate for the zero drift.

The total system concept is shown in the attached block diagram (Figure 14) and is discussed in the following section.

Block Diagram:

The illumination source for the fiber optic proximity probe is a high efficiency infra-red LED (e.g., Xciton XC88FC). The radiant output of this LED is held at a constant level by the lamp control circuit. The circuit functions, by converting the current output of a photodiode into a voltage proportional to the LED output intensity. This voltage is summed with a reference voltage and the integral of the sum is used to provide control of the LED current. As the reference voltage and the light level dependent voltage will be of opposite polarities, the integrator will act as an error amplifier whose output is related to the integral of the difference between the light level and a reference value.

Light returning to the Fotonic Sensor from the target (i.e., the transducer diaphragm) illuminates a second photodiode. Ideally, the current flowing in this diode will vary directly with the diaphragm displacement. The task of the electronics is to convert this current to an appropriate voltage.

The first stage of the receiver/amplifier converts the photodiode current to a low level voltage. The second and third stages provide a gain of approximately 20. The calibration capability of the instrument is provided by the independent, non-interactive offset and gain adjustments of these amplifiers.

In order to allow compensation for changes in diaphragm compliance and differential expansion of the proximity probe - diaphragm mechanical system over temperature, a temperature sensitive element (e.g., a nickel resistor)* will be added to the transducer body. A constant current source will drive the resistor and separate sensing leads will allow measurement of the voltage across the resistor. The temperature sensing circuit, then, provides a scaled, filtered voltage analog of the transducer temperature.

A simplified relationship between the output voltage of the instrument and the physical properties of the transducer may be written:

$$V \alpha C \times (P \times A) + X_o \qquad (1)$$

where

V is the instrument output voltage

C is the compliance of the diaphragm

P is the pressure

A is the diaphragm area

X_o is the 'zero pressure' probe-diaphragm gap.

*To avoid any electrical leads into the pressure transducer, a fiber optic temperature sensor was substituted for the nickel resistor in the final design, as is (also) shown in Figure 14.

In actual use, the output voltage due to the 'zero pressure' gap will be nulled by the offset adjustment of the receiver amplifier. Errors due to thermal drift of the probe-diaphragm gap, will be eliminated by adding a fraction of the transducer temperature analog to the same offset circuit.

As seen in Equation (1), the diaphragm compliance appears as a gain term in the relationship between pressure and output voltage. Compensation for drifts in the diaphragm compliance is accomplished, by using the temperature analog to adjust the multiplying input voltage (V_y) of a multifunction module whose transfer function is:

$$V_{out} = 10/9\ V_y \frac{V_z^m}{V_x}$$

(the output of the receiver/amplifier will be applied to V_z and V_x will be set to 1). Continuous linearization of the pressure-output voltage relationship may be accomplished by adjustment of the exponential term, m.

Separate outputs with bandwidths of 300 Hz and 20 kHz are produced by independent output amplifiers. These amplifiers provide buffering of the multifunction module output, final scaling of the output pressure analog, as well as precise bandwidth limiting.

APPENDIX 10

NASA-MSFC PRESSURE CALIBRATION TEST DATA SUMMARY

Three series of calibrations were made at MSFC, in October 1983, December 1983, and in February 1984. In the first calibrations, some equipment faults related to the power supply were experienced and repaired. In the second and third calibration series no equipment faults occurred. In all experiments where the sensor was at the temperature of liquid nitrogen, the response became disturbed. At all other temperatures, in the range of -300°F to +200°F, the response was stable and linear. Some of the data has been collected as shown on the graphs in Figures A10-1 through A10-4, and in Tables A10-1 and A10-2.

The overall performance of the sensor when not at the liquid nitrogen temperature is good to excellent. At ambient temperature the hysteresis and zero shift in the raw signal from the sensor, over a pressure cycle, are 0.1 to 0.2% F.S. (see Tables A10-1 and A10-2). At cryogenic temperatures, hysteresis is 0.1 to 0.5%, and zero shift is 0.1 to 2.2% F.S. After linearization, the linearity of the signal is (typically) as shown in Figure A10-1. The slope of the output signal varies over the F.S. range by ±2%. The deviation of the signal from the best straight line through the data points is (typically) ±1% F.S.

To gain some insight in the poor performance at liquid nitrogen temperature (-316°F), the graphs in Figures A10-2 through A10-4 were made. The three sets of data used in these figures were taken from the three sets of tests, made in October 1983, December 1983, and February 1984; therefore, all the available data were used to examine the disturbed -316°F response.

In the tests in December 1983 and February 1984, the fiber optic cable was purged with helium to remove air from inside the transducer. The purging gas could not be flowed through the transducer sensing volume, as no provision was made for that in the design. It was therefore possible that some air remained in the sensing gap, resulting in liquid air at -316°F*. If the liquid would enter the sensing gap, the gap would appear smaller by a factor equal to the refractive index of the liquid.

Figure A10-2 shows the response at -316°F and room temperature data taken after the cryogenic test. After a partial calibration cycle (from 0 to 1000 psi, back to 600 psi), there is an abrupt shift in output of +0.27 volt. The output due to a 1000 psi pressure is 0.65 volts. The diaphram deflection at 1000 psi is 0.0019 in. (see Table A10-3). Thus, the 0.27 volt reduction in absolute output level is equivalent to a gap reduction of:

$$0.27/0.65 \times 0.0019 \text{ in.} = 0.0008 \text{ in.}$$

The gap in the sensor at the moment that the 0.27 volt shift occured, can be found in Figure A7-10, where the operating point at 600 psi is at a gap of

---

*Liquid oxygen forms at -297°F and liquid nitrogen forms at -320°F. The refractive indices are: for O_2, n = 1.221; at -293°F, and for N_2, n = 1.2053 at -310°F.

about 0.004 in. Therefore, the 0.0008 in. apparent gap change was about 20% of the existing gap. This could be explained by having a change in the medium in the gap from gaseous air to liquid air, which would reduce the optical path length (and hence, the horizontal scale in Figure A7-10) by a factor 1.20 to 1.22 (the refractive index of the liquid medium). After the liquid enters the gap, the sensor pressure response must also appear reduced by a factor of 1.2. The slopes of the LN_2 and room temperature curves in Figure A10-2 are:

LN_2 (Top Curve): 0.5343 V/1000 psi
Ambient (Middle Curve): 0.6324/1000 psi.

The ratio of these two slopes is: 0.6324/0.5343 = 1.183. This ratio correlates well with the static apparent gap shift percentage calculated above at 1.20 X, and it correlates well with the effect that the refractive index change would have.

The data in Figure A10-2 supports the hypothesis of condensation of air in the gap. A similar response is shown in Figure A10-3, but a pressurization to 1000 psi could be made without a zero shift. The liquid entered the gap when the pressure dropped from 800 to 600 psi. This could relate to the amount of liquid air in the cavity and whether the pressure caused a change in the transducer tilt angle in that pressure range.

Figure A10-4 shows a similar pattern of zero shifts as the pressure traverses certain pressure intervals. Thus all of the available data points in the direction of condensation occurring in the diaphragm cavity after the temperature drops below the boiling point of oxygen.

TABLE A10-1

SUMMARY OF TEST RESULTS USING DATA TAKEN AT NASA-MSFC

Data Fit, $F(X) = A1 + A2 \times X$, X = Pressure (psi)

Date	Temp. (°F)	Raw Signal			0-5 V Output		0-30 mV Output		
		A1 (V)	A2 (V/1000 psi)	Hysteresis (%)	A1 (V)	A2 (V/1000 psi)	A1 (mV)	A2 (mV/1000 psi)	Hysteresis (%)
2/9/84	Ambient	-2.0561	+0.6580	-0.2	-2.1807	+5.6435	-1 2988	+33.622	
12/19/83	+75						-4.7465	+32.377	-0.25
12/19/83	+200						-7.2237	+33.919	11.23
2/8/84	-150	-2.0938	+0.6545	±0.1	-2.2090	+5.6511	-13 182	+33 67	
12/19/83	-150						-6.59	+32.89	+0.70
2/8/84	-272	-2.1079	+0.6460	-0.5	-2.1667	+5.5883	-12 936	+33.29	
12/19/83	-300						-5.75	+32.44	+0.65
2/9/84	LN2	Erratic Response							

TABLE A10-2

ZERO SHIFT IN SEVERAL SERIES OF CALIBRATIONS

Date and Time	Temp. (°F)	Raw Output at Zero Pressure (volts)	Zero Shift (volts)	Zero Shift (% F.S.*)
2/8/84 10:37 a.m.	-150°F	-2.0804 -2.0798	0 +0.0006	 +0.1
2/8/84 1:04 p.m.	-272°F	-2.0926 -2.0960	-0.0122 -0.0156	-1.9 -2.2
2/9/84 7:50 a.m.	Ambient	-2.0420 -2.0426	+0.0384 +0.0378	+5.7 +5.7
2/9/84 9:14 a.m.	LN2	-2.0958 -1.5704 -1.5708 -1.5704	-0.0154 +0.5100 +0.5096 +0.5100	-2.2 +78 +78 +78
10/20/83 10:08 a.m.	Ambient	-1.9459 -1.9467 -1.9466 -1.9466	0 -0.0008 -0.0007 -0.0007	0 -0.12 -0.11 -0.11
10/21/83 10:42 a.m.	LN2	-2.2495 -1.5262 -1.5256 -1.5250	-0.3036 +0.4197 +0.4191 +0.4185	-46 +65 +65 +65
10/21/83 12:25 a.m.	Ambient	-1.9439 -1.9438 -1.9437 -1.9442	+0.0020 +0.0021 +0.0022 +0.0017	+0.3 +0.3 +0.3 +0.3

*F.S. (full scale) output change of the raw signal is 0.65 V for a pressure of 1000 psi.

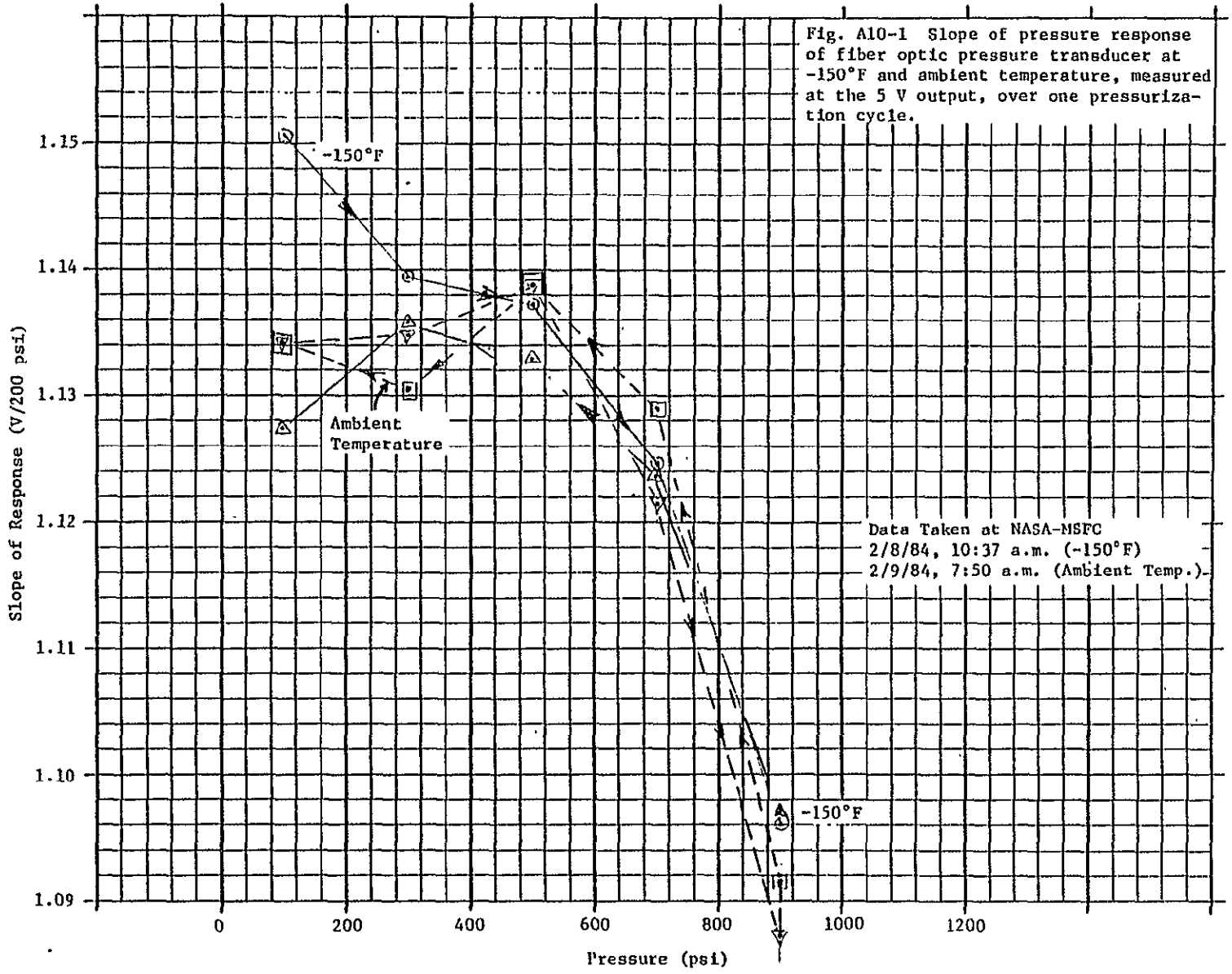

Fig. A10-1 Slope of pressure response of fiber optic pressure transducer at -150°F and ambient temperature, measured at the 5 V output, over one pressurization cycle.

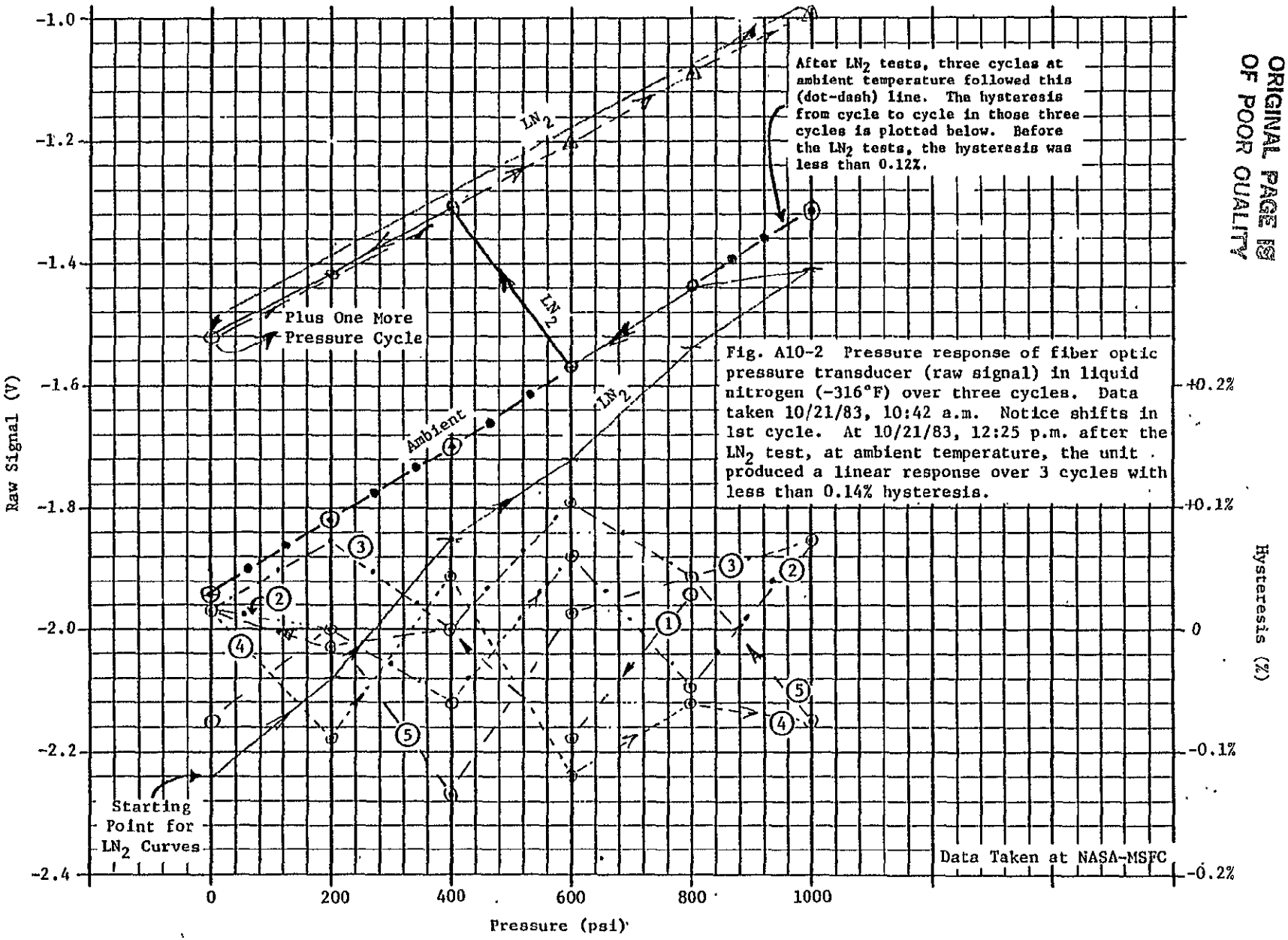

Fig. A10-2 Pressure response of fiber optic pressure transducer (raw signal) in liquid nitrogen (-316°F) over three cycles. Data taken 10/21/83, 10:42 a.m. Notice shifts in 1st cycle. At 10/21/83, 12:25 p.m. after the LN_2 test, at ambient temperature, the unit produced a linear response over 3 cycles with less than 0.14% hysteresis.

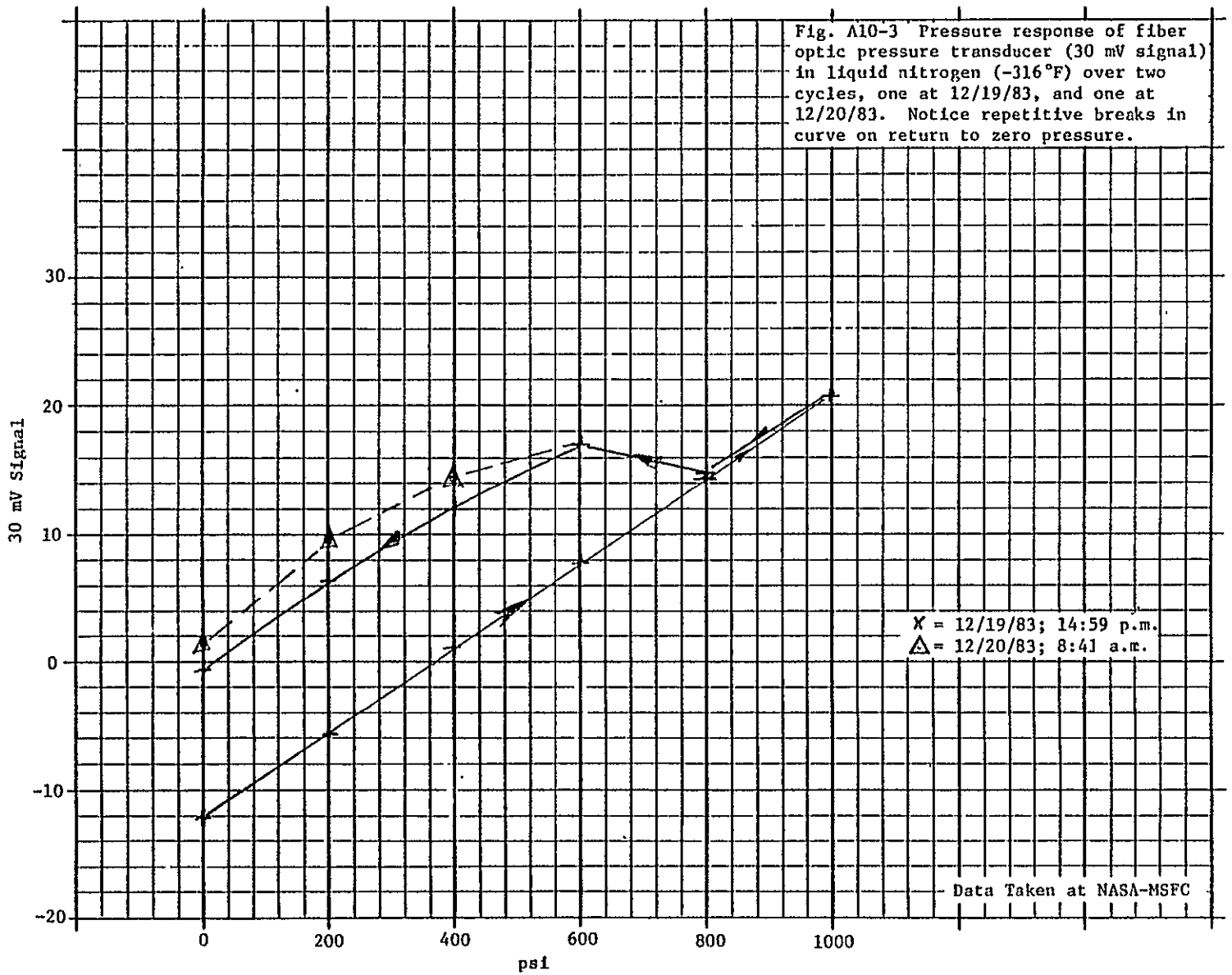

Fig. A10-3 Pressure response of fiber optic pressure transducer (30 mV signal) in liquid nitrogen (-316°F) over two cycles, one at 12/19/83, and one at 12/20/83. Notice repetitive breaks in curve on return to zero pressure.

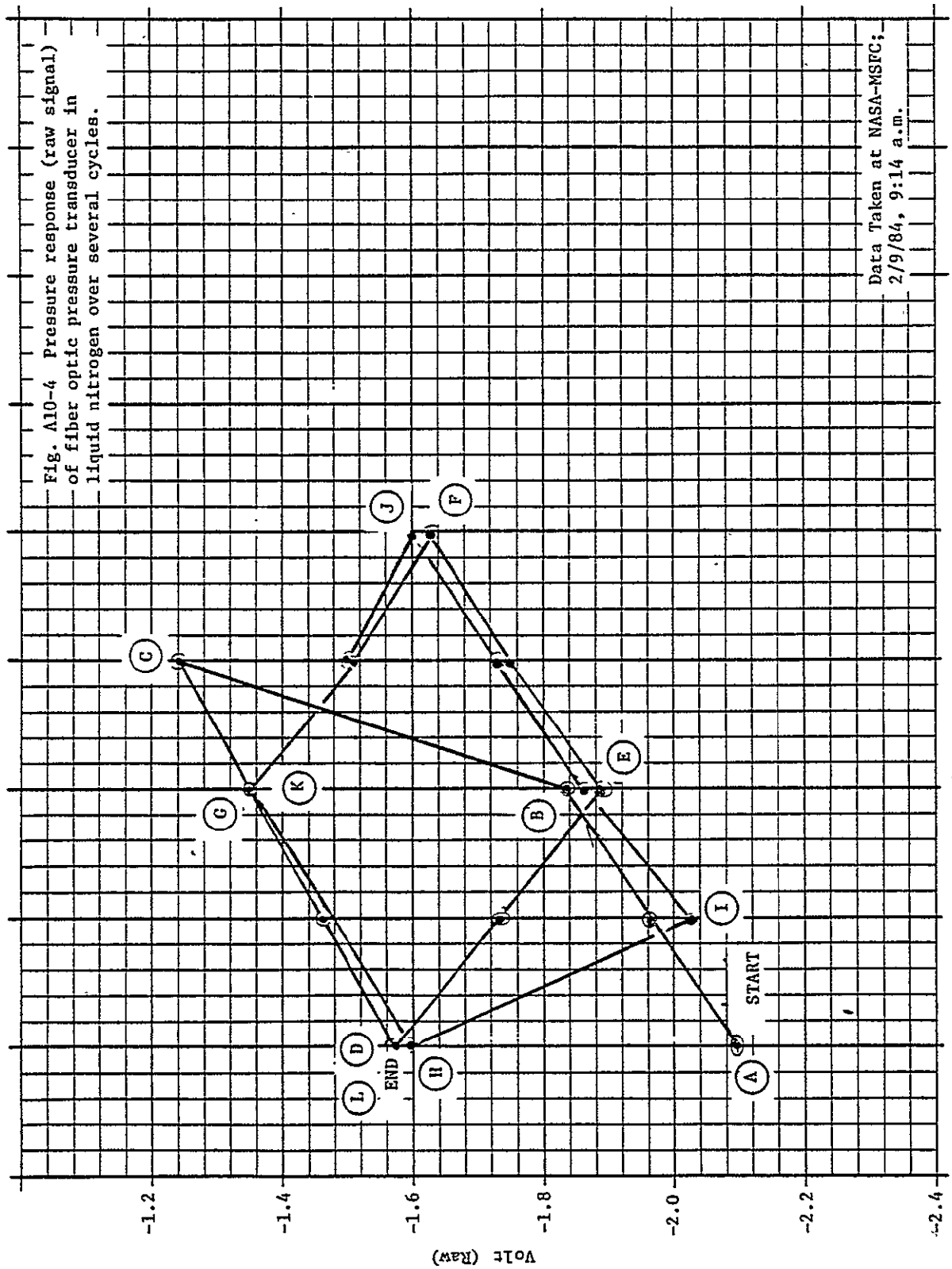

ORIGINAL PAGE IS
OF POOR QUALITY

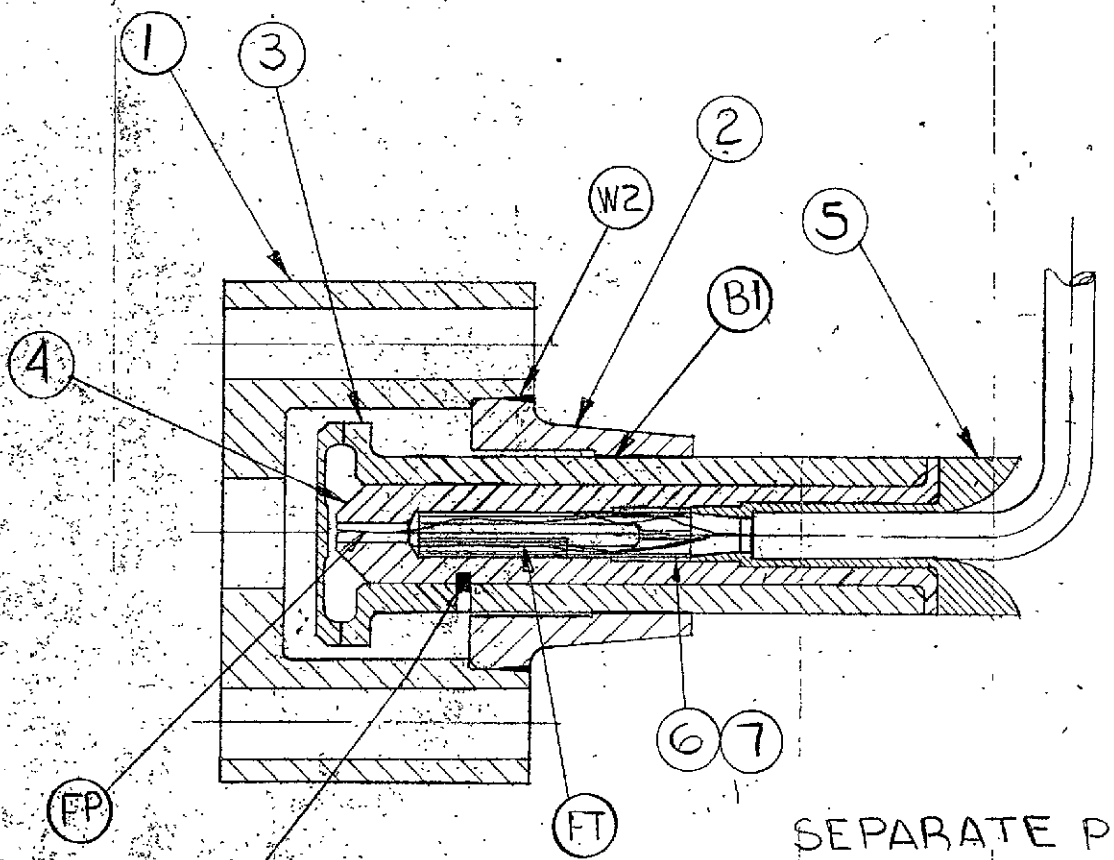

REVISIONS		SIZE B	SK-B-8454	REV. B
SYM.	DESCRIPTION	DATE	APPROVAL	
A	CORRECTED TO AGREE WITH DETAILS	5/30/83		
B	GEN. REV ADDED NOTE 1 CHANGED SCALE TO 2/1 9/27/84 JJD			

ORIGINAL PAGE IS
OF POOR QUALITY

NOTE:
1. TACK WELD THRU DRILL POINT IN ITEM 3 (3 PLACES 120° APART)

2 FOLDOUT FRAME

SEPARATE PARTS LIST ISSUED

UNLESS OTHERWISE SPECIFIED DIMENSIONS ARE IN INCHES TOLERANCES ON:		
DECIMALS	FRACTIONS	ANGLES
.XXX ±	±	±
.XX ±	ALL SURFACES ✓	
BREAK SHARP CORNERS AND REMOVE BURRS		
MATERIAL		
TREATMENT		

DRAWN	T. Bartnicki 9 JUNE '83
CHECK	
DESIGN	
ANALYTICAL	
MATERIALS	
MFG. ENGR.	
PROJ. ENGR.	
QUALITY CONTROL	

MECHANICAL TECHNOLOGY INCORPORATED
LATHAM NEW YORK

TITLE
FIBER OPTIC PRESSURE TRANSDUCER-NASA MSFC

CODE IDENT NO.	SIZE	
26741	B	SK-B-8454

ISSUED	SCALE	WT.	ACT. CALC.
	2/1		

FOLDOUT FRAME

ORIGINAL PAGE IS
OF POOR QUALITY

REVISIONS		SIZE C	SK-C-8473	REV. A
REVISION	DESCRIPTION	DATE	APPROVAL	
A	NOTE "PER ENGINEERING INSTRUCTIONS" WAS ".005 DEEP MIN." STEPS 5&6 .073 DIA. HOLES WERE .062 DIA.	6/6/97		

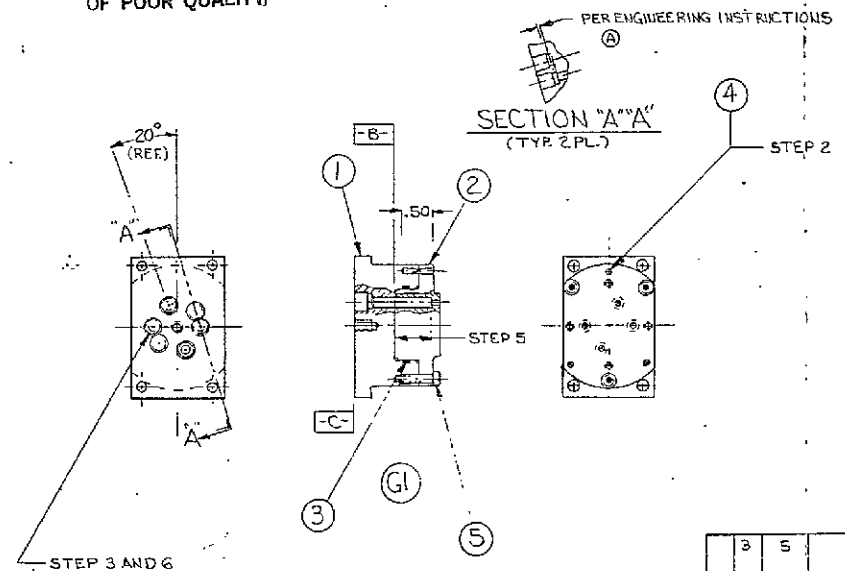

ORIGINAL PAGE IS
OF POOR QUALITY

STEP-1- ASSEMBLE ITEM 1&2 WITH CAP SCREWS ITEM 5
STEP-2-DRILL AND REAM TO DEPTH SHOWN 3 HOLES FOR .062 DIA. DIA. DOWEL PINS (ITEM 4). LOCATE FROM 3 EXISTING .031 DIA. HOLES IN ITEM 2. DOWELS TO BE PRESS FIT IN ITEM 1
STEP-3-DRILL 4- .073 DIA. HOLES THRU ITEMS 1 AND 2; LOCATE FROM 4- .031 DIA. HOLES IN ITEM 1.
STEP-4-DISASSEMBLE ITEMS 1&2
STEP-5-IN ITEM 2 DRILL THE 4-.073 DIA. HOLES TO .157 DIA. X .62 DEEP FROM SURFACE -B- FOR A PRESS FIT OF TUBES DWG. NO. SK-B-8471 P1 AND P2.
STEP-6- IN ITEM 1, DRILL & REAM THE FOUR .073 DIA. HOLES TO .159 DIA. THRU AND DRILL .234 (15/64) DIA. X .28 DP & REAM .250 (1/4) DIA. X .227 DEEP FROM SURFACE -C-

QTY/CP	ITEM NO.	PART NO.	DESCRIPTION
	3	5	HEX. SOCKET HEAD CAP SCREW #6-32 X .50 LONG; STEEL CAD PLATE
	3	4	DOWEL PIN – STANDARD .062 DIA. X .50 LONG – STEEL
	1	3	2-024 O-RING (.070 CROSS SECTION X 1 1/4 I.D. BUNA N) PARKER OR EQUIV.
	1	2	SK-B-8467 P1 PLUG BODY
	1	1	SK-C-8466 P1 RECEPTACLE BODY
	X	X	SK-C-8473 G1 ASSEMBLY

UNLESS OTHERWISE SPECIFIED DIMENSIONS ARE IN INCHES
TOLERANCES ON: DECIMALS .XX ± .02, .XXX ± .010; FRACTIONS ±; ANGLES ±
ALL SURFACES √
BREAK SHARP CORNERS AND REMOVE BURRS
MATERIAL
TREATMENT

DRAWN: Paul Swick 8 June 93
CHECK
DESIGN
ANALYTICAL
MATERIALS
SAFE. ENGR.
PROJ. ENGR.
QUALITY CONTROL

Mechanical Technology Incorporated
Latham, New York

TITLE: ASSEMBLY RECEPTACLE & PLUG

DODE IDENT NO. 26741 | SIZE C | SK-C-8473

ISSUED | SCALE 1/1 | SHT. ACT. ONLY

FOLDOUT FRAME

FOLDOUT FRAME

ORIGINAL PAGE IS
OF POOR QUALITY

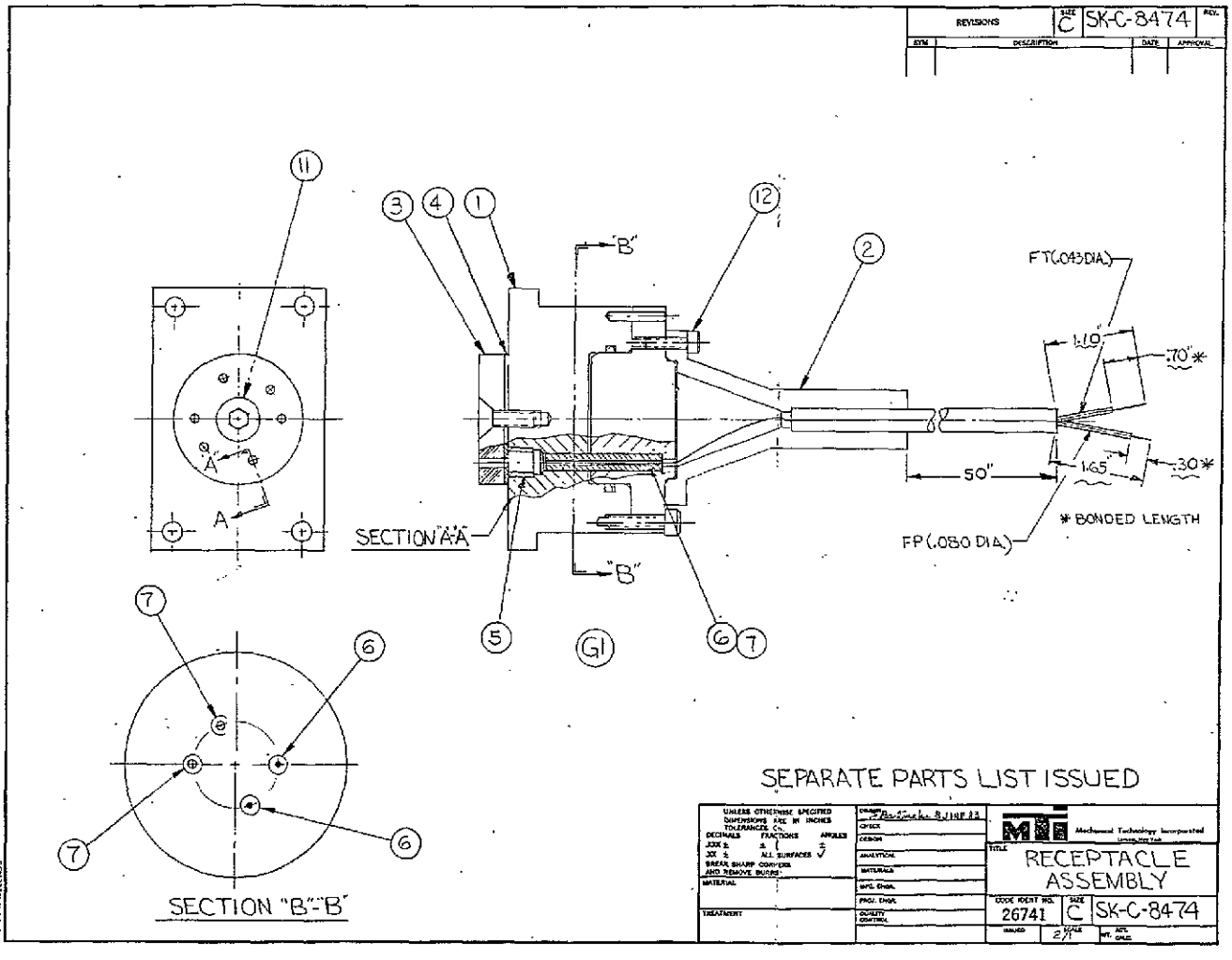

ORIGINAL PAGE IS
OF POOR QUALITY

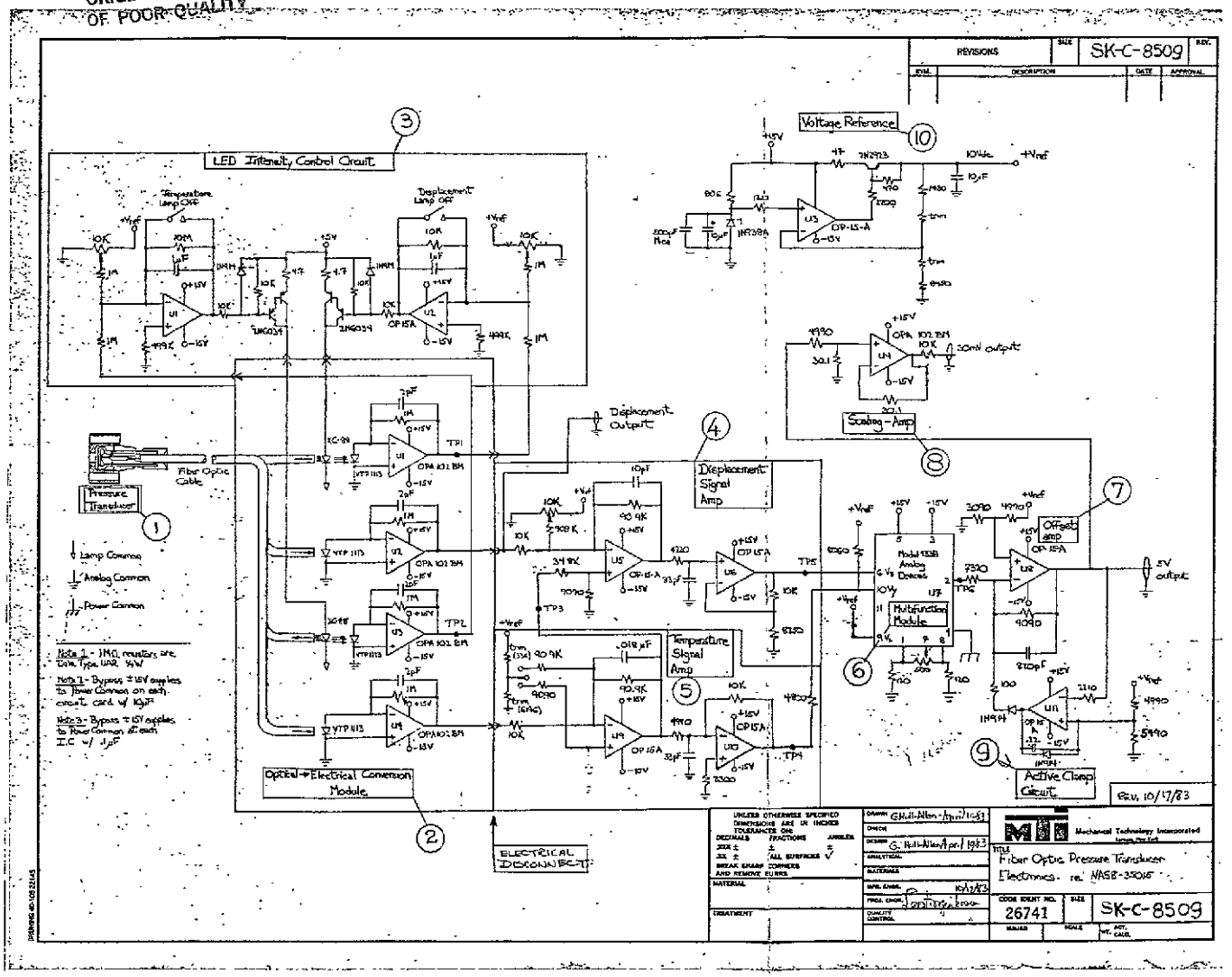

2 FOLDOUT FRAME